AN EXPERIMENTAL INVESTIGATION OF THE UREA-WATER DECOMPOSITION AND SELECTIVE CATALYTIC REDUCTION (SCR) OF NITRIC OXIDES WITH UREA USING V_2O_5-WO_3-TiO_2 CATALYST

A Thesis

by

JASMEET SINGH JOHAR

Submitted to the Office of Graduate Studies of
Texas A&M University
in partial fulfillment of the requirements for the degree of

MASTER OF SCIENCE

August 2005

Major Subject: Mechanical Engineering

AN EXPERIMENTAL INVESTIGATION OF THE UREA-WATER DECOMPOSITION AND SELECTIVE CATALYTIC REDUCTION (SCR) OF NITRIC OXIDES WITH UREA USING V_2O_5-WO_3-TiO_2 CATALYST

A Thesis

by

JASMEET SINGH JOHAR

Submitted to the Office of Graduate Studies of
Texas A&M University
in partial fulfillment of the requirements for the degree of

MASTER OF SCIENCE

Approved by:

Chair of Committee,	Jerald A. Caton
Committee Members,	Kalyan Annamalai
	Cady Engler
Head of Department,	Dennis O'Neal

August 2005

Major Subject: Mechanical Engineering

ABSTRACT

An Experimental Investigation of the Urea-Water Decomposition and Selective Catalytic Reduction (SCR) of Nitric Oxides with Urea Using V_2O_5-WO_3/TiO_2 Catalyst.

(August 2005)

Jasmeet Singh Johar, B.En., University of Delhi

Chair of Advisory Committee: Dr. Jerald A. Caton

Two flow reactor studies, using an electrically heated laminar flow reactor over Vanadia based (V_2O_5-WO_3/TiO_2) honeycomb catalyst, were performed at 1 atm pressure and various temperatures. The experiments were conducted using simulated exhaust gas compositions for different exhaust gases. A quartz tube was used in order to establish inert conditions inside the reactor. The experiments utilized a Fourier transform infrared (FTIR) spectrometer in order to perform both qualitative and quantitative analysis of the reaction products.

Urea-water solution decomposition was investigated over V_2O_5-WO_3/TiO_2 catalyst over the entire SCR temperature range using the temperature controlled flow reactor. The solution was preheated and then injected into pure nitrogen (N_2) stream. The decomposition experiments were conducted with a number of oxygen (O_2) compositions (0, 1, 10, and 15%) over the temperature range of 227^{o}C to 477^{o}C. The study showed ammonia (NH_3), carbon-dioxide (CO_2) and nitric oxide (NO) as the major products of decomposition along with other products such as nitrous oxide (N_2O) and nitrogen dioxide (NO_2).

The selective catalytic reduction (SCR) of nitric oxide (NO) with urea-water solution over V_2O_5-WO_3/TiO_2 catalyst using a laboratory laminar-flow reactor was investigated. Urea-water solution was injected at a temperature higher than the vaporization temperature of water and the flow reactor temperature was varied from 127^{o}C to 477^{o}C. A FTIR spectrometer was used to determine the concentrations of the product species.

The major products of SCR reduction were NH_3, NO and CO_2 along with the presence of other minor products NO_2 and N_2O. NO removal of up to 87% was observed.

The aim of the urea-water decomposition experiments was to study the decomposition process as close to the SCR configuration as possible. The aim of the SCR experiments was to delineate the effect of various parameters including reaction temperature and O_2 concentration on the reduction process. The SCR investigation showed that changing parameter values significantly affected the NO removal, the residual NH_3 concentration, the temperature of the maximum NO reduction, and the temperature of complete NH_3 conversion. In the presence of O_2, the reaction temperature for maximum NO reduction was 377°C for β ratio of 1.0.

DEDICATION

To my parents and two younger sisters
For their love, support and patience.

ACKNOWLEDGEMENTS

I would like to give special thanks to my adviser, Dr. Jerald A. Caton, for giving me an opportunity to work on this thesis project. He offered me his constant guidance and enhanced my technical knowledge about scientific work. Dr. Caton has been an untiring teacher and a great advisor.

I am very grateful to Dr. Annamalai who helped me build strong combustion and thermodynamic fundamentals and has always shown a willing attitude towards clarifying my doubts from the fruitful discussions.

I would like to thank Hyukjin Oh and Younghun Park for providing me guidance on experimental calibration and procedures. Great appreciation goes to Sharef A. Abdelfattah for his good team spirit and his assistance with the experimentation.

This research project was sponsored in part by a grant from the Texas Higher Education Coordinating Board under Grant No. 000512-0012-2001. The contents of this thesis, however, do not necessarily reflect the opinions or views of the sponsors.

TABLE OF CONTENTS

Page

Page

LIST OF FIGURES

FIGURE Page

FIGURE Page

FIGURE Page

FIGURE Page

FIGURE Page

FIGURE Page

LIST OF TABLES

1. INTRODUCTION

Combustion can be defined as a process of burning, or rapid oxidation which is accompanied by release of energy in the form of heat and light. Combustion is an essential process in order to obtain useful forms of energy either directly or indirectly. Almost 90% of the current energy production is based on the combustion of fossil fuels and biomass [1]. The combustion process does not come without any downsides, environmental pollution being one of the major drawbacks resulting in the production of many harmful exhaust gases. One of the dictionaries refers to pollution as a synonym for contamination. Introduction will provide a brief overview of different combustion-related pollutants, and describe their effects on the environment and human health. Nitrogen oxides (NO_x) will be discussed in detail since the aim of the research was NO_x abatement. Finally the SCR process will be discussed along with a brief insight into the Vanadia based (V_2O_5) catalyst.

1.1 Overview on pollutants

Many substances can be found in the air which may impair the health of plants and animals (including humans), or reduce visibility. These arise both from natural processes and human activity. Substances not naturally found in the air or at greater concentrations or in different locations from usual are referred to as 'pollutants' [2].

National Ambient Air Quality Standards (NAAQS's) have been established for six air pollutants of which five are primary and one is secondary. Primary air pollutants are the pollutants in the atmosphere that exist in the same form as in the source emissions. Examples of primary air pollutants include sulfur dioxide (SO_2), carbon monoxide (CO), nitrogen dioxide (NO_2), particulate lead and particulate matter less than 10 μm in diameter (PM-10). Secondary air pollutants are formed in the atmosphere as a result of reactions such as hydrolysis, oxidation and photochemical oxidation [3]. Secondary

---

This thesis follows the format and style of Combustion and Flame.

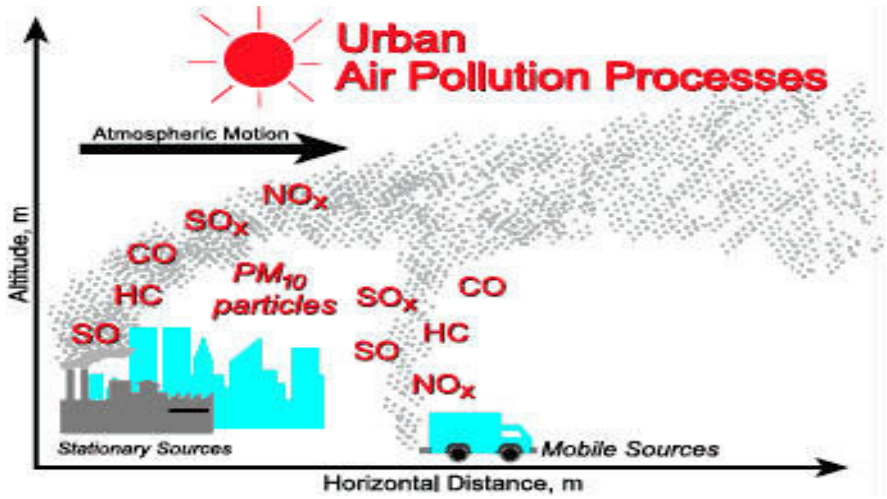

Figure 1. Urban air pollution processes [4].

pollutants include some particles formed from gaseous primary pollutants, acidic mists and compounds in photochemical smog, such as nitrogen dioxide, ozone and peroxyacetyl nitrate (PAN) [2]. Some pollutants which may be both primary and secondary: that is, they are both emitted directly and can be formed from other primary pollutants. Figure 1 shows several pollutants coming from both stationary and mobile sources. Figure 2 shows the various pollutants and their affect on the atmosphere.

CO_2 is one of the preferred products of combustion and yet it leads to serious environmental problems like global warming and greenhouse effects [5]. CO_2 is a product of complete combustion. U.S. Environmental Protection Agency (EPA) originally viewed carbon dioxide as a product of "perfect" combustion, but now views CO_2 as a concern for a different kind of pollution. Carbon dioxide has not been shown to impair human health, but it is a "greenhouse gas" that traps the earth's heat and contributes to the issue of global warming [6].

SO_2 and sulfur trioxide (SO_3), collectively known as sulfur oxides (SO_x) are mostly produced as a result of oxidation of fuel-bound sulfur whose portion is relatively significant in coals (i.e. lesser of 10% in coal, of 4% in heavy fuel oil, and of 0.06% in gasoline by weights [7]). SO_2 is a primary pollutant in the atmosphere which arises from both natural and human activities. Natural processes that contribute sulfur compounds to

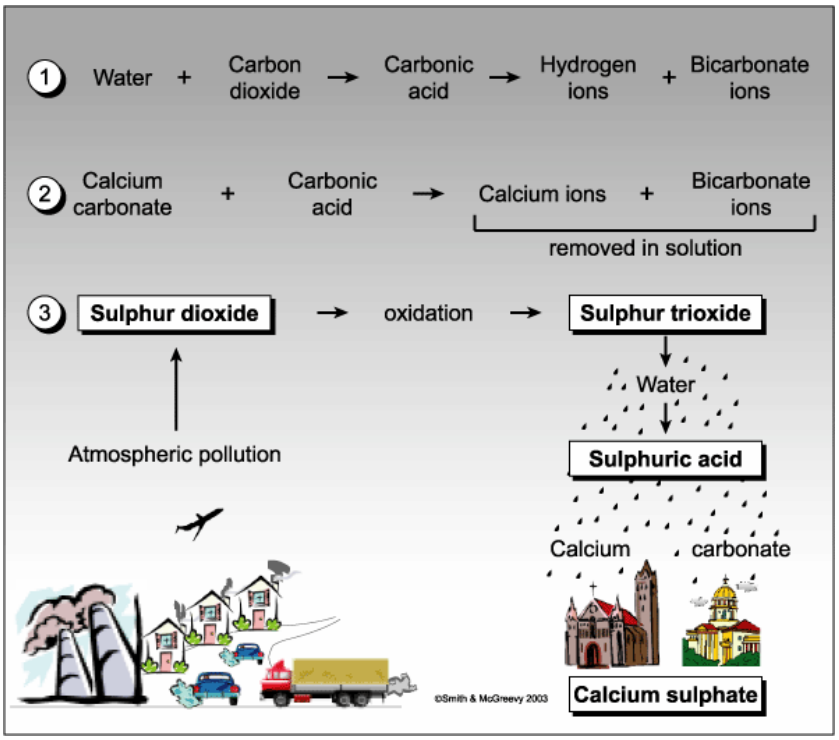

Figure 2. Pollutants and their effect on atmosphere [8].

the atmosphere include decomposition and combustion of organic matter, spray from the sea, and volcanic eruptions. The main human activities leading to the production of SO_2 are smelting of mineral ores containing sulfur and combustion of fossil fuels. SO_2 dissolves in water to form sulfuric acid and this is a corrosive substance that can cause damage to materials and the tissue of plants and animals by forming acid rain. SO_2 has been found to contribute to regional haze and fine particulate that cause visibility impairment, most noticeably in national parks [9]. SO_2 is also a respiratory irritant and may worsen existing respiratory illness; its prolonged exposure leading to chronic bronchitis. Since the SO_x emissions are proportional to the sulfur content of the fuel being used, a primary measure for SO_x reduction is to use low sulfur fuels. Other approaches for SO_x emission reduction include fuel cleaning or reduction of sulfur in the feed: beneficiation; use of appropriate combustion technologies such as fluidized bed combustion (FBD); and flue gas treatments – sorbent injection and flue gas desulfurization (FGD) [10]. SO_x

regulations and the development of various control methods have significantly reduced SO_x emissions in Europe and North America [11].

In addition to the gaseous pollutants suspended in air, there are also solid or liquid particles that may be suspended and are regarded as pollutants. Referred to as 'particulate matter' (PM), these particles range in size up to 50 micrometers (μm) in diameter and may reduce visual amenity and badly impact human health. Examples of particles in the air include smoke, bacteria, plant spores, metal fumes, aerosols and dust. Particulate matter may be a primary pollutant, such as smoke particles, or a secondary pollutant formed from the chemical reaction of gaseous pollutants. Human activities that result in particulate matter in the air include mining; burning of fossil fuels; transportation; agricultural and hazard reduction burning; the use of incinerators; and the use of solid fuel for cooking and heating. Particulate matter generally causes breathing and respiratory symptoms, aggravation of existing cardiovascular disease, damage to lung tissue and alteration in the body's defense mechanisms. High concentration of particulate matter could lead to aggravation of bronchitis, asthma and a decrease in lung function. Rainfall is an important mechanism for removing particles from the air. Particulate matters can also be reduced by combustion modifications or by trapping them using post combustion technologies [7].

N_2O is known to be a green house gas and also caused stratospheric ozone (O_3) depletion. NO_2 is a respiratory irritant which may worsen the symptoms of existing respiratory illness. Many nitrogen oxides come in the category of pollutants and would be discussed in detail in the next section.

CO is a colorless, odorless gas produced by incomplete oxidation (burning). CO is produced naturally by oxidation in the oceans and air of methane produced from organic decomposition and by wildfires. Vehicles are by far the largest human source in cities, although any combustion process may produce it. It is removed by oxidation to form carbon dioxide, absorption by some plants and micro-organisms, and rain. When inhaled, carbon monoxide binds to the oxygen-carrying site on the blood's haemoglobin,

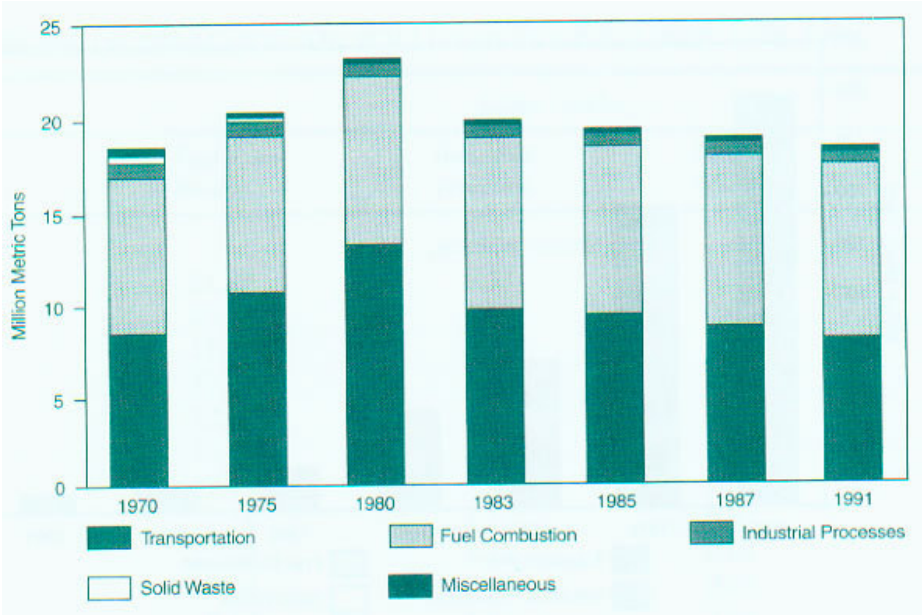

Figure 3. US emissions of NO_x by source [3].

which reduces oxygen carrying capacity of the blood. At high concentrations it is very toxic, causing nausea, dizziness, headaches and reduced ability to think.

1.2 NO_x : A harmful pollutant

There are seven nitrogen oxides known to occur: NO, NO_2, NO_3, N_2O, N_2O_3, N_2O_4 and N_2O_5 [12, 13]. The main oxides of nitrogen present in the atmosphere are nitric oxide (NO), nitrogen dioxide (NO_2) and nitrous oxide (N_2O). Amongst these, Nitric oxide (NO) and nitrogen dioxide (NO_2) are two species that are regulated [14]. N_2O occurs in much smaller quantities than the other two, but is of interest as it is a powerful greenhouse gas and thus contributes to global warming.

Figure 3 shows the relative contribution of different sources in US on a nationwide basis to the overall NO_x emissions. The major human activity which generates NO_x is fuel combustion, especially in motor vehicles. Oxides of nitrogen form in the air when fuel is burnt at high temperatures. The main sources of NO_x in the lower atmosphere are

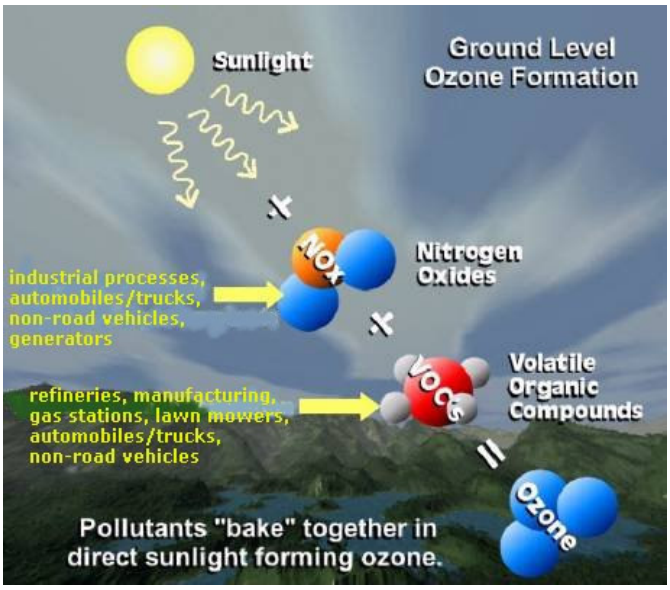

Figure 4. Formation of ozone in the atmosphere [16].

the combustion of fossil fuels and the burning of biomass including forest fires. Other sources are nitrogen fixation by lightening, volcanic activity, the oxidation of ammonia in the troposphere, and the ammonia oxidation from the decomposition of proteins [15]. NO_x is formed largely by the reaction of nitrogen and oxygen under extremely high temperature that occurs during the combustion process in internal combustion engines [16].

Figure 4 show the formation of ozone by the reaction of NO_x with unburned hydrocarbon (HC) or VOC in the presence of sunlight in the lower level of the atmosphere leading to ground level ozone [17]. The concentration of ozone depends on the amount of NO_x and hydrocarbon present in the atmosphere [16]. The formation of ozone in the upper levels of the atmosphere adsorbs the harmful ultraviolet rays from the sun, while the ground level ozone causes human respiratory problems. Ozone at ground level is one of the irritant secondary pollutants in photochemical smog and is often used as a measure of it. Ozone is strongly oxidizing and can irritate the eyes and the respiratory tract. It also damages plants. From one third to one-half of the Americans reside in areas that exceed the standard ozone levels at least once a year [3].

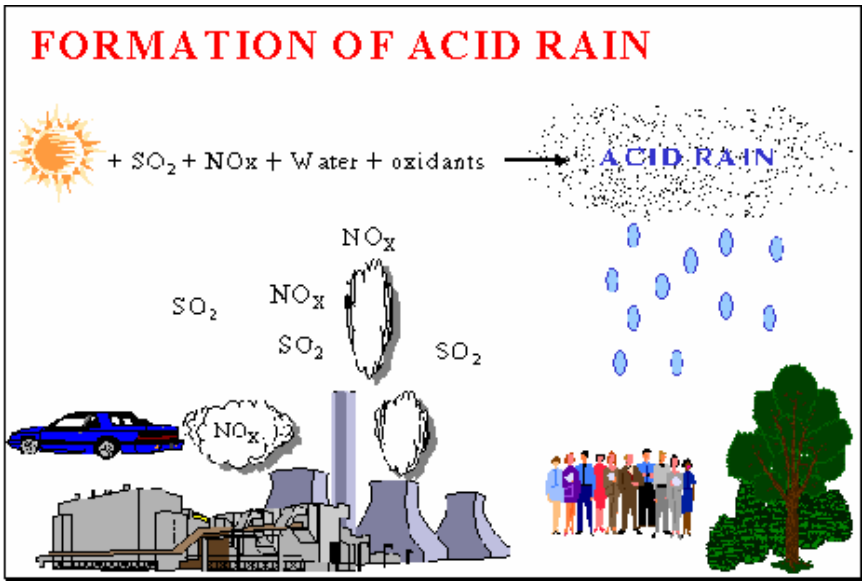

Figure 5. The formation of acid rain [18]

The oxides of nitrogen may remain in the atmosphere for several days and during this time chemical processes may generate nitric acid (HNO_3), and nitrates and nitrites as particles. These oxides of nitrogen play a major role in the chemical reactions which generate photochemical smog. HNO_3 formed due to the reaction of NO_x with water (moisture) is absorbed in the form of drops and hence contributes to the acidification of rain [19]. Figure 5 shows how SO_2 and NO_x contribute to the formation of acid rain. Acid rain causes acidification of water bodies and contributes to damage of trees and many sensitive forest soils. In addition, acid rain accelerates the decay of building materials and paints, including irreplaceable buildings, statues, and sculptures.

1.3 NO_x formation

Nitrogen is found to be inert at lower temperatures. In the case of combustion devices, high temperatures are prevalent and at temperatures higher than 1100°C, nitrogen reacts with oxygen to produce NO_x. Higher temperatures and the availability of oxygen are the two main reasons for the formation for NO_x. Strictly speaking, the formation of NO_x can be attributed to three different mechanisms namely thermal NO_x (Zeldovich mechanism), fuel NO_x and prompt NO_x (Fenimore mechanism).

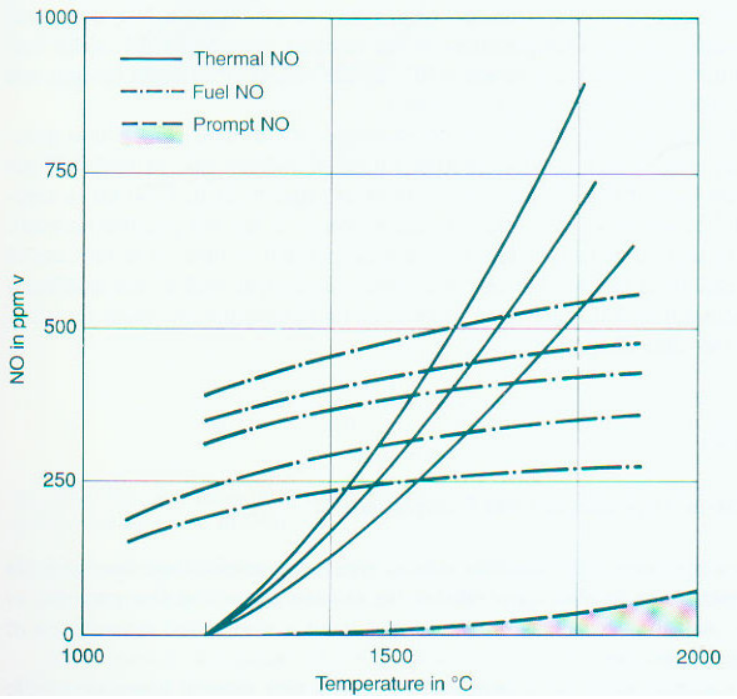

Figure 6: NO_x formation versus combustion temperature [19].

At high temperatures the nitrogen (N_2) begins to oxidize, forming NO through a number of chain reactions. Formation of thermal NO_x proposed by Zeldovich consists of two main reactions:

$$O + N_2 = NO + N \tag{1.1}$$

$$N + O_2 = NO + O \tag{1.2}$$

In case of fuel-rich flames, one additional reaction is important:

$$N + OH = NO + H \tag{1.3}$$

Figure 6 shows the temperature range for the formation of thermal NO_x. Note how the thermal NO_x is strongly dependent on temperature and increases almost exponentially with temperature rise. Temperature dependence of prompt and fuel NO_x is not much as can be seen in the figure.

The quantity of thermal NO_x formed depends primarily on the "three t's" of combustion: temperature, time, and turbulence. Thus flame temperature, the residence time at temperature, and the degree of fuel/air mixing, along with the nitrogen content of the fuel and the quantity of excess air used for combustion, determine NO_x levels in the flue gas [20]. Thermal NO_x is significant above 2,800 ^oF Adiabatic Flame Temperature (AFT) [21] and increases exponentially (about the fourth power) with the absolute temperature [22].

Fuel NO_x is formed due to the oxidation of the chemically bound nitrogen to the fuel. Fossil fuels such as coal and coke consist of a number of chemicals, which can also contain nitrogen. Fuel NO_x is independent of the temperature of the flame at normal combustion temperatures and is also insensitive to the nature of the organic nitrogen compound [15].

According to Fenimore [23], prompt NO_x on the other hand, is rapidly produced during the combustion process in the flame zone long before there would be time for the formation of thermal NO_x. The formation of prompt NO_x has a weak temperature difference and a short lifetime of several microseconds [15]. In hydrocarbon flames of fuel rich conditions, hydrocarbons react with N_2 to form amines or cyanides. These compounds are then converted to intermediate compounds like NCO, and NH which are in turn converted to NO.

1.4 US and European emission laws and regulations

In the following section, current as well as future US and European regulations pertaining to NO_x emissions will be discussed to show the change in the regulation trends with time as the environmental pressure of pollutants gets more severe every year. As an example, the pollution laws dealing with heavy duty engines will be discussed as they would provide a general picture of the need to making the laws stricter and hence necessitating better emission control technologies.

The first major national legislation that was passed in the US was the Air Pollution Control Act in 1955. The passing of Clean Air Act (CAA) in 1963, along with

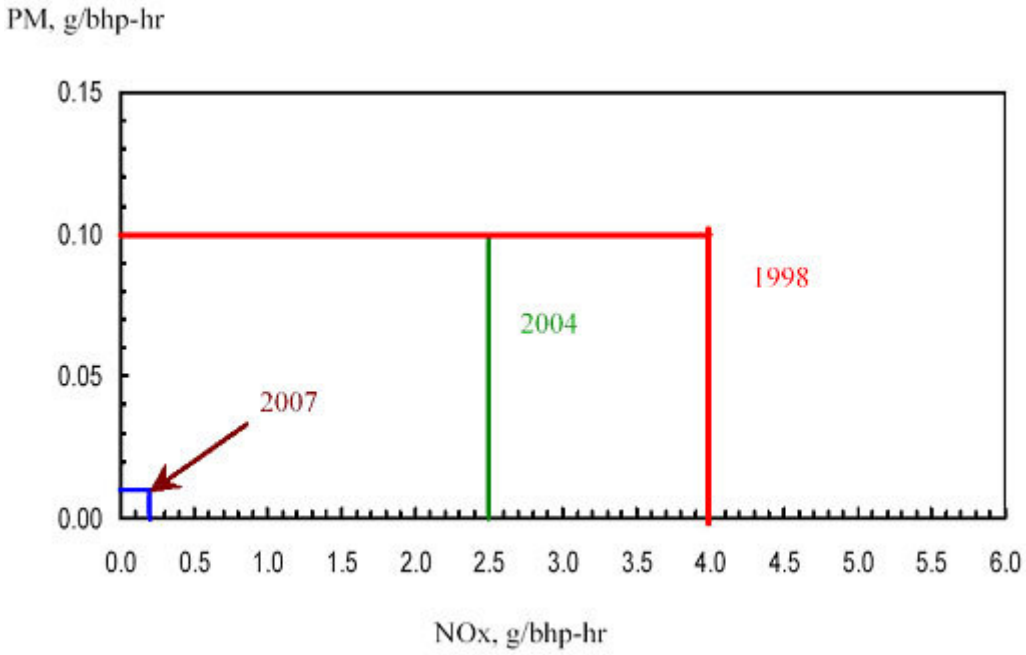

Figure 7. US heavy duty diesel emission standards over time [25].

the establishment of the US Environmental Protection Agency (EPA) and CAA Amendments in the 1970's led to the introduction of the National Ambient Air Quality Standard (NAAQS). The amendments made to the CAA between 1970 and 1975 served as a basis for the new source performance standards (NSPS) which apply to both new and modified stationary sources. In 1977, CAA was once again amended with the addition of two additional programs: the non-attainment (NA) program and the prevention of significant deterioration (PSD) program [24]. These two programs aimed at achieving the previously established ambient air quality standards for the air quality control regions. While the NA program was applicable regions that were unable to meet the ambient air quality standards, the PSD program was designed to preserve the air quality in regions doing better than the national standards.

Figure 7 shows the US emission standards for NO_x emissions versus PM. It can be clearly seen that emission regulation aim for achieving a tradeoff between the NO_x and PM. In general, there is a clear trend towards achieving lower emission standards in the future, which would go as low as 0.01 g/bhp-hr for PM and 0.20 g/bhp-hr for NO_x in

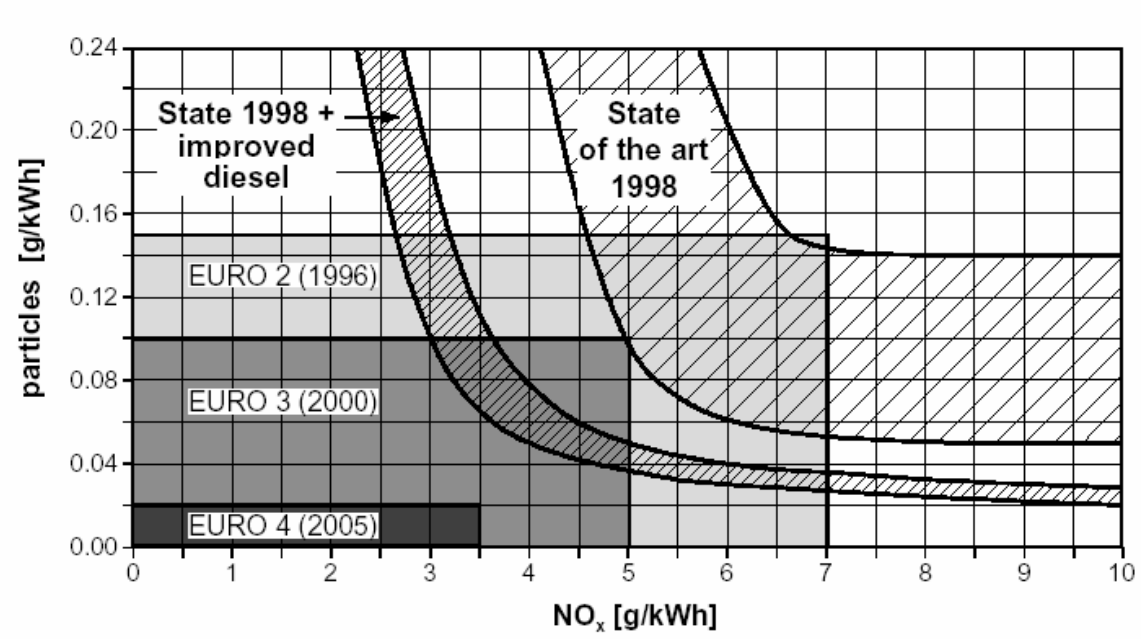

Figure 8. NO_x and PM tradeoff for heavy duty trucks and prospected EURO emission standards [27].

the year 2007 [26]. In US, the emission levels can vary appreciably from one region or state to another hence it is imperitive that the regulations for the NO_x emissions be changed with geographical location, and with the varieties and variances of the combustion sources. Owing to the noxious effects of NO_x as discussed in the previous sections, the regulatory standards to be introduced in the years to come would enforce stringent limits on emission from both stationary and mobile sources.

A number of directives were passed in the EU, pertaining to different emissions and a variety of combustion sources. In the member states of EU, the passed directives were required to be converted into national laws or regulations within a certain period of time and they could also contain requirements pertaining specifically to a particular state concerned or requirements which were more stringent than the original directive [19]. Figure 8 gives an insight of the European regulations for NO_x and PM. It shows the large gap between feasible raw emissions of heavy-duty diesel engines and forthcoming emission standards [27].

1.5 NO_x emissions control and abatement techniques

With the advent of new technology and more fuel burning devices, the quality of air is deteriorating day by day. As the quest for greater efficiency and power continues,

Reduction of the flame temperature	Avoidance of local oxygen deficit	Slow combustion
■ delayed injection timing ■ exhaust gas recirculation (EGR) ■ water-fuel mixture injection ■ combustion air cooling	■ central trough-shaped combustion zone ■ central injection ■ reduction of the ignition delay ■ increase of cetane number ■ control of the combustion air temperature	■ prolonged injection ■ control of the injected fuel ■ smaller dose diameter ■ use of common rail system ■ increase of cetane number

Figure 9. Primary measures for NO_x emission reduction [29].

serious effort in pursuit of curbing the environmental pollution must go hand in hand. New regulatory norms being introduced strive for checking the pollution limits and hence the need for NO_x control technologies arises in order to meet the stringent emission standards.

The NO_x emission control techniques can be broadly classified as pre-combustion and post-combustion methods [28]. Pre-combustion techniques include primary measures or combustion modifications and Figure 9 gives a list of all the primary measures that are adopted for NO_x emission reduction. Various combustion modifications include low NO_x burners, oxyfuel burners, reburning, burner NO_x tuning, eliminating nitrogen-bearing fuels, eliminating air pre-heat, flue gas recirculation, water injection and lime/reagent injection. With the introduction of stringent emission regulations, pri-

mary abatement techniques cannot meet the requirements alone making it imperative to look for post-combustion techniques. Post combustion modifications involve SCR (low-temp), SNCR (high-temp), Wet scrubbers/neutralizers, Urea-Water Injection, Ammonia injection, Methanol, lime and caustic injection. A common feature of SCR and SNCR processes is that they occur within a particular temperature range and the temperature range is different for each of the processes. Each of the processes listed above has its own advantages and shortcomings.

1.6 Selective Catalytic Reduction (SCR) of NO_x

One of the most effective and widely used post combustion technologies to tackle NO_x is Selective Catalytic Reduction (SCR) of NO_x. It is called 'Selective' because it does not reduces the excess oxygen which is typical to a lean exhaust in a diesel engine. SCR technology was first developed in Japan in the 1970s and employed in fossil fuel power plants all over the major Japanese cities [30]. It involves mixing the exhaust air with a gaseous reagent, typically ammonia or urea, and passing the homogenous mixture over a bed of catalyst which causes the reaction to undergo completion at the air stream temperature. The NH_3 selectively reacts with the NO_x component in the gas stream without reacting with the O_2 available in large excess [31]. The catalyst promotes the reduction of NO_x with NH_3 in the presence of O_2 in the exhaust stream, forming nitrogen (N_2) and water (H_2O). The SCR process makes use of various types of catalysts, mostly in the form of oxides of metals such as titanium, vanadium or molybdenum, impregnated onto a metallic or ceramic substrate. The present study is based on the SCR of NO_x with a commercially available vanadia-based catalyst, V_2O_5-WO_3/TiO_2 commonly known as VWT. Typical operating temperatures for an SCR application ranges from 200-500^oC [11]. SCR technology accounts for more than 90-95% of the total De-NO_x flue gas treatments in Europe and Japan [32].

NH_3 as well as aqueous solutions of urea ($(NH_2)_2CO$) are the most widely used reducing agents for SCR reduction of NO_x. Urea may be considered as a NH_3 storage solid compound which is produced commercially by reacting ammonia with carbon di-

oxide. Vanadia is proven to show superior performance for the selective catalytic reduction of NO_x and hence V_2O_5-WO_3/TiO_2 has been investigated in detail. Urea SCR is presently considered as the most promising way to mitigate NO_x emissions originating from heavy duty vehicles, especially trucks [33]. Urea is an environmentally benign chemical which makes it more suitable for application to the SCR process. Some of the drawbacks of using SCR technology are (a) *Secondary NH_3 emissions (NH_3 slip),* (b) *Process control at variable flow rates,* (c) *Handling and storage of reagents,* (d) *Reaction of HCN with urea to form undesirable high molecular weight products,* (e) *High equipment and control system costs, and* (f) *catalyst deactivation due to the deposit formation.* Adoption of urea SCR over NH_3 SCR could be gaining momentum due to a number of drawbacks associated with the use of ammonia. Ammonia is corrosive and toxic in nature. It is also a primary as well as a secondary pollutant. Use of ammonia entails careful and accurate handling requiring pressure. In order to introduce NH_3 into the exhaust gas stream, accurate dosage control mechanism is required which can be expensive. Urea on the other hand is non-toxic being extensively used in agriculture as well as in the industry and it is available in a number of quality grades [34]. Urea SCR though seems to be the most plausible and safe technique also suffers from some drawbacks and challenges. It is really important to design a urea SCR system in a way to ensure that maximum NH_3 conversion takes place and that the system responds to the engine operation at different loads effectively. It has been shown that best SCR performance is obtained with gaseous ammonia, followed by ammonia solution, solid urea and finally urea solution [35]. The urea mixing problems have been found to be further aggravated if an additional precatalyst for oxidizing NO is used. HNCO emissions from urea SCR could lead to hyperreactive respiratory diseases. Other problems with the use of urea include high freezing point of aqueous urea solution and possible formation of high molecular weight compounds like cyanuric acid, biuret and melamine. In humans, urea causes redness and irritation to eyes and skin [36].

Table 1 compares the characteristics of SCR and SNCR reduction of NO_x.

Table 1. Comparison of SCR and SNCR emission control techniques [37].

Characteristic	SCR	SNCR
NO_x removal efficiency (%)	70 - 90	30 – 80
NH_3/NO molar ratio	0.4 – 1.0	0.8 – 2.5
Operating temperature (°C)	200 - 500	800 – 1100
Operating cost	Moderate	Moderate
Capital cost	High	Low
NH_3 slip (ppm)	< 5	5 – 20

1.7 Vanadium (V_2O_5)- based catalysts

Selective catalytic reduction of NO_x has been used for over 30 years for NO_x abatement from the industrial boiler flue gas and power plants. Vanadia is proven to show superior performance for the selective catalytic reduction of NO_x and hence V_2O_5-WO_3/TiO_2 has been investigated in detail. Urea SCR is presently considered as the most promising way to mitigate NO_x emissions originating from heavy duty vehicles, especially trucks [33]. The most common catalysts in commercial material today are vanadia-based catalysts [38]. The supports including alumina, silica, zirconia, and titania were commonly used for vanadia-based catalysts. Alumina has a higher specific surface area, superior mechanical strength, and is highly resistant to sintering, compared to titania [38]. However, for the SCR of NO_x with NH_3 using alumina support (Al_2O_3), SO_2 in the flue gas reacts with ammonia and then deactivates the catalytic activity [19]. It indicates that Al_2O_3 is weakly poisoned by sulfur and its compounds.

Among many metal oxide supports, TiO_2 support has been found to be highly effective for the selective catalytic reduction of NO_x with NH_3 because of its durability to sulfur compounds [39]. The sulfation of the TiO_2 supported catalyst has been found to even enhance the level of NO removal [39]. Hence, due to its high activity and durability to sulfur compounds, V_2O_5 supported on TiO_2 is well known to be the most effective and widely used commercial catalyst for the SCR processes [39].

A ternary catalyst, V_2O_5-WO_3/TiO_2, was also recently introduced. Promoters such as WO_3, SiO_2 and MoO_3 are usually added to V_2O_5/TiO_2 catalyst in order to enhance the catalyst activity [40, 41]. The promoters lead to the formation of acid sites on the surface of the catalyst, and the catalysts exhibit a higher catalytic activity than that of a single TiO_2 supported vanadium catalyst [40]. The addition of WO_3 provides some poison resistance and improves NH_3 oxidation. There are many studies to promote the activity of vanadia-based catalysts, but V_2O_5-WO_3/TiO_2 has shown a high efficiency for removal of NO_x. Performance of V_2O_5-WO_3/TiO_2 catalysts has been stated to be insufficient at low and high temperatures.

TiO_2 in the anatase form is used as high surface area carrier in order to support the active components. Vanadia is added for increasing the activity of the catalyst in the reduction of NO_x and also for the undesirable oxidation of SO_2 to SO_3. In typical SCR applications, size/volume of the catalyst is dependent on a number of parameters [30] such as (a) *catalyst activity*, (b) *exhaust gas flow*, (c) *ammonia misdistribution*, (d) *desired NO_x conversion*, (e) *accepted ammonia slip*, (f*) temperature and pressure*. Volume of the catalyst is often expressed by the term "space velocity", abbreviated as NHSV (Net Hourly Space Velocity), which expresses the number of m^3 per hour of exhaust gas that can be treated effectively by one m^3 of catalyst. It has been stated that the ternary catalyst system TiO_2-WO_3-V_2O_5 is resistant to sulfur, but at low temperatures (below 250^{o}C) temporary deactivation might take place due to the deposition of ammonium sulfates in the pores [33]. However, this deactivation can be reversed or eliminated when the catalyst again reaches higher temperatures [35]. These types of catalysts have also been found to be sensitive to compounds with alkaline properties and phosphorous.

2. LITERATURE REVIEW

In this section, previous studies on the urea-water thermal decomposition and selective catalytic reduction (SCR) of nitrogen oxides process using urea as the reducing agent over vanadia (V_2O_5)-based and oxide supported catalysts will be presented. Since the study deals with vanadia based catalysts, it would be discussed in more detail. Transient results over catalyst not based on vanadia have been shown for reference.

2.1 Urea-water decomposition

In the automotive application of the SCR process, the preferred reducing agent is urea due to toxicological and safety reasons [42]. An aqueous solution of urea (32.5 wt-% urea) is usually atomized into the hot exhaust upstream of the SCR catalyst. The thermohydrolysis of urea into ammonia and carbon dioxide precedes the SCR reaction [42].

2.1.1 Urea-water decomposition mechanism

Urea decomposition does not reach completion in the gas phase at temperatures that are prevalent during a light-duty diesel engine operation (below 300 ºC) [43]. Stradella et al. [44] studied the thermal decomposition of urea and related compounds. Their investigations were based on TGA and DSC, together with the evolved gas analysis (EGA) with the help of an FTIR spectrometer. They were able to identify biuret, ammelide and cyanuric acid as intermediate compounds but tracking of residue species and synthetic details are still lacking [45]. Schaber et al. [45] found that the urea melted at 133^{o}C and precipitates started to form prior to 225^{o}C. The first decomposition reaction is the complete evaporation of water molecules from the aqueous solution leading to solid urea:

$$(NH_2)_2CO\ (\text{aqueous}) \rightarrow (NH_2)_2CO\ (\text{solid}) + x\ H_2O \qquad (2.1)$$

Melting point of urea used is 132.9°C [46]. Schaber et al. [45] studied pyrolysis of urea and found that a complete melt of urea is not achieved until 135°C. Hence solid urea would melt after the urea injector to give molten urea:

$$(NH_2)_2CO\ (solid) + heat \rightarrow (NH_2)_2CO\ (melt) \quad (2.2)$$

$$(NH_2)_2CO\ (melt) + heat \rightarrow (NH_2)_2CO\ (gas) \quad (2.3)$$

Also urea decomposition begins at around 152°C noted by vigorous gas evolution from the melt [33, 47, and 48].

$$(NH_2)_2CO\ (melt) + heat \rightarrow NH_3\ (gas) + HNCO\ (gas) \quad (2.4)$$

Schaber et al. [45] also noted that biuret is first produced at this temperature according to the reaction:

$$(NH_2)_2CO\ (melt) + HNCO\ (gas) \rightarrow (H_2N)CO(NH)CO(NH_2)(solid) \quad (2.5)$$

The next step in the process of urea decomposition is the hydrolysis of isocyanic acid (HNCO) formed to produce additional NH_3. Isocyanic acid is very stable in the gas phase, but it hydrolyzes easily with the water arising from the combustion process:

$$HNCO\ (gas) + H_2O\ (gas) \rightarrow NH_3(gas) + CO_2(gas) \quad (2.6)$$

According to Blakeman et al. [49], the above reaction takes place at temperatures around 120°C. SCR catalysts are very effective for the above reaction. The overall decomposition process is not as simple as shown above. Intermediate reactions might take place owing to the non-ideal behavior, such as incomplete decomposition of HNCO, trimerization of HNCO to form cyanuric acid as well as other reactions that reduce the overall NH_3 available for NO_x reduction [35, 50, 51, and 52].

The thermohydrolysis of urea is globally an endothermic process - the heat being provided by the hot exhaust. Kleemann et al. [36] have found that SCR catalysts are also effective in the hydrolysis of isocyanic acid (reaction 2.6). Reactions (2.2), (2.3) and (2.4) may also occur in the gas phase upstream of the catalyst, whereas the hydrolysis of the isocyanic acid (reaction 2.6) proceeds mainly on the SCR catalyst itself. Catalytic tests have shown that the reaction rates of HNCO hydrolysis are much higher than the rates of the standard SCR reaction at low to medium temperatures on usual SCR catalysts. Therefore, Kleemann et al. [36] suggested that ammonia is the effective reducing agent also when urea is used. One way to promote the thermohydrolysis of HNCO is to introduce a hydrolyzing catalyst in front of the catalyst [53, 54].

Sullivan et al. [55] studied the temperature-programmed decomposition of urea by wetting the catalyst with aqueous solution of urea and then placing in the reactor in a flow of He. They reported very low levels of HNCO and that too at low temperatures. Similar studies conducted by Koebel et al. [35] have also reported the presence of HNCO downstream of undersized Vanadia based SCR catalysts at low concentration using Vanadia-based catalysts. On the other hand FTIR data collected by Sluder et al. [43] did not reveal any HNCO downstream of the SCR monolith.

Jones et al. [56] studied temperature programmed urea decomposition by adsorbing urea on the FeZSM-5 and HZSM-5 samples and then thermally treating them at different temperatures (25^{o}C, 50^{o}C and 250^{o}C). Urea was found to decompose into ammonia (ammonium ion) and CO_2 after pretreatements at 150 and 250^{o}C. The decomposition of urea was complete after thermal treatment at 250^{o}C.No isocyanic acid was observed in the study. They also studied the reactions of urea, NO and O_2 on HZSM-5 and FeZSM-5 to try to observe the formation of N_2 which is a desired SCR product. The above experiments resulted in the formation of CO_2, NH_3 (NH_4^+), and N_2.

Koebel et al. [57] studies the thermal decomposition study of urea using high-performance liquid chromatography. They proposed that large molecules may also be formed during urea decomposition due to the secondary reactions with highly reactive isocyanic acid. Trimerization of isocyanic acid leads to the formation of cyanuric acid which is a very stable compound. Reaction with isocyanic acid with urea would lead to the formation of biuret. Other possible high molecular weight compounds include ammeline, ammelide, melam, melem and melamine. Chromatographic study conducted by Koebel et al. on the study of by-product of the urea-SCR process showed the presence of acetic acid at low engine loads (for low catalyst temperatures). Tests were conducted by injecting urea in the form of a solution in front of the catalyst connected to a variable load engine. Urea was detected at lowest catalyst temperature (230^{o}C) and at 330^{o}C. Isocyanic acid was detected at lowest catalyst temperature (230^{o}C) and could be attributed to the fact that at lower temperature greater amount of gaseous urea entered the catalyst and are decomposed there to isocyanic acid and ammonia. The hydrolysis reaction of

isocyanic acid therefore, does not take place completely. Emission of cyanuric acid was found to be low under all conditions. Overall, the emission of higher molecular mass compounds urea and cyanuric was low under all the conditions examined.

Schaber et al. [45] studied the thermal decomposition of urea between 133^{o}C and 450^{o}C. Analytical analysis of the decomposition products was achieved using TGA, HPLC, FTIR and an ammonium ion selective electrode. They proposed some additional thermal decomposition reactions apart from the ones mentioned above. They found that urea decomposition begins at 152^{o}C in the following way:

$$NH_2CONH_2(m) + \text{heat} \rightarrow NH_4\ NCO^-(m) + NH_3(g) + HCNO(g) \qquad (2.7)$$

175^{o}C marked the commencement of production of cyanuric acid and ammelide.

$$NH_2CONH_2\ (m) + HCNO\ (g) \rightarrow \text{Cyanuric acid (s)} + NH_3(g) \qquad (2.8)$$

$$NH_2CONH_2\ (m) + HCNO\ (g) \rightarrow \text{ammelide (s)} + H_2O\ (g) \qquad (2.9)$$

Decomposition of biuret into urea and HCNO is observed resulting in mass loss at 190^{o}C

$$NH_2CONHCONH_2\ (m) \rightarrow NH_2CONH_2\ (g) + HCNO\ (g) \qquad (2.10)$$

Ammeline was produced as a result of biuret decomposition but at a slower rate at 225^{o}C.

$$NH_2CONHCONH_2(m) + HCNO(g) \rightarrow \text{ammeline (s)} + 2\ H_2O(g) \qquad (2.11)$$

Melamine was also found to occur at temperature range of 325 and 350^{o}C.

$$\text{Ammeline (s)} + NH_3\ (g) \rightarrow \text{melamine (s)} + H_2O\ (g) \qquad (2.12)$$

Hence it can be seen that urea decomposition process consists of a number of re-actions which governs the gaseous products formed. During urea-water decomposition, deposit formation has been noticed and mentioned in the literature. Deposit formation has been explained in the next section. Figure 10 shows a general thermal decomposition reaction mechanism for urea. It has been derived and reproduced from Ball et al [36].

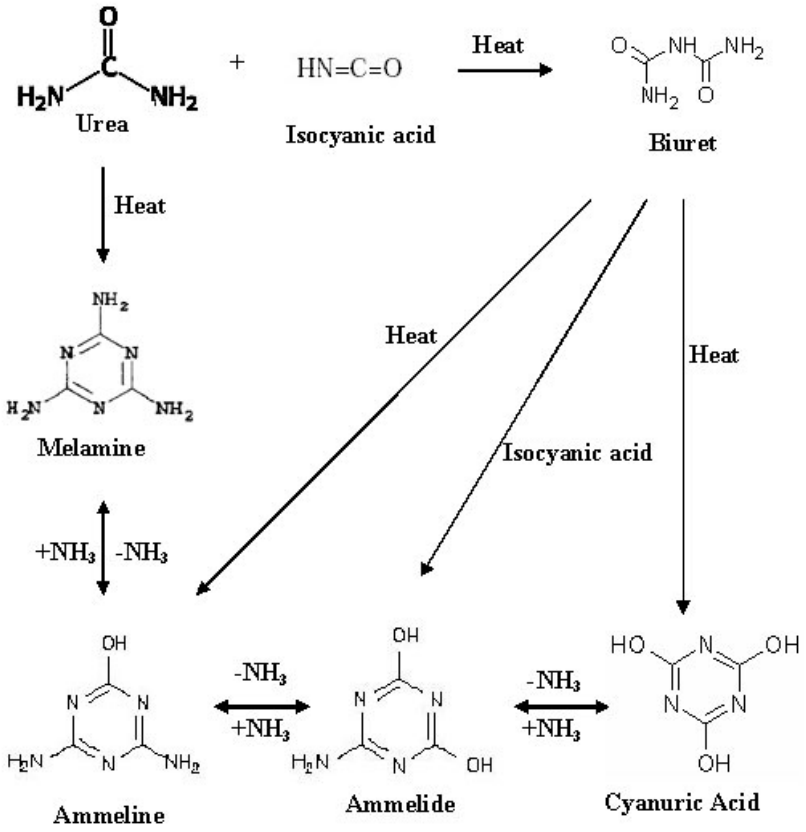

Figure 10. Decomposition products of urea (reproduced from [36]).

2.1.2 Urea-water thermal decomposition deposit analysis

Deposit formation deactivates catalytic performance by not only consuming part of ammonia produced during urea decomposition but also degrading the structural and thermal properties of the catalytic surface [47]. The formation of stable decomposition products also means that higher amount of urea would be required than the theoretical value for producing a certain amount of ammonia.

Fang et al. [47] conducted urea decomposition experiments by mixing the powdered catalyst ($V_2O_5/WO_3/TiO_2$) with urea. Their studies utilized thermal gravimetric analysis (TGA) and differential scanning calorimetry (DSC) along with spectroscopic techniques such as Diffuse Reflectance Infra-red Fourier Transform Spectroscopy (DRIFTS) and Raman in order to characterize the urea decomposition with and without

SCR catalyst. They suggested that the urea decomposition process does not take place in the simple steps as mentioned in equations (2.1 to 2.6) but can be given by the reaction:

$$(x+1)(NH_2)_2CO + H_2O \rightarrow (HNCO)_x + (x+2)NH_3 + CO_2 \qquad (2.13)$$

where $(HNCO)_x$ represents isocyanic acid for x=1, or cyanuric acid if x=3.

Their study without catalyst showed that urea thermolysis exhibits two decomposition stages, involving ammonia generation (at 250°C) and consumption (at 360°C) respectively. Decomposition occurring after the second stage leads to the production of melamine complexes, $(HNC=NH)_x(HNCO)_y$, that hinder the overall performance of the catalyst and lead to the consumption of the NH_3 formed after the first stage. They asserted that polymeric melamine complexes can be formed both with and without the catalyst and they do not undergo further decomposition (at least up to 320°C). Fang et al. also investigated the effect of moisture on urea decomposition process and found that the moisture could assist the hydrolysis of HNCO only in the temperature region below the first decomposition stage (below 250°C). The DRIFTS measurements showed that the final brown color product formed at 450°C could be a chemical complex of polymeric melamines with high molecular weights which might actually block the active sites on the catalyst surface.

Seker et al. [58] have also reported “white precipitates” but they did not discuss the chemical composition of these precipitates. Greenish-brown deposits were also found on the glass surface of the water condenser. Some deposits were found just ahead of the catalyst and were not dissolvable in water. Their composition is unknown and needs to be investigated. Urea thermolysis study conducted by Fang et al. [47] found similar solid deposits by the thermolysis of neat urea without the catalyst. The experiments conducted by Fang et al. reported a severe deposit formation along the exhaust pipe prior to the catalyst if the urea spray was not appropriately monitored. The deposit had a pale beige color at an early period of operation which changed to dark brown after a long period of heating and the morphology changed from a turbostratic structure into a relatively amorphous solid. Their study showed that urea thermolysis exhibits two decomposition stages, involving ammonia generation and consumption respectively. Decomposition occurring

after the second stage leads to the production of melamine complexes, $(HNC=NH)_x(HNCO)_y$, that hinder the overall performance of the catalyst. They asserted that polymeric melamine complexes can be formed both with and without the catalyst and they do not undergo further decomposition (at least up to 320^{o}C).

Sullivan et al. [55] studied the temperature-programmed activity of a series of oxide supported (TiO_2, Al_2O_3, and SiO_2) Cu catalysts for the selective catalytic reduction of NO_x using urea solution as a reductant. This data was compared with the data obtained from SCR reduction over the same catalysts using NH_3 in the presence of H_2O. It was found that the catalysts that were active for the selective reduction of NO_x with NH_3 were inactive for its reduction using urea solution. It was hypothesized that urea was oxidizing to form N_2 or was forming passivated layers of polymeric melamine complexes on the surface.

2.2 SCR reduction of NO_x using urea as a reducing agent

The overall process of SCR reduction of NO_x with urea can be subdivided into two steps for easy understanding: first involving urea decomposition leading to the generation of NH_3 and CO_2, and second being the reduction of NO in the exhaust by the NH_3 generated. In addition to the afore mentioned stages, urea and HNCO may take part in direct reduction of NO, as explained later.

2.2.1 SCR reduction mechanism

Several reaction pathways have been proposed and documented to explain the function of SCR systems. These have been discussed in detail in the literature [35, 49, 50, 51, and 52] and are repeated here in order to discuss the experimental results. The first pathway, which is referred to as "standard-SCR" occurs according to equation 2.14 for NO in the presence of O_2.

$$4\ NH_3 + 4\ NO + O_2 \rightarrow 4\ N_2 + 6\ H_2O \qquad (2.14)$$

This reaction is relatively a slow reaction. This reaction implies a 1:1 stoichiometry for ammonia and NO and the consumption of some oxygen. The more desired pathway is

the "fast-SCR" reaction, shown in equation 2.15 which occurs in the presence of NO_2. This pathway is much faster, but requires equal amounts of NO and NO_2 in the feed gas.

$$4\ NH_3 + 2\ NO + 2\ NO_2 \rightarrow 4\ N_2 + 6\ H_2O \quad (2.15)$$

Sluder et al. [43] found that NO_x reduction was at its peak when the NO_2/NO ratio was nearly 1, irrespective of the catalyst temperature (at least in the range from 180 – 250 ºC). The production of NO_2 in the exhaust is usually achieved by placing a strong oxidation catalyst upstream of the catalyst which produces NO_2 in the right proportion [35]. Too much of NO_2 generation is undesirable as it would result in the production of undesirable NO_2 [43]. A third pathway which is slower than either standard- or fast-SCR reduces NO_2, and is shown in equation 1.19.

$$8\ NH_3 + 6\ NO_2 \rightarrow 7\ N_2 + 12\ H_2O \quad (2.16)$$

It has been reported that when the NO_2: NO ratio exceeds 1, N_2O formation tends to take place at high temperatures (>400^{o}C) [52, 35]. N_2O formation pathways have also been reported when NO_2 content exceeds the NO content in the feed gas [52]. These pathways are particularly important for intermediate operational temperatures that are prevalent in case light duty applications. These pathways are shown in equations 2.17 and 2.18.

$$6\ NH_3 + 8\ NO_2 \rightarrow 7\ N_2O + 9\ H_2O \quad (2.17)$$

$$4\ NH_3 + 4\ NO_2 + O_2 \rightarrow 4\ N_2O + 6\ H_2O \quad (2.18)$$

Thus, when the NO_2/NO ratio is higher than unity, NH_3 may react with the excess NO_2 leading to the formation of N_2O. While the SCR process takes place on the catalyst surface, the urea decomposition process takes place both prior to and on the surface of the catalyst. At high temperatures N_2O can be formed in the incomplete reduction of NO with ammonia:

$$4\ NH_3 + 4\ NO + 3\ O_2 \rightarrow 4\ N_2O + 6\ H_2O \quad (2.19)$$

At even higher catalyst temperatures, the catalyst tends to lose its reducing property and facilitates the oxidation of ammonia to NO. The selective catalytic oxidation of ammonia (SCO) to N_2 becomes increasingly important at high temperatures.

$$4NH_3 + 5O_2 \rightarrow 4NO + 6H_2O \quad (2.20)$$

$$4\,NH_3 + 3\,O_2 \rightarrow 2\,N_2 + 6\,H_2O \quad (2.21)$$

Although this reaction does not lead to the formation of undesired products, it is highly undesirable due to an increase in the consumption of reducing agent.

The reaction of ammonia and NO in the absence of oxygen is very slow and is definitely not relevant in lean conditions:

$$4\,NH_3 + 6\,NO \rightarrow 5\,N_2 + 6\,H_2O \quad (2.22)$$

Seker et al. [58] studied the NO_x reduction by urea over sol-gel Pt/alumina catalysts in which the NO conversion temperature is strongly dependent on O_2 and water when urea is present. In addition to the reactions above, urea and isocyanic acid alone could react with NO directly according to the reactions

$$2(NH_2)_2CO + 6NO \rightarrow N_2 + 4H_2O + 2CO_2 \quad (2.23)$$

$$4HNCO + 6NO \rightarrow 5N_2 + 2H_2O + 4CO_2 \quad (2.24)$$

Table 2 shows the SCR mechanism in the presence of Vanadia based catalyst. NH_3 is first chemisorbed at the V^{5+}=O sites (Eley-Riedel model where NH_3 reacts with NO after being adsorbed, as described by Miyamoto et al. [59]). The NO_x reduction reaction occurring over these sites causes the V^{5+}=O sites to get reduced to V^{4+}-OH. The

Table 2. SCR mechanism over vanadium based catalysts [47].

Reduction of vanadia surface by the activation of NH_3 :

$$V^{5+} = O + NH_3 \rightarrow HO - V^{4+}...N^{\bullet}H_2$$

$$HO - V^{4+}...N^{\bullet}H_2 + {}^{\bullet}NO \rightarrow HO - V^{4+}...(NH_2) - NO$$

$$HO - V^{4+}...(NH_2) - NO \rightarrow HO - V^{4+} + N_2 + H_2O$$

Re – oxidation of the surface by NO_2 radicals :

$$OH - V^{4+} + {}^{\bullet}NO_2 \rightarrow V^{5+} = O + HNO_2$$

Adsorbed NH_3 neutralized by HNO_2

$$HNO_2 + NH_3 \rightarrow [NH_4NO_2] \rightarrow N_2 + 2H_2O$$

loss of catalyst surface leads to deterioration of the catalyst activity which needs to be replenished by adding oxidizing agents such as NO_2 or SO_2 [60]. The table shows how re-oxidation of the surface takes place with the addition of NO_2.

All the reactions from the literature review have been summed up in Table 3 for easy reference. Some of the reactions which are undesirable should be tried to be minimized as much as possible. The reactions which are desirable have been arranged in an increasing order of fastness.

Table 3. Urea-SCR reactions (undesirable/desirable) [47, 33].

Direct urea reduction :

$$2(NH_2)_2CO + 6NO \rightarrow 5N_2 + 2CO_2 + 4H_2O$$

Desirable reduction (In the increasing order of degree of fastness) :

$$4NH_3 + 6NO \rightarrow 5N_2 + 6H_2O$$

$$4NH_3 + 3NO_2 \rightarrow \tfrac{7}{2}N_2 + 6H_2O$$

$$4NH_3 + 4NO + O_2 \rightarrow 4N_2 + 6H_2O \quad \text{standard SCR}$$

$$4NH_3 + 2NO_2 + 2NO \rightarrow 4N_2 + 6H_2O \quad \text{fast SCR}$$

$$4NH_3 + 4NO + 3O_2 \rightarrow 4N_2O + 6H_2O \quad \text{Temp.} > 400^{\circ}\text{C}$$

$$2HNCO + 6NO \rightarrow 5N_2 + 2H_2O + 4CO_2 \quad \text{degree of fastness not known}$$

Undesirable reaction/oxidation :

$$6NH_3 + 8NO_2 \rightarrow 7N_2O + 9H_2O$$

$$4NH_3 + 4NO_2 + O_2 \rightarrow 4N_2O + 6H_2O$$

$$2NH_3 + 8NO \rightarrow 5N_2O + 3H_2O$$

$$4NH_3 + 4NO + 3O_2 \rightarrow 4N_2O + 6H_2O$$

$$4NH_3 + 4O_2 \rightarrow 2N_2O + 6H_2O$$

$$4NH_3 + 3O_2 \rightarrow 2N_2 + 6H_2O$$

$$4NH_3 + 7O_2 \rightarrow 4NO_2 + 6H_2O$$

$$4NH_3 + 5O_2 \rightarrow 4NO + 6H_2O \quad \text{high temperature}$$

Undesirable degradation :

$$2NH_3 + SO_2 + \tfrac{1}{2}O_2 + H_2O \rightarrow (NH_4)_2SO_4$$

$$NH_3 + SO_2 + \tfrac{1}{2}O_2 + H_2O \rightarrow NH_4(HSO_4)$$

$$(NH_2)_2CO \rightarrow \quad \text{polymeric compounds}$$

$$2NH_3 + 2NO_2 \rightarrow NH_4NO_3 + N_2 + H_2O$$

$$HNCO + 3NH_3 \rightarrow \quad \text{melamine } (C_3N_6H_6)_z$$

2.2.2 Effect of reaction temperature

Figure 11 shows a comparison in the SCR reduction performance between NH_3 with H_2O and with urea for different catalysts [55]. The activity of all the catalysts was found to be much lower than the equivalent reactivity using NH_3 as a reducing agent. The presence of H_2O had no severe effect on the SCR performance, and it just pushed the required temperature up for the TiO_2-supported catalysts and improved the catalytic activity for Al_2O_3 and SiO_2-supported materials.

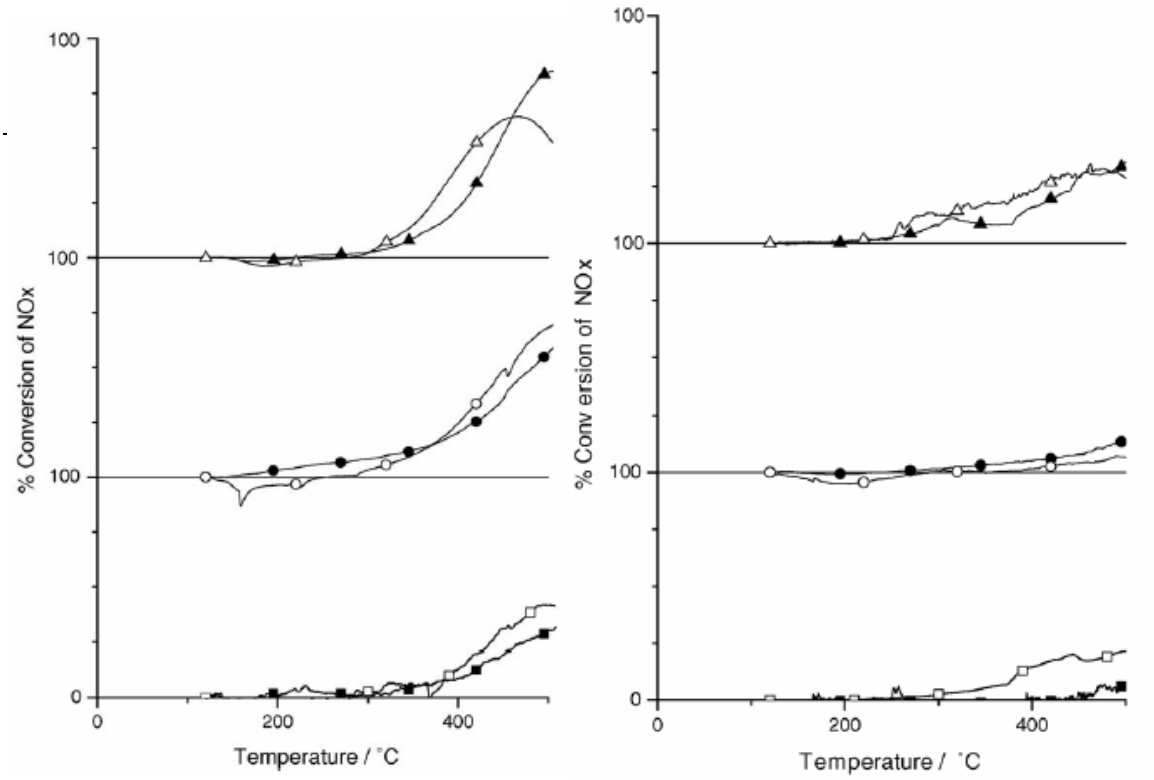

Figure 11. Comparison of NO_x reduction efficiencies for various catalysts in case of SCR-NH_3 reaction in presence of H_2O (left) and in case of SCR-urea reaction (right). Cu/SiO_2(□,■); Cu/Al_2O_3 (○,●); Cu/TiO_2 (Δ,▲). Open symbols ex-NO_3^-, filled symbols ex-SO_4^- [55].

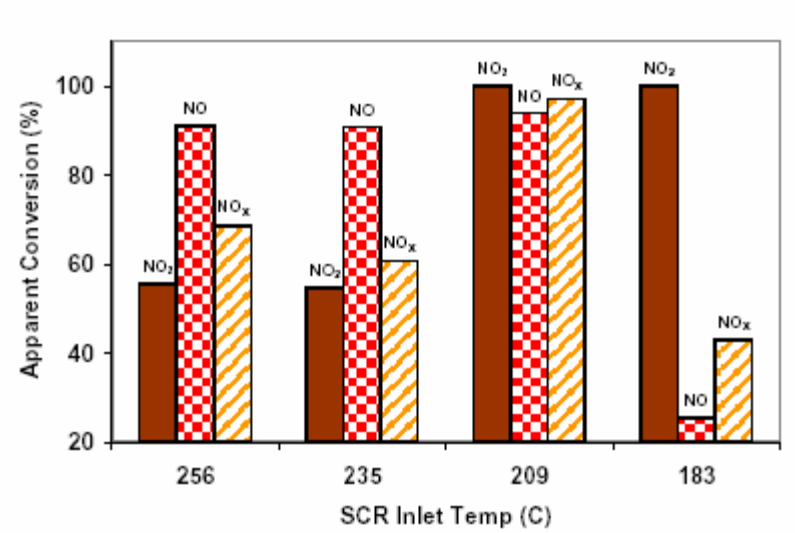

Figure 12. NO and NO_2 conversion results for the 76-mm long SCR monolith [43].

Sluder et al. [43] studied the apparent conversion efficiency for NO and NO_2 using urea solution. Figure 12 shows that NO conversion is preferred over NO_2 at higher temperatures, with this preference being reversed at temperatures below 200°C. They found out that conversion efficiency for a species that was of a lower concentration was higher than the one in greater concentration at a given temperature. Hence fast SCR reaction was predominant for temperatures above 200°C where NO_2 was present at a greater concentration.

2.2.3 Effect of urea concentration (β Ratio)

Koebel et al. [33] conducted SCR reduction of NO_x using a laboratory scale reactor with synthetic exhaust gas and applied experiments on a diesel test stand. Figure 13 shows the NH_3 and HNCO slip for various reducing agents that were investigated. Reducing agent with the minimum NH_3 slip would be favorable. It was found that best performance was obtained by gaseous ammonia, followed by ammonia solution, solid urea and finally urea solution.

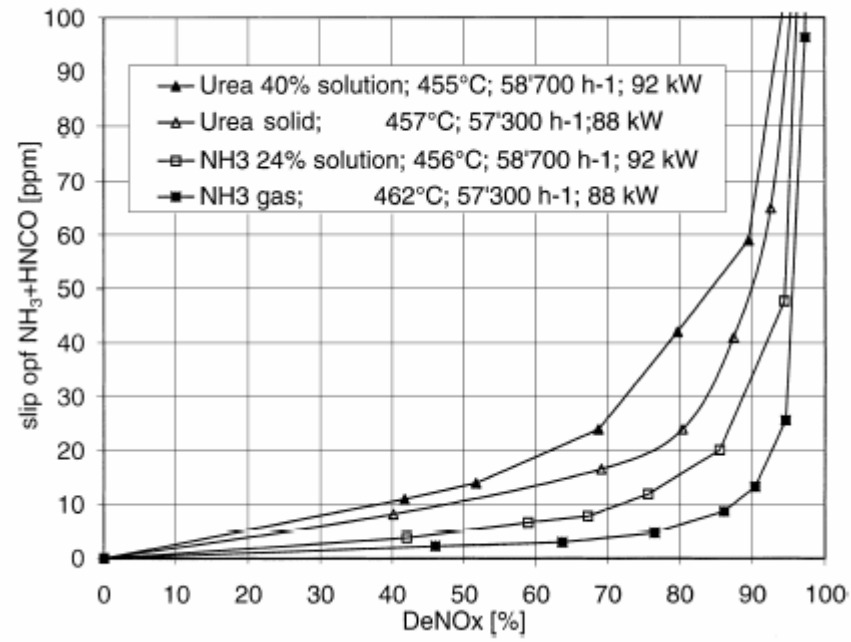

Figure 13. Performance of catalyst K53 on the diesel test stand with various reducing agents at 460°C [33].

2.2.4 HCN and N_2O and production

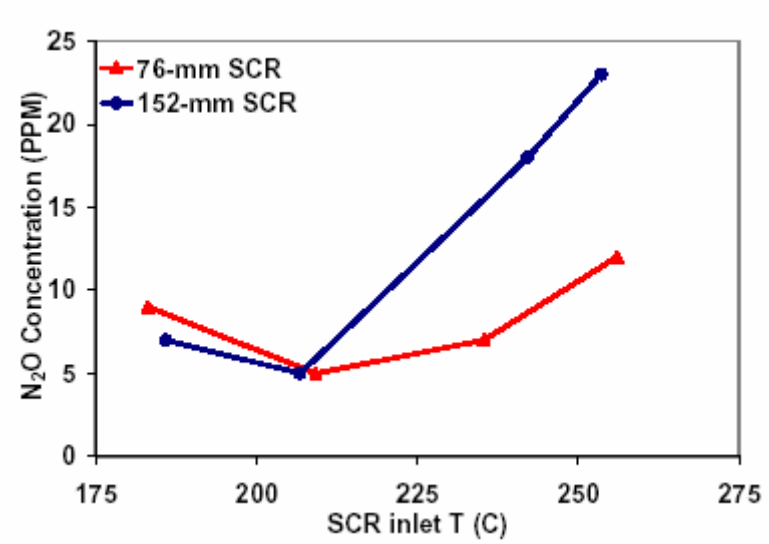

Figure 14. N_2O concentration for SCR reduction of NO_x using urea-water solution for two catalyst lengths [43].

Sluder et al. [43] studied the apparent conversion efficiency for NO and NO_2 using urea solution as shown in figure 14. Studies of urea-SCR systems to date have shown that N_2O production is likely if the NO_2/NO ratio is too high. N_2O was formed in significant quantities for temperatures above 200°C. Longer SCR catalyst was found to produce nearly double the amount of N_2O as compared to the shorter catalyst of almost half the volume [43].

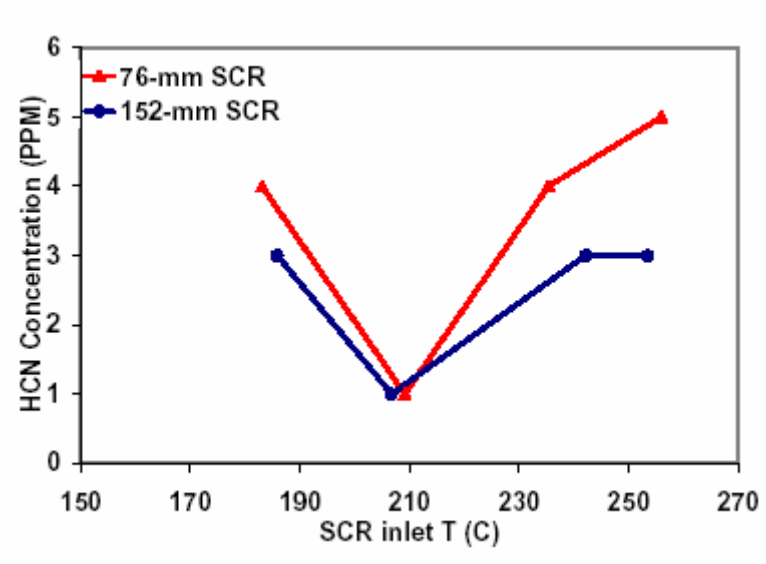

Figure 15. HCN emission profiles for SCR reduction of NO using urea-water solution for two different catalyst lengths [43].

HCN formation was also found to take place for both the catalyst samples that were investigated. Figure 15 gives the results for HCN formation from the study of Sluder et al. [43]. HCN formation was found to decrease with temperatures from 180°C to 210°C. For temperatures higher than 210°C, HCN was found to occur at higher concentration.

2.2.5 Transient results

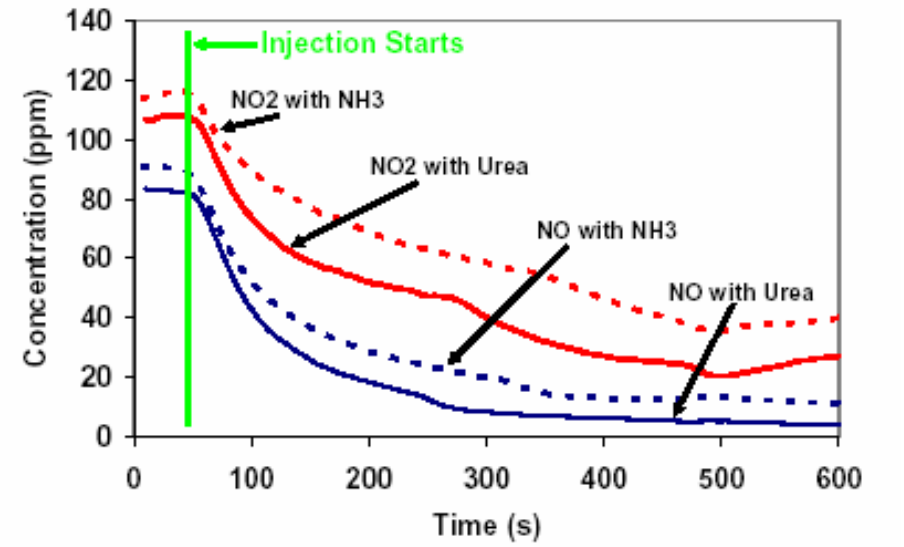

Figure 16. Transient experiments showing post-SCR NO and NO_2 profiles with time (205°C inlet temperature).

Sluder et al. conducted SCR experiments on a Mercedes Benz 1.7 L turbo-charged, direct-injection compression ignition engine (OM668). An oxidation catalyst was mounted upstream of the SCR catalyst and urea injector port was located before the SCR catalyst but after the oxidation catalyst. The SCR catalyst was a zeolites formation that did not contain Vanadia.

The data shown in Figure 16 were taken using the 76-mm long SCR monolith at an inlet temperature of 205 ºC. Urea and NH_3 were both injected at stoichiometric rates. The two curves with NH_3 injection are very similar to their counterparts with urea injection. The small offset in both NO and NO_2 prior to injection accounts for much of the difference between the two curves. Note the transient behavior of the catalyst when urea was used. Both NO_2 and NO concentrations took time to stabilize and overcome to transient state.

3. OBJECTIVES

The overall goal of the current research project is to investigate the urea-water decomposition products and selective catalytic reduction (SCR) of NO by ammonia over vanadia-based (V_2O_5-WO_3/TiO_2) catalyst. Typical vanadia-tungsta-titania catalysts show their optimum SCR performance in the temperature range of 300-400°C. On the other hand, the automotive application of the SCR process calls for a high NO_x removal over a much wider temperature range (150-550°C). The scope of this thesis was to investigate the possibilities of widening the temperature window of the SCR reaction (127-477^{o}C) in order to adapt the process to the applications with mobile diesel engines.

The first part of the work is to investigate the urea-water thermal decomposition products and the SCR of NO_x of nitric oxide (NO) with urea (NH_2CONH_2) over V_2O_5-WO_3/TiO_2 catalyst using a laboratory laminar-flow reactor. It would involve development of an effective and reliable urea injection system for the continuous addition of urea into the exhaust gas stream. The main focus will be to develop an effective urea injection system capable of operating continuously. The system would be flexible enough to govern the urea injection flow rate easily. This temperature-controlled decomposition study will be conducted with a number of O_2 gas compositions (0, 1, 10 and 15%).

The second part of this work is to study the SCR reduction of NO_x over V_2O_5-WO_3/TiO_2 catalyst for a number of oxygen concentrations (1, 0.5, 1 and 3%) and different reactor temperatures. The urea-water injector would be used to generate ammonia indirectly from the thermal decomposition of the aqueous solution which would in turn react with NO_x over the surface of the catalyst to bring about the NO_x reduction process.

4. EXPERIMENTAL SYSTEMS AND DESCRIPTIONS

For the current study of selective catalytic reduction (SCR) of NO_x by urea-water injection, exhaust gases are simulated by combining pure gases in laboratory facilities, rather than using actual exhaust from a combustion device. This ensures a clean study in a controlled environment with the help of FTIR, free from as much particulate matter as possible. Figure 17 shows the experimental setup, which composed of seven distinct units: (1) a simulated exhaust gas source unit, (2) flow control unit consisting of mass flow controllers (MFC), (3) urea-water injector unit, (4) temperature controlled furnace and reactor unit containing a catalyst sample in the reaction zone, (5) water condenser unit for collecting the water after the reactor and before the FTIR, (6) filtration unit for filtering out undesirable particles from the gas stream, and (7) output gas measurement and analysis unit comprising of the Fourier transform infrared spectrometer. Each of these systems is described in the following section.

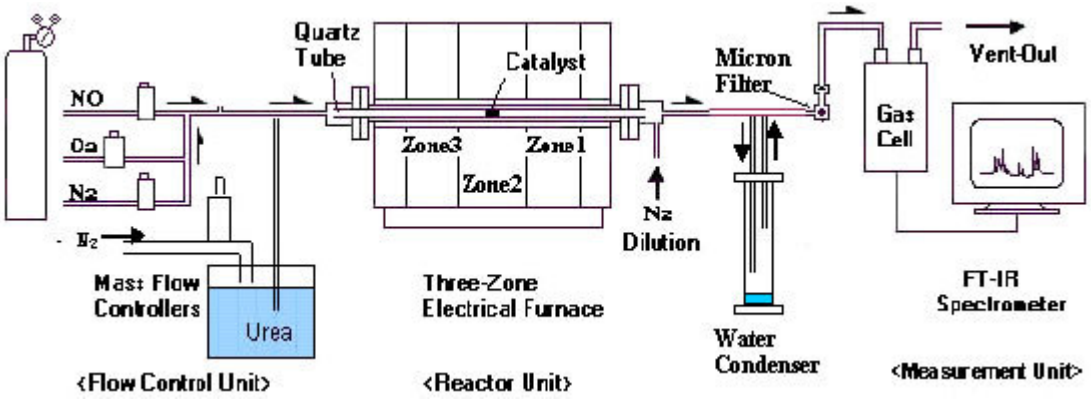

Figure 17. Schematic diagram of the experimental apparatus used to perform NO_x removal study.

4.1 Overview of the experimental setup

The main components of the experimental setup have been mentioned before. Figure 17 is a schematic of the experimental system. All of the experiments utilized simulated exhaust gas mixture as opposed to the actual exhaust gases from a combustion device. The gases were stored in standard gas cylinders up to a pressure of 2000 psi. The mass flow controllers were calibrated individually with various gases (NO, O_2, CO_2, N_2O, and N_2) and had accuracies ± 1.0% of full scale. MFC calibration has been described in more detail in Appendix A. The urea-water solution was placed in a glass reservoir and with the help of a calibrated pressure control gauge was pressurized using N_2 gas. Due to the pressure of N_2 gas, urea solution flowed out of the reservoir and then flowed through the small injection capillary tube. Urea injector calibration has been described in great detail in Appendix B. Also the corresponding water injection flow rate calculations have been described in Appendix C.

Upon exit from the capillary tube, the solution was vaporized with the help of a heating tape wrapped around a metal pipe concentric with the capillary tube and then injected into the simulated exhaust gas stream in the pre-heat section before entering the reactor unit. The mixture entered the reactor inside the furnace and the temperature of the reactor was varied from 127^{o}C to 477^{o}C in steps of 50^{o}C. The total flow rate of the entering gas was 1100 sccm (standard cubic centimeter per minute at 0°C and 1 atm). Care was taken to accommodate volume occupied by the NH_3 and CO_2 originating from the urea-water solution and subtracting it from the total flow rate to get the correct amount of balance N_2 required. This has been explained with great detail in Appendix D. In order to avoid too much H_2O in the gas mixture, the feeding rate of the urea solution was set to have less than 5% of H_2O in all gas mixtures. A quartz tube (ID=20 mm, length=1.04 m) was placed in a three-zone reactor that has an electronic control unit to furnish accurate temperature control. The catalyst sample was placed inside the quartz tube approximately at its center. The gas exiting the reactor was diluted with 5000 sccm of N_2 in order to minimize any further secondary reactions and to decrease the temperature to a level amenable to the gas analyzer. A condenser for H_2O was placed right after

the end of reactor to minimize the H_2O going into the gas cell of the FTIR (Fourier transform infrared) spectrometer. The output gas from the condenser was allowed to pass through two filters of 140 and 60 µm size. The output gas along with the dilution N_2 gas was then allowed to flow into the gas cell of the FTIR spectrometer. Necessary calibrations were done beforehand in order to quantify the FTIR spectrum for each species, prior to the main experiments. The gases were finally vented out to the atmosphere.

4.2 Source of simulated exhaust gas

The gases were stored in standard gas cylinders up to a pressure of 2000 psi. The pressure was regulated to about 40 psi prior to the mass flow controllers (MFC). Figure 18 shows the pressurized gas cylinders which were used to simulate the exhaust gases and pressure regulators which were used for regulating the pressure after the gas cylinder before the MFCs.

Figure 18. High pressure gas cylinders to simulate combustion exhaust gases (NO, NH_3, N_2)

Standard Teflon tubes were used to transport the gases to the Mass flow controllers after the pressure regulators of each pressurized gas cylinder. A simulated stream of combustion gases was mixed at atmospheric pressure after proper monitoring of their mass flow rate with the help of mass flow controller (MFC). The gas compositions were chosen based upon actual exhaust gas configurations for practical combustion. A source of simulated exhaust gas was used in order to avoid any inherent complexities of dealing with the exhaust gas from actual combustion sources, such as particulate emissions, transient irregularities in NO concentrations or excess sulfur content in the exhaust which may deactivate the catalyst being used. Each species was stored in the standard gas cylinder at pressures up to 2000 psi (pound per square inch). The concentrations of each gas species in the standard gas cylinder are listed in table 4. 1.04% NO in N_2, 100% N_2 and 48.91% O_2 in N_2, were used for this work. The pressure of the simulated gas stream was reduced down to 40 psi by standard gas regulators before being regulated by the flow controllers. NO, balance N_2, and O_2 (if used) were mixed first to form the simulated exhaust gas stream, and aqueous urea solution was then injected into this simulated exhaust gas stream before entering the reactor system.

Table 4. Compositions of gas species in the gas cylinders used for experiments at STP (273.15 K and 1 atm).

Pure Gas/ Balance	Compositions in the cylinder	Purity	Supplier
NO/N_2	1.04% NO and 98.96% N_2	± 1%	Scott Specialty Gases, Inc.
O_2/N_2	48.91% O_2 and 51.09% N_2	± 1%	Scott Specialty Gases, Inc.
N_2	100 % N_2	99.99%	BOTCO

4.3 Mass flow controllers (MFC)

As a means of controlling the flow of each constituent of the simulated exhaust gas into the experimental system, four mass flow controllers were used (two of the PFD 401 series by Precision Flow Devices, Inc., and two of the MKS type 1179A by MKS Instruments).Each mass flow controller was calibrated exclusively for a particular gas specie (NO/ O_2 / N_2) and could monitor their flow with ± 1% full-scale accuracy.

Table 5 shows the list of mass flow controllers that were used, MFC manufacturers, their maximum flow capacity (sccm) and list of the gas species for which they had been used and calibrated. MFC #1-4 and #2-4 were used for dilution N_2 of 5000 sccm and balance N_2, respectively, while MFC #1-3 was used for NO. O_2 was governed with the help of MFC # 2-2. It should be noted that the flow capacity of each MFC is in the unit of sccm (standard cubic centimeters per minute), where standard conditions were at T = 0^oC and pressure P = 1 atm as defined previously. The maximum flow capacities for the four MFCs were 200 sccm for MFC #1-3, 5000 sccm for MFC #1-4, 300 sccm for MFC # 2-2 and 1000 sccm for MFC #2-4.

Table 5. Mass flow controllers used for the experimental system.

MFC #	Manufacturer	Serial Number	Maximum flow capacity (sccm)	Gas used
1-3	MKS Instruments	4012772	200	NO/N_2
1-4	MKS Instruments	4012767	5000	N_2 (Dilution)
2-2	Precision Flow Devices	4012770	300	O_2/N_2
2-4	Precision Flow Devices	4012768	1000	N_2 (Balance)

Figure 19. Mass flow meters for regulating the gas flow rates in ppm.

Figure 19 gives a snapshot of the MFC's that were used for the gas flow measurements and regulation prior to the reactor. Each MFC was connected to the respective

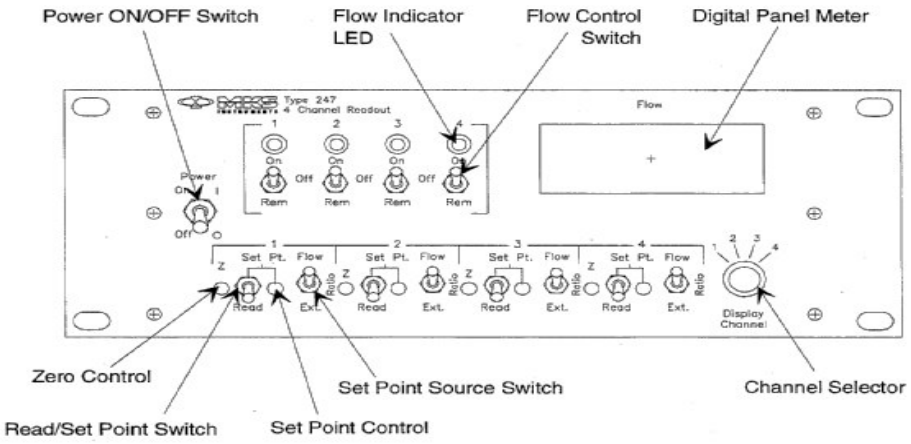

Figure 20. Front panel controls for MKS type 247D four-channel readout [61].

gas cylinder pertaining to the gas specie it was calibrated for. Figure 20 presents a diagram of the front panel controls of the MKS type 247D four-channel power supply/readout that connected to the MKS type mass flow controllers [61]. To set the desirable concentration of each species, the respective MFC was selected using the channel selector, read/set point switch was then lifted up and then revolved the set point control. The MFC control system only works after a sufficient warm up period to provide stability. After the warm up period, sufficient pressure was built up before the MFCs for the respective gas species. The power supply was used to set the switch in the center to the 'Set' position for the controller that was desired to be used. Then the controller was set to 00.0% flow rate (of the maximum flow rate) by turning the switch to read 00.0% on the screen. The controller switch was then brought to the 'Servo' position. After this, the power supply was set to 'Read' position in order to measure the flow rate values from the panel. If the flow rate registered on the screen was anything other than '00.0', the controller was adjusted to zero which is also known as the 'zero correction'. A precision screw driver was used in order to bring the potentiometer into a position where the power supply part showed '00.0'. Once the system was adjusted for zero correction, it was ready to be used. Since the MFC #2-4 was used to balance all other constituents in the simulated exhaust gas stream by N_2, which usually occupied a major fraction in the exhaust gases, the standard total flow rates of simulated exhaust gases including the reducing agent was set to be 1100 sccm. This was kept constant for any compositions of simulated mixture over the entire experimental sets.

4.3.1 MFC calibration process

Prior to the experiments, all the MFCs were calibrated with the corresponding gas species with the help of water displacement method. The details of the calibration method, the results of the MFC calibrations and the calibration procedure have been explained in Appendix A. The gas flowing through the experimental system was collected in a glass flask. Initially, the glass flask was completely filled with water, and held in an inverted position in a tub full of water. The water inside the flask was displaced by the

gas over time in ambient conditions of temperature and pressure [62]. The time and displacement volume were measured, and the volume flow rate ($\dot{\forall}$) was obtained through the following equations [52]:

$$\dot{\forall} = \frac{\Delta \forall}{\Delta t} \equiv \frac{M_1 - M_2}{\rho_{H2O} \cdot t} \tag{4.1}$$

where M_1 and M_2 are weights of water at the beginning and the end.

In order to accommodate the pressure difference from the changing water level in the glass flask during the displacement process, a correction term for the volume is required [62]:

$$\frac{\Delta \forall_{adjusted}}{\Delta t} = \left(\frac{P_0 - \rho_{H2O} \cdot gh}{P_0} \right) \left(\frac{T_0}{T} \right) \left(\frac{M_1 - M_2}{\rho_{H2O} \cdot t} \right) \tag{4.2}$$

The calibration procedures are described in more detail in Appendix A.

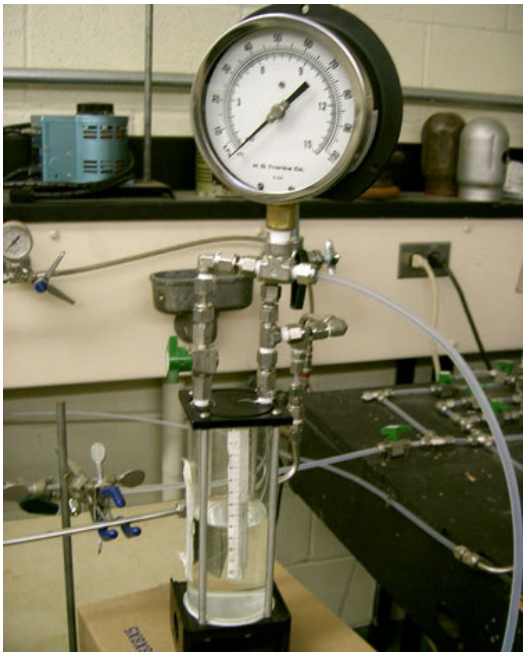

Figure 21: Pressure driven urea injector designed for injecting aqueous urea solution into the gas stream.

4.4 Urea-water injector

Pressure-driven injection of urea-water solution was achieved with the designed urea-water injector, which injected the required quantity of the aqueous solution into the gas stream after vaporizing it completely. Figure 21 shows the designed urea-water injector. Pressurized N_2 gas was used to inject urea-water solution into the gas stream after heating the solution prior to the reactor. The pressure gauge on top of the injector was used to calibrate the injection and to measure the pressure of the gas required for achieving a desired injection rate. A specific amount of urea was dissolved in water (as explained earlier) depending upon the concentration of NH_3 that was required to be achieved in order to reduce a given amount of NO (ppm). The amount of urea dissolved would theoretically result in 330 ppm of NH_3 production after thermal decomposition. The feed rate of the solution was 0.06 ml/min. This was necessary to ensure that the concentration of H_2O in the exhaust gas stream mixture was as minimal as possible.

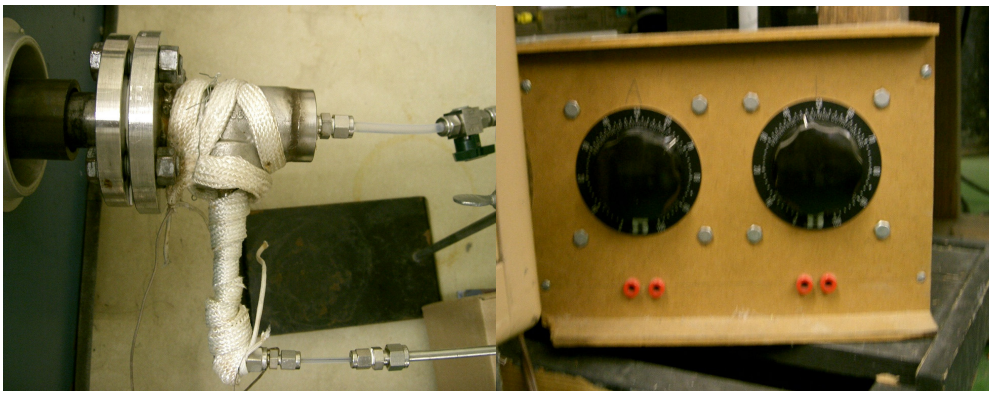

Figure 22. Picture of the heating zone (left) for the injector and the temperature controller (right) for the heating tape used.

Figure 22 (left) shows the inlet line before the reactor with a heating zone to heat the aqueous urea-water solution prior to mixing with the gas stream. The heating was done with the help of a heating tape. The picture on the right in Figure 22 (right) shows the temperature controller that was used for heating the heating tape up to a desired temperature. Figure 23 shows the initial injector design that was proposed but failed to operate effectively. It was proposed to have a capillary tube (27 gauge) run through a metal tube which was totally covered with a heating tape.

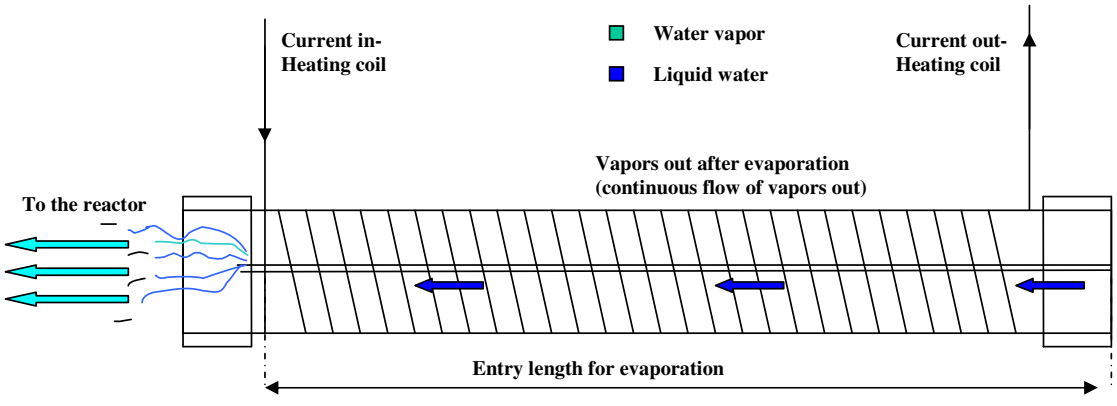

Figure 23. Initial proposed design for the urea-water injector

The urea-water solution would then flow through the capillary tube and by the time it would come out of the tube, it would be completely evaporated (vapor form) by the heat convected by the outer metallic tube to the capillary. However, it was observed that the flow of urea-water solution eventually stopped after a while. This could be attributed to the phenomenon of vapor lock which might have taken place due to a two-phase flow taking place inside the capillary tube. The vapor lock eventually stopped or choked the system resulting in no flow through the tube. Hence the injector had to be redesigned.

Figure 24 shows the new design which was incorporated and how the vapors were generated using the modified injector design. The new design was effective and was able to produce continuous flow of vapors after the injector which were allowed to mix with the simulated exhaust gases before entering the reactor. The modified injector design did not have a problem of vapor lock even at high temperatures of the heating tape. A small capillary tube (27 gauge - 0.007 inch diameter) was used to transport urea-water solution inside a concentric metal tube. At the end of the loop on the left, heating tape was wound around the outer metal tube in order to heat the solution immediately as

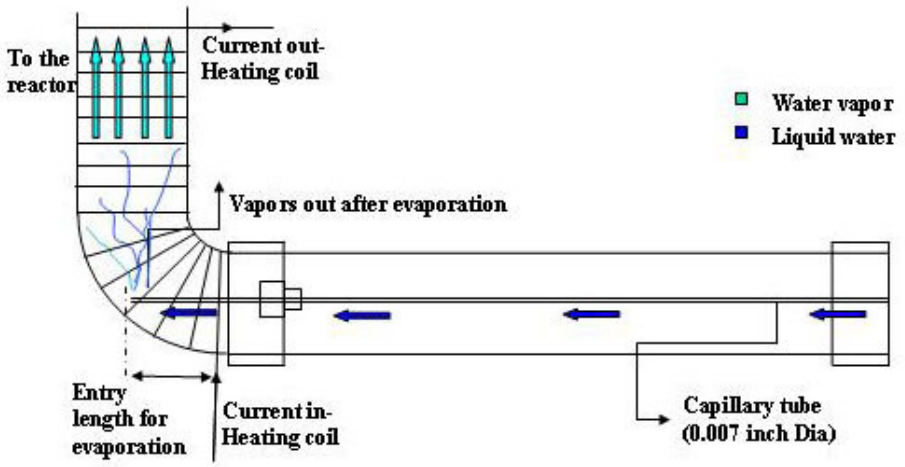

Figure 24. Final urea-water injector design for achieving complete vapors after the injector outlet.

it came out of the capillary tube. The temperature of the heating tape was high enough to ensure complete vaporization of the aqueous solution. Typically the temperature of the heating tape was maintained at around 160^{o}C in order to make sure that urea completely melted after the injector and was able to generate ammonia upon thermal decomposition. In order to ensure complete vaporization of water and also that the urea melts completely, the heating tape temperature was well above the melting point of urea. The vapors mixed completely with the simulated gas stream and entered the temperature controlled reactor unit. The mass flow meters along with the urea-water injector were so adjusted so as to produce 1100 sccm (standard cubic centimeter per minute at 0°C and 1 atm) of total gas flow.

4.4.1 Injector calibration process

The pressure regulator which was used to regulate the pressure of N_2 gas used for injection controlled the urea-solution feeding rate. Using the pressure regulator, which has range 0 to 15 psi, made possible of controlling low feeding rate. Using the pressure regulator, outlet pressure of regulator set from 4 psi to 0.05 psi. Setting 1 psi as the pressure regulator resulted in 0.053ml/min. After flowing through an injection pipette, before entering the reactor, urea-water solution should be vaporized. A metal tube (length = 1 feet) was injected between the injection capillary and the heating tape, and the heating tape provided the solution evaporation. The heating tape was set to the desired temperature with the help of the temperature controller described before so that complete melting of urea and its vaporization could take place prior to the entry into the reactor.

4.4.2 Urea-water solution preparation

The urea used in the series of experiments was obtained from OmniPur, E. M. Industries (99.5% pure). The distilled water used in the aqueous solution preparation was acquired from OmniSolv, E. M. Industries (extra pure). A urea-water solution with 7.67 grams of urea per liter was prepared such that it resulted in 165 ppm of urea inside the reactor. Table B-2 of Appendix B gives details regarding the calculations were done us-

ing Excel spreadsheet for the amount of urea required to be dissolved into the right amount of distilled water. While making the solution, care was taken so that no foreign matter or particles got into it which might flow through the small capillary tube being used and ultimately block the flow of urea-water solution through it. It was also ensured that no urea was left undissolved which might lead to the same problem mentioned above.

4.5 Reactor unit

Figure 25 shows the flow reactor which was used to supply energy to heat the flowing gas mixture with the catalyst in place. Reactor unit comprises of a furnace used to supply heat to the exhaust gases and the flow reactor. The flow reactor equipped inside the furnace consists of two parts: a stainless steel pipe assembly and a quartz tube that is concentrically aligned in the steel pipe. Zone 2 specified in the figure was used to place the catalyst in the middle of the quartz tube. The simulated gas mixture flowing through the reactor was heated to reach the desired temperatures by a three-zone furnace

Figure 25. Picture of the furnace and reactor assembly used to heat the catalyst.

(Lindberg model number 54259), which has an electronic control unit (Lindberg model number 58475). Flow of simulated exhaust gases took place from right to left in the figure shown and zone 3 was the first one to come in contact with the gases, followed by zone 2 and then zone 1 on the left. This section provides information on the configurations of the reactor part and the placement of the catalyst inside the flow reactor zone.

4.5.1 The furnace and reactor assembly (reaction zone)

Figure 26 represents the schematic of the three-zone furnace system. It shows the placement of the three reactor zones along with their individual lengths in inches. The initial and final heating zones of the furnace are 5.9 inches (15.2 cm) each long while the center zone is 11.81 inches (30.5 cm) in length. The energy produced by the heating zones is transferred to an Inconel 600 steel pipe throughout the entire length of the furnace. The quartz-tube, which prevents catalytic reactions with the steel surface, is centrally located within the steel pipe. The reactor (represented by dotted lines in the figure) is 25.4 mm internal diameter tube of Inconel 600 which is 1.06 m long.

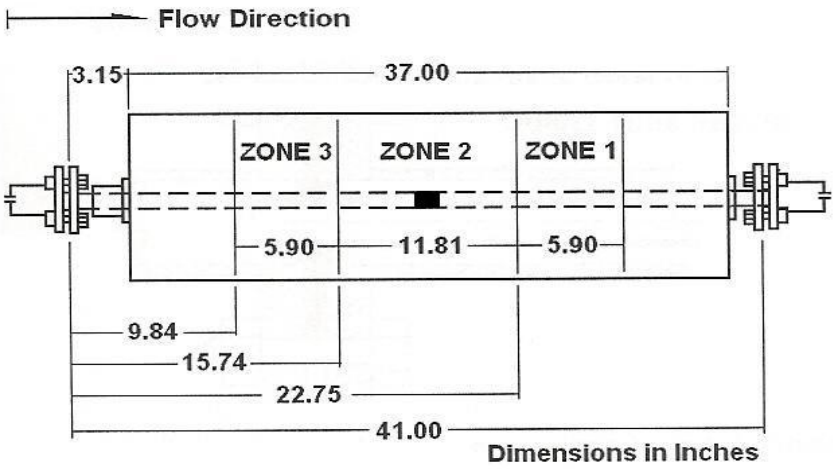

Figure 26. Schematic of the temperature controlled furnace and reactor system. All lengths in inches [63].

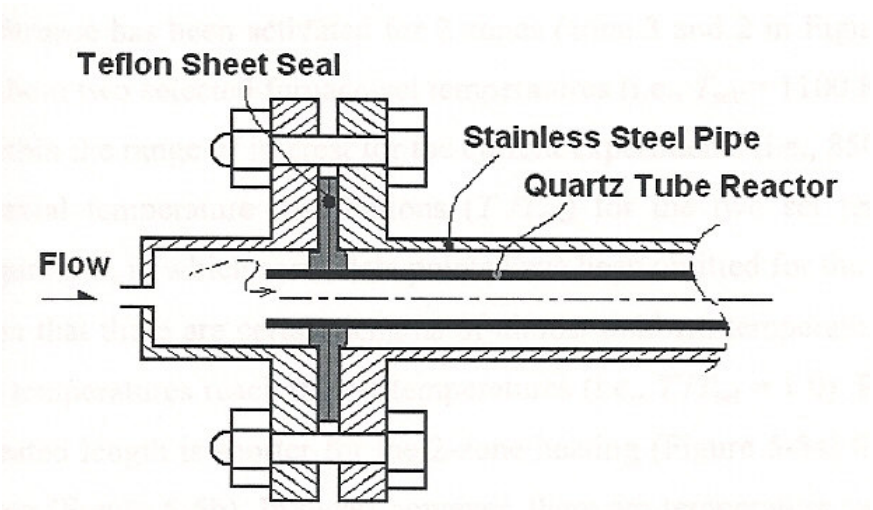

Figure 27. Teflon-sheet sealing between quartz-tube and steel tube [9].

The catalyst was placed near the center of the quartz-tube along the length where is in the middle of heating zone 2. In order to settle and secure the catalyst sample in one place in the quartz-tube, a "dent" on the inside surface of the quartz-tube was made in the middle of heating zone 2. The dent is too small to change any conditions of the experiments but was sufficient enough to hold the catalyst in place at any desired orientation.

The steel pipe is threaded at both ends, and two 4.5 inches (11.43 cm) bolt flanges of 304 stainless steel are screwed on the ends as shown in Figure 27 [9]. The quartz-tube is located in the center of the reactor with the support of graphite Teflon gaskets made from Grafoil^{TM} sheets. The Teflon gaskets were cut in annular shape with outer diameter greater than that of the steel pipe and the internal diameter slightly smaller than that of the quartz-tube. The Teflon gaskets are used to seal the flanges on each end of the reactor.

4.5.2 Reactor temperature control and distribution

The electric control unit shown in Figure 28 was coupled with the furnace and is a 58475 model Eurotherm electronic control unit capable of attaining temperatures of up to 1371^{o}C.

Figure 28. Electronic temperature control unit for the furnace.

The desired temperature of the furnace was set with the help of the electronic control unit readout at the bottom of each individual zone temperature panel. In the middle of each zone panel, the unit showed the temperature of that zone in ^{o}C. It took around 17 minutes for the reactor to attain a stable desired temperature. More details on the temperature increase of the furnace have been provided in the next section.

The temperature distribution inside the reactor was measured prior to the actual experiments. This was done with the help of thermocouple (OMEGA® Type K) at the flow conditions which were similar to the normal experimental conditions. The temperature distribution in the furnace is described in more detail in Appendix E. By opening the outlet side of the reactor and allowing 1100 sccm of N_2 through a quartz tube of 2 cm internal diameter, the data for gas temperature were taken at increments of 4-6 cm from the outlet side of the reactor. Temperature analysis was done along the entire length of the quartz tube along the center (from upstream to downstream). Data for the gas temperatures was measured after allowing ample time for the steady state conditions over the whole reactor length.

4.5.3 Flow regime

In order to consider an internal flow through a circular tube (or pipe), it is necessary to find whether the flow is laminar or turbulent for this work. The flow through the quartz tube has an entry length were the flow is developing and after sometime the flow is fully developed. Hence it is imperative to define the region (fully developed region) where the internal flow can be defined. In fully-developed region in a circular tube, the velocity profile has a parabolic distribution as shown in Figure 29 [9]. To determine laminar flow or turbulent flow, the Reynolds number must be obtained. Mean velocity is used to calculate the Reynolds number according to the formula given below:

$$\mathrm{Re} = \frac{\rho VD}{\mu} = \frac{VD}{\nu} \tag{4.3}$$

where ρ is the fluid density (kg/m^3), μ is the dynamic viscosity (kg/sec·m), ν is kinematic viscosity (m^2/sec), V is the mean velocity of fluid, and D is the internal diameter of the quartz-tube (or pipe). In general, the Reynolds number for a laminar flow less than 2300 [64].

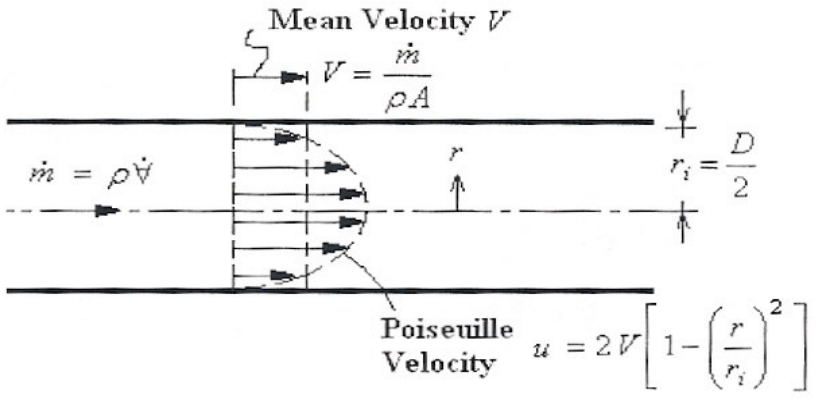

Figure 29. Fully-developed laminar flow regime and velocity distribution in a circular tube [9].

Considering a gas mixture flowing through a quartz-tube of cross-sectional area (A), the mass flow rate can be given by

$$\dot{m} = \int_A (\rho u)\, dA = \rho A V \tag{4.4}$$

where u is the flow velocity at a particular location.

The mean velocity V in the above equation can be obtained from the knowledge of the volume flow rate $\dot{\forall}$ and the cross-sectional area A by

$$V = \frac{\dot{m}}{\rho A} = \frac{\dot{\forall}}{A} \tag{4.5}$$

The initial volume flow rate ($\dot{\forall}_0$) in the reactor is 1100 sccm at atmospheric pressure (P = P_0) and ambient temperature (T_0 = 25°C) in these experiments. The volume flow rate which is dependent on temperature can be related to the standard flow rate by

$$\dot{\forall} = \dot{\forall}_0 \left(\frac{P_0}{P}\right)\left(\frac{T}{T_0}\right) = \dot{\forall}_0 \left(\frac{T}{T_0}\right) \tag{4.6}$$

Hence the new expression for the mean velocity can be written as

$$V = \frac{\dot{\forall}_0}{A}\left(\frac{T}{T_0}\right) = \frac{4\dot{\forall}_0}{\pi D^2}\left(\frac{T}{T_0}\right) \tag{4.7}$$

Table 6. The Reynolds number at various temperatures for the current study.

Temperature (T)	Volume flow rate ($\dot{\forall}_0$) (sccm)	Diameter (D) (cm)	Kinematic viscosity (ν) of N_2 (m^2/sec)	Reynolds #
Ambient (25˚C)	1100	2.0	15.5×10^{-6}	75.29
127°C	1100	2.0	26.5×10^{-6}	44.04
477˚C	1100	2.0	74.74×10^{-6}	15.61

Therefore, the Reynolds number is

$$\mathrm{Re} = \frac{4\dot{\forall}_0}{\pi D \nu}\left(\frac{T}{T_0}\right) \tag{4.8}$$

For the current experimental investigation, the temperature varied from 127°C to 477°C, and the inner diameter of the quartz-tube was 2 cm. The thermodynamic properties of the simulated gas mixture were assumed to be those of pure nitrogen due to the high percentage of N_2 (balance) concentration in the simulated gas.

Table 6 shows the maximum and minimum Reynolds number for the current study. The maximum Reynolds number takes place at 127°C and minimum takes place at the highest temperature of 477°C. Figure 30 presents the Reynolds number as a function of the reaction temperature. Using the equation (4.8), the Reynolds numbers were calculated at constant volume flow rate and tube diameter. The Reynolds number was the greatest at 127°C and declines with an increase in the reaction temperature.

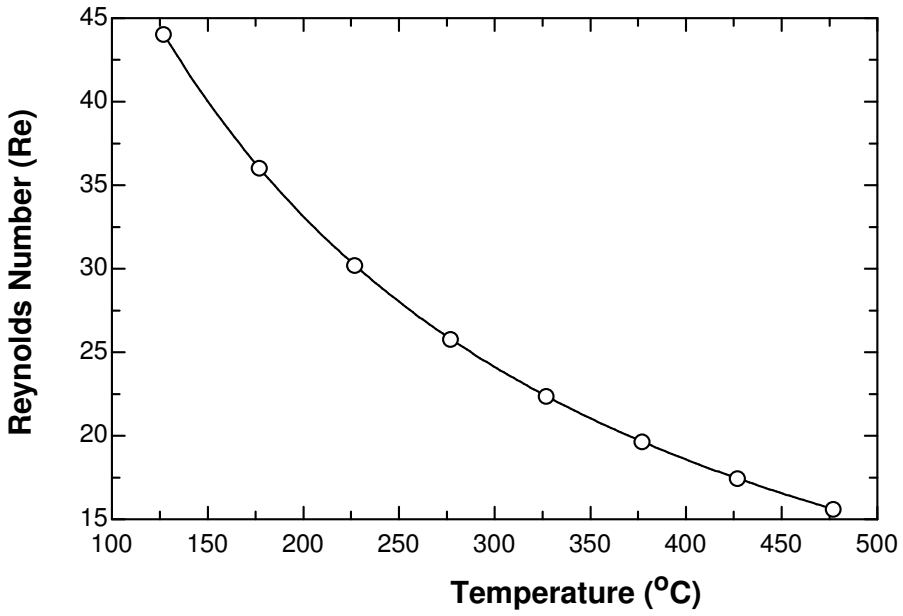

Figure 30. The flow Reynolds number as a function of the reaction temperature.

4.5.4 Catalyst sample

The experiments were performed on a vanadia-based (V_2O_5-WO_3/TiO_2) catalyst samples. Figure 31 shows the V_2O_5-WO_3/TiO_2 monolithic honeycomb catalyst sample [63]. More details about supplier and specifications for the catalyst sample are listed in Appendix F.

The catalyst sample was carefully handled because of its toxic components to inhale or swallow. Original sample from supplier was too big to be used for the current experiments. In order to obtain the desirable space velocity, the sample had to be carefully cut off to make a snug fit into the quartz-tube. Special gloves were used in order to handle and cut the sample carefully into the required size. Ordinary saw with thin blade was used to cut out two identical samples so that a new sample could be used for both the two experiments: first one on urea-water decomposition products and the second one on the SCR reduction of NO_x using urea as a reducing agent. While cutting it was noticed that the sample was hard and brittle and required careful cutting strokes from the blades of the hand-saw.

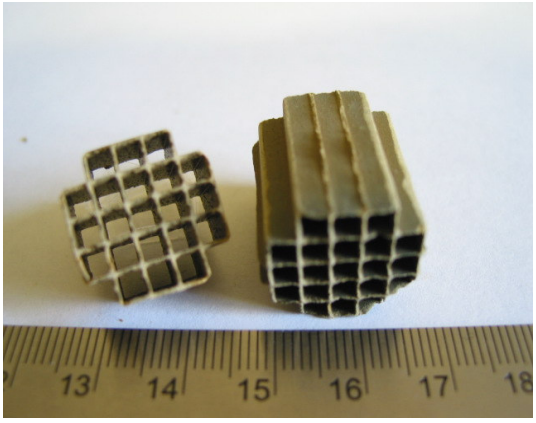

Figure 31. V_2O_5-WO_3/TiO_2 catalyst sample cut to the required size [63].

Table 7. Variation of space velocities with catalyst length.

Catalyst length (cm)	Tube Diameter (cm)	Catalyst volume (cm^3)	Space velocity (h^{-1})
1	2	3.142	21000
2 (standard)	2	6.283	10500

A 2 cm long monolithic catalyst was used for all the experimental cases. In order to minimize the 'slip' of gases past the catalyst surface it was essential to ensure that the catalyst was able to snug fit inside the quartz tube.

The space velocity is an important design parameter for chemical reactors and represents the number of reactor volumes of feed, measured at normal conditions, processed per unit of time [1]. Space velocity is defined as the ratio of the total simulated gas flow rate to the volume of the catalyst, expressed in per-hour. At a constant gas flow rate, space velocity is inversely proportional to catalyst volume so that increasing the catalyst volume corresponds to a decrease in the space velocity. The volumetric activities of two catalysts can be compared considering the conversions obtained at the same value of GHSV. Table 7 lists how the space velocities change with the length of the catalyst. A catalyst sample with the same diameter but greater axial length (2 cm) would have a lower space velocity that the one having a smaller length (1 cm). The following equation gives the relationship between the space velocity and catalyst volume used.

$$\text{Space Velocity } (h^{-1}) = \frac{\text{Total Flow Rate}}{\text{Catalyst Volume}} \tag{4.9}$$

4.6 Water condenser unit

The simulated exhaust gases got reduced over the catalyst surface and exited the reactor where they were diluted with 5000 sccm of N_2 as mentioned before. The exiting gases were at high temperature but after exiting from the reactor they were exposed to the room temperature conditions resulting in a temperature drop. The temperature drop was further enhanced due to the dilution of the gas stream by the dilution N_2 line. This would result in the shedding of moisture from the gas stream due to the cooling of the

Figure 32. Water condensing unit installed after the reactor.

gas after the reactor. Hence it was imperative to install a water condenser soon after the gas stream was allowed to exit the reactor and diluted with 5000 sccm of N_2. When the gases were made to pass though the water-collector, it collected/condensed some of the water vapor before the gas analyzer and also helped in collecting some of the particulate matter with the moisture. Reducing the moisture content prevented the pores of the filter from blockage and ensured a steady operation of the gas analyzer. Figure 32 shows the water condenser which was designed for the experimental setup.

4.7 The filtration system

A filtration system was placed after the water condenser unit and prior to the gas analyzer so as to filter out any gas impurities such as particles from the catalyst, foreign material, dust particles, or any urea particulates. This was necessary so as to make sure no particulate matter entered the FTIR which could damage the reflecting mirrors and spoil the readings. After passing through the furnace, the output gas diluted by 5000 sccm of pure N_2 passed through two tee type filters which were 140 micron (μm) and 60

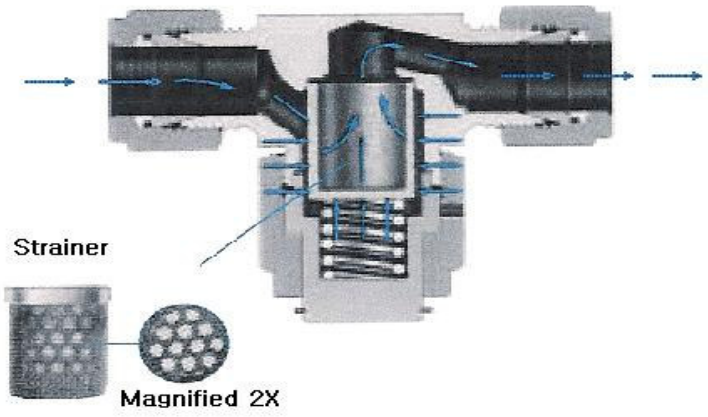

Figure 33.Sectional view of a tee type filter and a strainer [65].

micron (μm) filters in sequence as listed in table 8. The gas stream was first made to pass through the 140 micron filter and then through the 60 micron filter. The filters were maintained at room temperature and any worn out strainers of the filtration system were replaced with new ones provided by Swagelok Company [64] prior to the experiment. Figure 33 shows a schematic sectional view of the tee type filter system that was used. The strainer shown in the figure had minute pores which got clogged with time and had to be replaced. Use of a finer strain filter resulted in an increase in the back pressure which in turn resulted in an increase in the injection pressure required for the same rate of injection of the urea-water solution. Clogging of the filter pores also increased the

Table 8. Filtration systems for the current experiments.

Filter size	Body material	Part #	Type
140 micron	stainless steel	SS-4FT-140	Tee type
60 micron	stainless steel	SS-4FT-60	Tee type

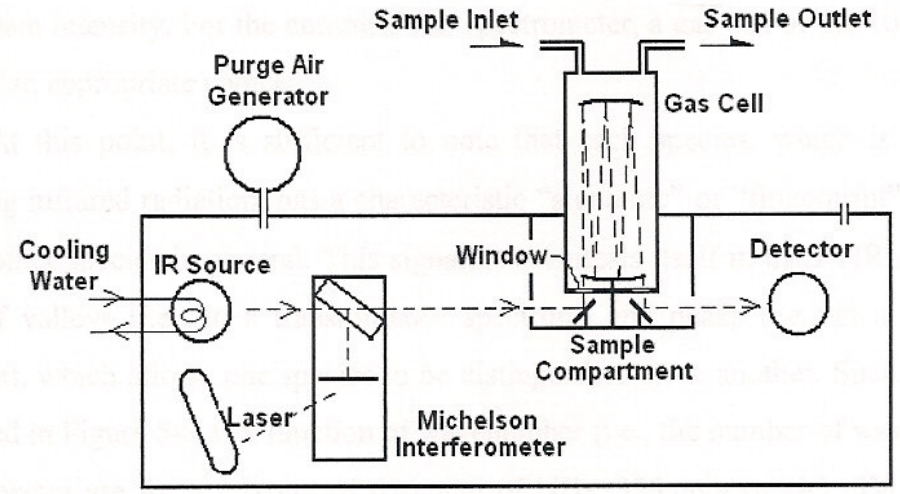

Figure 34. Schematic of FTIR spectrometer and the gas cell [9].

back pressure and it was easy to detect it with the help of the urea-injector attached to the system requiring a greater injection pressure. Table 8 gives the details about the two filters that were used including the body material, the part # and the filter type.

4.8 The gas analysis system (Fourier Transform Infrared Spectrometer)

In order to analyze the various gas species after exiting the reactor and to determine their concentration, a Fourier transform infrared (FTIR) spectrometer was used. Figure 34 shows the schematic of FTIR spectrometer, a gas cell and a purge gas generator [9]. The current Bio-Rad FTIR (FTS-60A) utilizes a software package (WIN_IR Pro) in order to collect and quantitatively analyze the data obtained from the FTIR. It is equipped with He-Ne laser and a liquid nitrogen-cooled MCT (Mercury-Cadmium-Tellurium) detector which works in the range of wavenumber of 4000 to 400 cm^{-1}. The main component of the FTIR is the Michelson interferometer, by which infrared (IR) radiation from the IR source is carefully modulated to various intensities and optical path lengths. The modulated infrared beam is then directed though the gas cell which is equipped in the sample compartment. After being absorbed (or transmitted) by the gas sample in the gas cell, the infrared beam is redirected to a detector. At the detector a

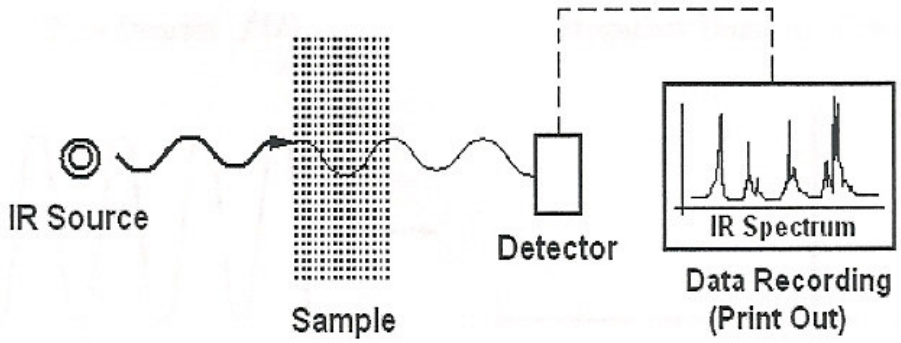

Figure 35. Simple representation of IR spectrometer [9].

continuous electrical signal (called an interferogram) is generated. The laser working near the IR source generates a reference signal which enables the spectrometer to collect the interferogram at precise intervals, generating a digital signal which is compatible with the FTS computer software. Figure 35 shows a simple system of an IR spectrometer, in which infrared radiation emitted from a source passes through a sample that absorbs the radiation. The remaining radiation which has not been absorbed by the sample is transmitted to the detector which transfers data to a data processing and recording device. Bio-Rad WinIR-pro version 2.96 software was used to collect data from FTIR for the current experiment. In order to determine the frequencies that have been absorbed by the sample, the data processing device analyzes the transmitted radiation by means of IR spectrum. To operate the FTIR spectrometer properly, three coolants were used: the liquid nitrogen, water and ambient air. Water and ambient air flowed inside FTIR all the time, and the liquid nitrogen had to be recharged daily before conducting the experiments.

The total simulated mixture gas stream of 6100 sccm after dilution entered into the cylindrical-shape gas cell (Permanently Aligned Long Path cell) as shown in figure 35. Two beam splitters of both top and bottom in the gas cell create 10 meters of optical path (which can be varied), contained in a volume of 2.3 liters and analyze the output

Figure 36: FTIR setup along with the data acquisition system.

gas compositions. The gas sample was vented out into the atmosphere after analysis into the atmosphere. Figure 36 shows the complete FTIR system along with the data acquisition system for collection of data.

Since the gas cell is made out of KBr crystal, which is sensitive to ambient air

Figure 37. Purge gas controller coupled with the FTIR.

conditions, it is necessary to use a purge gas generator is used to ensure proper air conditions. The purge gas generator is utilized to purge unwanted CO_2 and water vapor from the IR beam paths. Figure 37 shows the purge gas controller that was utilized for the experimental setup and was coupled with the FTIR throughout the experimentation.

More details about various components of FTIR spectrometer, Permanently Aligned Long Path cell, and the purge gas generator are reported by Baek [9]. Appendix G gives details on the FTIR calibration procedure which was done prior to using the FTIR for data acquisition. The calibration procedure and obtaining method of data for the different species used in the experiments for FTIR spectrometer have been described in more detail by Park [61] and Baek [9].

5. EXPERIMENTAL PROCEDURES AND OBSERVATIONS

The actual experiments for the urea-decomposition and NO_x reduction study were performed by flowing 1100 sccm (standard cubic centimeter per minute at 0°C and 1 atm) of simulated mixture in the quartz-tube, regulated by the mass flow controllers. The standard condition is consistent with former studies completed by Gupta [64] and Oh [63]. The temperature was varied from 227°C to 477°C for urea-water decomposition study and from 127°C to 477°C for SCR reduction of NO_x experiments. The following sections describe the experimental procedures, the data collection and the processing of data using example plots.

5.1 Experimental procedure

Before starting the flow of gas it was necessary to stabilize the MFC readings which fluctuated as soon as the MFCs were switched on. In order to stabilize the flow rate from the mass flow controllers, the MFCs and the four-channel power supply/readout needed to be turned on at least two hours before the experiment begins. One way to prevent the two hour delay everyday was to let the MFC turned on the entire time. This was a risky affair since all the MFCs are sensitive to power surges and lightening strikes especially on a cloudy day. Liquid nitrogen, used as a coolant for the FTIR spectrometer, was added to the MCT detector everyday prior to the run. The whole system was tested for leakage before the main experiment. This was done by turning on the valves after the MFCs and allowing the gases to flow through the system with the valve before the FTIR closed. In case of leak free system, no gas flow would be registered by the MFCs ensuring a totally sealed environment. In case the MFCs showed any readings, the water condenser, quartz tube, or pipe connections were checked for any leakage or loose connections. The three furnace zones were set to the lowest temperature to be tested and the preheating tape for the urea solution was turned on. MFC #1-4 and #2-4 which controlled the balance and dilution nitrogen were switched on and only water from the urea injector was allowed to flow in order to take a background scan with the

FTIR. Flowing water through the system would make sure that while taking sample scans least amount of base line correction would be required. The background scan must be taken for each experiment. After obtaining the background scan, the other species were flowed. While performing the experiments, catalyst was placed inside the quartz tube in the middle and the quartz tube as sealed from both the ends at the inlet and outlet of the reactor to prevent leakage of gas into the atmosphere. Also during experimentation, water inside the injector was replaced with the urea-water solution made to the concentration required. Calculations on determining the right amount of urea to be added in a given quantity of water have been shown in Appendix B.

The set points of each mass flow controller were determined using an Excel spreadsheet, which included the calibration data for each specific mass flow controller. The set points of the mass flow controllers were double-checked to ensure the flow of the correct quantities of each component in the mixture. In order to calculate the set points, care was taken to ensure that the CO_2 and NH_3 being generated by urea injection was also accommodated in calculating the balance N_2 required. During the complete running time of the experiments, the furnace remained on all the time to ensure thermal stability. The temperature of the furnace was increased by a temperature step of 50°C from the 127^{o}C to 477°C. The reason of performing the experiments by means of increasing the reactor temperature is due to the fact that it requires more time to cool down the rector than to heat it up.

After taking the last reading at 477°C, the flow of all species except N_2 was stopped. Only the balance nitrogen of 1100 sccm flowed so as to purge out the remaining gases of NO, NH_3 and O_2 in the system and the gas species that might have been absorbed by the catalyst. The heated reactor needed to cool back to the ambient temperature, which normally took about 5 hours with compressed air assistance. The slow cooling down of the reactor with the help of compressed air in an even way prevented any stress formation in the reactor or the stainless steel pipe.

Table 9. The average time to obtain the final value for each reaction temperature.

Reaction Temperature (°C)	Average time to obtain the final value (mins)
	V_2O_5-WO_3/TiO_2 sample
127	100
177	84
227	70
277	57
327	40
377	28
427	15
477	10

5.2 Procedures for data collection

During data collection at steady state, strictly speaking, all the species in the product gas for a fixed set of temperature should not vary at any time. However, the ideal situation is not expected experimentally due to minute variations of the given experimental conditions.

5.2.1 Detection of species that were calibrated

In order to process the data of a FTIR scan, Bio-Rad WinIR-pro version 2.96 software was used which allowed for the quantitative analysis of the gas species based on the calibration files. The scans of the output gas in the FTIR gas cell were taken after the steady state for both NO and NH_3 was established. For most of the species, more than one wavenumber were chosen and were calibrated. However, for some species some peaks had to be excluded during analysis (eg, interaction of NO_2 with water). To determine whether the steady state condition was reached, scans of the FTIR were repeatedly taken. The values of the last 25 scans fluctuated within the error ranges of $\pm$ 0.5 ppm were considered to be in the steady state condition. Then, the average value of the

last 25 scans was obtained, and the final value, the closest value to the average value, was determined at the reaction temperature.

The average time taken to obtain the final values for each temperature is listed in table 9. The average time is decreasing with an increase in the reaction temperature. In the beginning of the experiments at lower temperatures, it took a very long time (~ 115 mins) to reach the steady state, and the high urea concentration was responsible for that. The lowest values of the average time for V_2O_5-WO_3/TiO_2 at 400°C were corresponding to the occurrence of 100% NH_3 conversion. After collecting the final scan for every single reaction temperature, the concentration data was then plotted as a function of the reaction temperature.

5.2.2 Detection of species that were not calibrated

In order to quantify the gas species detected by the FTIR, it was necessary to calibrate the FTIR for the detected absorbance versus a known concentration of the gas species. However, it was not possible (or difficult) to calibrate some species and their detection could only be done by checking for its absorbance spectra in the data obtained. This was the case for HNCO for which absorbance spectra was checked at every temperature so as to detect its presence.

5.3 Urea injection procedure and difficulties

In the urea decomposition and the NO_x reduction experiments, the urea concentration was set to 165 ppm so that 330 ppm of NH_3 would be generated. Various factors such as urea-water mixture, pressure setting of the injector, or resolidification of urea inside the reactor could lead to experimental errors. Since the urea injection rate was small, even a slight variation due to any of the above factors could cause the readings to fluctuate a lot. Higher urea-water injection rates would also lead to higher moisture content in the FTIR making it difficult to detect some of the species which lie in the same wavenumber region as H_2O. Moisture poses a major threat as it results in the deactivation of the catalyst in the long run by plugging the pores of the

catalyst and reducing the "Effective Surface Area" over which NOx reduction takes place. The quartz tube was cleaned and compressed air was allowed to pass through it after every run. It was ensured that the pressure of the compressed air was not very high. Blowing the air through the tube served 2 purposes: (1) It helped in the removal of any residual moisture/water vapors which may deactivate the catalyst if present. (2) It helped in reducing the temperature of the heating chamber. This helped in expediting the process of cooling of the reactor so that the next set of readings could be taken starting from the lowest temperature. Regulating the moisture content in the gases is also necessary in order to ensure that FTIR works properly. Greater is the moisture content, greater effort is required for the baseline correction, which is extremely important. The 7 μm filter used initially before the FTIR was removed so as to reduce the back pressure to an accepted value. Too much back pressure required higher urea-injection pressure and also made the system too unstable. Even a minor change in injection pressure was found to affect the urea injection rate tremendously at higher injection pressures. After removing the filter 0.052 ml/min of injection rate was observed at about 0.5 psig injection pressure which gave stable urea-injection rate and was also safe for the bottle used as a reservoir of the urea-water solution.

5.4 Experimental uncertainty and error range

Though it was ensured that readings were only taken when the system had reached a steady state, performing the experiments under the exact same condition was very hard. The room temperature varied slightly (~ 3°C) all the time because of the air conditioning and the frequent opening and closing of the door. Hence though we base our calculations on the ambient air conditions of 25^{o}C, it may not be the same in actual sense. The different condition of nitrogen (N_2) in a cylinder (could occur during the recharging process of a gas) affected the background scan. Clogging of the filter pores by the deposits or foreign material could result in a change in the system backpressure which would render the urea injector calibration useless. Hence it was necessary to

check the FTIR scan to check if the results were off than the expected values by more than 50 ppm. However, during the experimental process the change of back pressure was noticed once and the strainers were replaced with new ones.

5.5 Temperature increase of the furnace

The reaction temperature of the furnace was increased by the temperature step of 50°C or 100°C from the ambient temperature (approximately 25°C) to 400°C for studying the temperature increase of the reactor furnace with temperature. Figure 38 shows the transition of the temperature of the furnace for the heating for zone 1, 2 and 3 at the

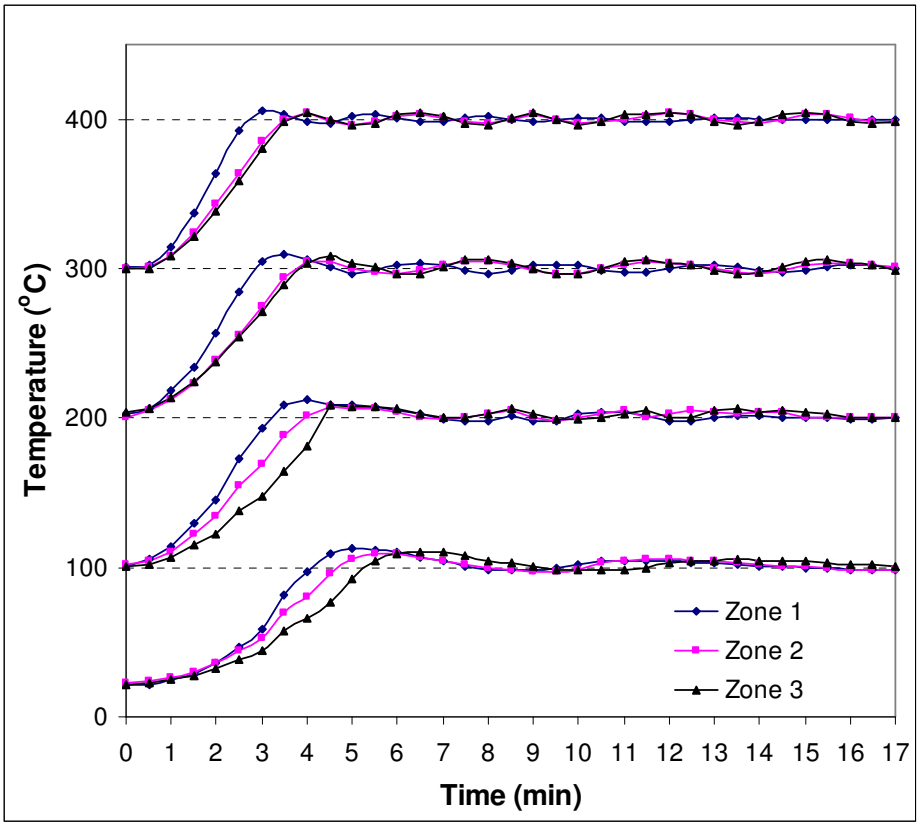

Figure 38. Temperature variation of the reactor with time for a temperature increase of 100°C from ambient.

Table 10. Temperature variation values for two cases of set temperature (100°C and 200°C)

Set Temperature 100 °C Measured Temperature				Set Temperature 200 °C Measured Temperature			
Zone 1	**Zone 2**	**Zone 3**	**Time (min)**	**Zone 1**	**Zone 2**	**Zone 3**	**Time (min)**
22	23	22	0	101	102	101	0
22	24	23	0.5	106	104	102	0.5
25	26	25	1	114	111	107	1
29	30	28	1.5	130	123	115	1.5
36	36	32	2	145	135	122	2
47	44	38	2.5	173	155	138	2.5
59	53	45	3	193	169	148	3
82	70	58	3.5	209	188	165	3.5
97	81	66	4	212	202	181	4
109	96	77	4.5	209	208	209	4.5
113	106	92	5	209	207	208	5
112	109	104	5.5	208	207	208	5.5
110	109	109	6	205	204	207	6
107	107	110	6.5	203	200	203	6.5
104	105	110	7	199	199	200	7
101	102	108	7.5	198	201	200	7.5
99	100	105	8	198	203	203	8
98	98	103	8.5	202	205	206	8.5
98	97	101	9	198	201	203	9
100	97	99	9.5	198	198	199	9.5
102	99	98	10	203	201	199	10
104	103	98	10.5	204	203	200	10.5
104	105	98	11	204	205	203	11
104	106	100	11.5	202	200	205	11.5
104	106	103	12	198	203	201	12
103	105	105	12.5	198	205	201	12.5
103	104	105	13	201	204	205	13
102	103	106	13.5	202	203	206	13.5
101	102	105	14	202	204	204	14
101	101	105	14.5	201	204	205	14.5
100	101	104	15	200	201	204	15
100	100	103	15.5	200	200	203	15.5
99	99	102	16	199	200	201	16
99	99	102	16.5	199	201	200	16.5
99	99	101	17	200	200	201	17

temperature steps of 100°C. The heating zones 1, 2 and 3 were heated simultaneously in order to produce the required reaction temperature on the catalyst. After the final values of NO and NH_3 concentrations were obtained at ambient, the temperature was increased to100°C. Five minutes later, the temperature reached 100°C and fluctuations were seen in the temperature readings which die out completely after about fifteen minutes. To get the final species values at 100°C, more than an hour is required as listed in table 10. Again, after final concentrations were obtained at 100°C, the reaction temperature was increased to 200°C. The temperature reached 200^{o}C in less than five minutes and remained constant with only slight fluctuation after 13 minutes. It was noticed that the time taken to reach the desired temperature decreased with an increase in the furnace temperature. In general, zone 1 reached the set temperature earliest followed by zone 2 and then zone 3. As mentioned earlier, all the three zones had to be heated for the experimental cases in order to prevent moisture condensation in the reactor especially on the surface of the catalyst.

5.6 NO_x conversion

The NO_x conversion ($DeNO_x$) is defined as follows:

$$DeNO_x = \frac{NO_{x,IN} - NO_{x,OUT}}{NO_{x,IN}} \times 100 \quad (5.1)$$

Strictly speaking, the definition of $DeNO_x$ should be based on the conversion of $NO_x = NO + NO_2$. Since no NO_2 was part of the simulated exhaust gas, the $DeNO_x$ definition can be solely based on the reduction of NO input to the system. The main product of the NO_x reduction is generally N_2, a high $DeNO_x$ indicating a high SCR activity of the catalyst. If the selectivity for SCR is low, the reduction of NO_x is not complete and nitrous oxide may be formed. However, the formation of nitrous oxide consumes NO, thus enhancing the $DeNO_x$. Some of the NO_2 formed as an intermediate product would also react with NH_3 in the presence of NO to lead to fast SCR process. Therefore, in the case of low SCR selectivity, a high $DeNO_x$ does not correspond to a high SCR activity of the catalyst (see chapter 7).

5.7 Stoichiometric ratio β

The stoichiometric ratio β represents the ratio between the moles of nitrogen added as reducing agent and the moles of NO_x contained in the feed. A value of β =1 means that, in case of a high selectivity for SCR, the amount of reducing agent which is added to the feed results in the total removal of NO_x. If ammonia is used as reducing agent, then β is evaluated as follows:

$$\beta = \frac{NH_{3,IN}}{NO_{x,IN}} \quad (5.2)$$

For stationary source and automotive applications, urea is used as the reducing agent. In that case β is given by:

$$\beta = \frac{2 \times urea_{IN}}{NO_{x,IN}} \quad (5.3)$$

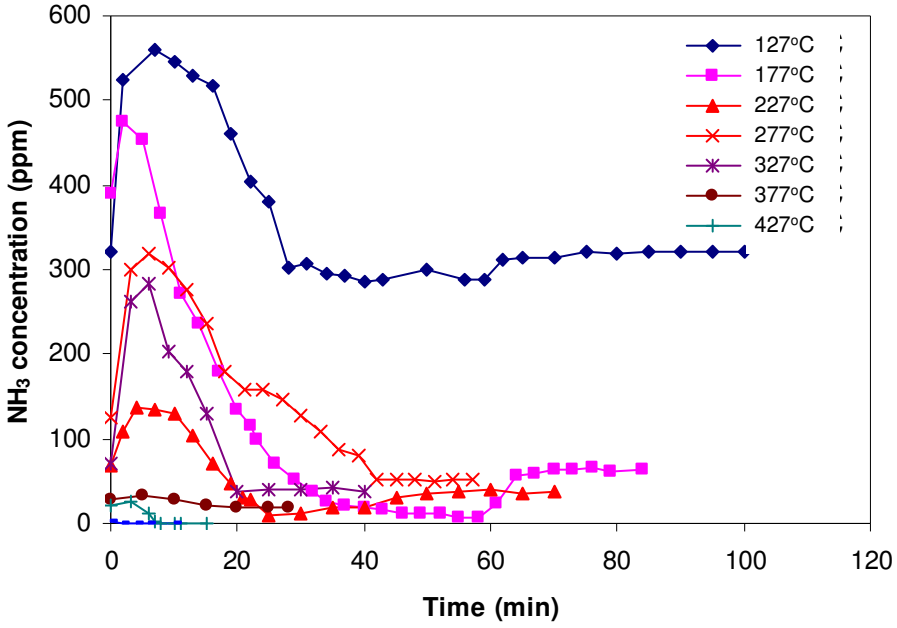

Figure 39. NH_3 concentration as a function of time at different reaction temperatures over V_2O_5-WO_3/TiO_2. Reaction conditions: [NO] = 330 ppm, [urea] = 165 ppm, 1% O_2, heating area of zone 1 + 2 + 3, and SV = 10500 h^{-1}.

5.8 Observation of NH_3 concentration

Prior to running the main experiments, each reading normally took around 20 - 25 minutes to reach steady state during the NO calibration process. On the other hand, it took up to more than one hour to stabilize during the NH_3 calibration. NH_3 was found to require a longer time to stabilize than NO in the main experiment as well as the calibration process.

After the background scan, all species (such as 330 ppm of NO, 165 ppm of urea, 0 - 3.0% O_2, balance N_2, and dilution N_2 of 5000 sccm) were allowed to flow through the system. Initially when the gas species started to flow, the catalyst sample apparently absorbed mostly ammonia. Thus, the concentration of NH_3 in the output gases very gradually increased up to 330 ppm (theoretical value of NH_3 concentration produced from the urea) at the lowest temperature studies (127°C). This is the reason that the average time at the lowest temperature (127°C) was the longest one as listed in table 9.

Figure 39 represents the NH_3 concentrations as a function of time at various reaction temperatures over V_2O_5-WO_3/TiO_2 under the reaction conditions of [NO] = 330 ppm, [urea] = 165 ppm, 1% O_2, heating area of zone 1 + 2 + 3, and SV = 10500 h^{-1}. Every time the reaction temperature of the furnace was increased by the temperature step of 50°C, a sudden 'burst' of NH_3 concentration was detected by FTIR spectrometer. Though the urea concentration metered by the injector (165 ppm) should theoretically produce 330 ppm of NH_3, NH_3 concentration of around 560 ppm was measured during the transient stage. The concentration declined after it reached the maximum level around 10 minutes after the experiment started. The time during which NH_3 remained in the transient state varied for different temperatures. The sudden 'burst' was most obvious for the lower reaction temperatures. The maximum levels of the NH_3 concentration that was reached during transient state were all different at various reaction temperatures. This phenomenon was observed for every single experiment. Considering figure 39 and figure 40 together, the time region between 0 and 10 minutes, reaction temperatures increase and stabilize. Though the temperature of 100°C increases to 200°C within 5 minutes and stabilizes, NH_3 and NO concentration increase during this moment. More details concerning these observations will be provided in Chapter 6, Experimental Results and Discussion.

5.9 Observation of NO concentration

Figures 40 shows the NO concentrations as a function of time at various reaction temperatures over V_2O_5-WO_3/TiO_2 under the reaction conditions of [NO] = 330 ppm, [urea] = 165 ppm, 1% O_2, heating area of zone 1 + 2 + 3, and SV = 10500 h^{-1}. Unlike ammonia species, the concentrations of NO were decreased as soon as the reaction temperature increased as shown in figure 40. A sudden decrease of NO concentration was detected and was also greater at lower reaction temperatures. More detail will be discussed in the Chapter 6, Experimental Results and Discussion.

To determine the final scan, not only the NO concentration should be stabilized, but also the NH_3 concentration should reach the steady state and no transient characteris-

tics should be observed in the FTIR data. When the ammonia concentration was completely stabilizes (i.e., 100% NH_3 conversion), the final scan depended only on the NO condition.

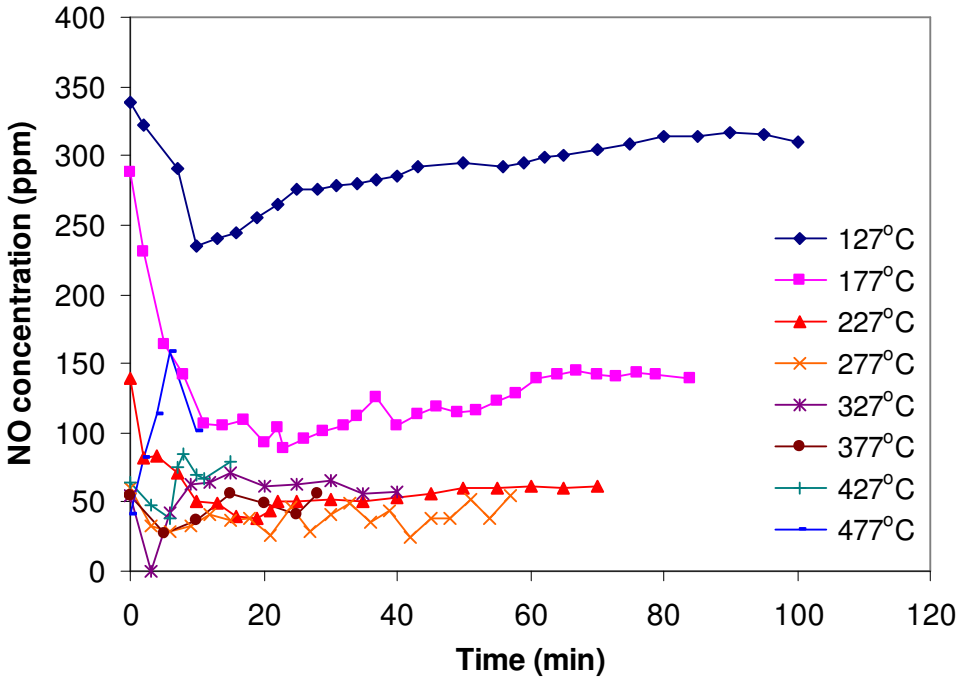

Figure 40. NO concentration as a function of time at different reaction temperatures over V_2O_5-WO_3/TiO_2. Reaction conditions: [NO] = 330 ppm, [urea] = 1665 ppm, 1% O_2, heating area of zone 1 + 2 + 3, and SV = 10500 h^{-1}.

6. EXPERIMENTAL RESULTS AND DISCUSSION

The results obtained for the urea-water thermal decomposition and selective catalytic reduction (SCR) of NO with ammonia as the reducing agent over vanadia-based (V_2O_5-WO_3/TiO_2) monolithic honeycomb catalyst are presented and discussed in this chapter. As a preface to this section, lines in all figures used to connect data points are only for the purpose of helping the reader differentiate one set of data from another. In all the following figures, NH_3 conversion is defined as the ratio of the output NH_3 concentration (as measured by the FTIR) to the input NH_3 concentration (from the injector) in percentage. NO reduction is defined as the ratio of the output NO concentration to the input NO concentration (as metered through the MFC) in percentage form. Therefore, higher NO reduction or higher NH_3 conversion means more NO or NH_3 removal from the exhaust.

6.1 Urea-water decomposition study

Since the main aim of the research study was to investigate the NO_x reduction using urea as a reducing agent, it is essential to study the urea-water decomposition process as much in detail as possible. It was ensured that the thermal decomposition study was carried out at the same experimental conditions as the NO_x reduction experiments. This study is an investigation into the products of thermal decomposition and oxidation of urea-water solution for a typical SCR process over Vanadia based catalyst. This has been done so as to study the decomposition process as close to the SCR configuration as possible. The decomposition experiments discussed in this section do not necessarily relate to the actual chemistry of the SCR-urea reaction. However these studies give a good insight into the interaction of the catalysts with urea as well as the behavior of urea molecules in the presence of moisture and in the absence of other reacting gases.

The decomposition studies related to SNCR done till now at Texas A&M University have been conducted at high temperatures.

Table 11. Experimental parameters for urea-water decomposition study.

Parameter	Value/Source
Urea	Extra Pure (EM Industries)
Distilled water	OmniSolv with purge gas in bottle
Temperature Range	227-477^{o}C
Total Flow Rate	1100 sccm
Urea in water solution (mass percentage)	0.76%
Temperature after injector	160 ^{o}C
Inlet Species (concentration in the reactor)	
Urea ($(NH_2)_2CO$)	165 ppm
Oxygen (O_2)	0%,1%,10%,15 %
Nitrogen (N_2)	Balance

Caton and Siebers [67] published the decomposition study of dry urea in a N_2 stream which indicated that urea splits up equally into NH_3 and HNCO. Urea-water decomposition studies conducted by Gentemann [62] later at high temperatures (527^{o}C to 1027^{o}C) showed that urea decomposition leads to a number of gaseous species like NH_3, CO_2, HNCO, NO, and N_2O. Park [61] carried out urea decomposition studies for a temperature range of 227^{o}C to 527^{o}C and urea-water decomposition studies for temperatures of 177^{o}C to 527^{o}C. The above study was conducted in the absence of a catalyst and no species other than HNCO, NH_3 and CO_2 were reported. The present study investigates urea-water solution decomposition as it takes place in a SCR process using a catalyst. Additional species apart from the ones mentioned above will also be reported such as NO_2 and N_2O.

Table 11 presents the experimental cases and injection conditions for the urea/water decomposition experiments that were conducted. Urea injection rate was kept constant and O_2 was varied for four different cases (0%, 1%, 10% and 15%). Temperature of the reactor was varied from 227^{o}C to 477^{o}C in steps of 50^{o}C. The catalyst was placed inside zone 2 of the reactor and the urea-decomposition products were measured and analyzed using FTIR. 1.92 g of urea was dissolved in 250 ml of water to produce a

0.76% (mass) solution. The major species noted in the output were NH_3, CO_2, NO, and H_2O. Minor species that were noted were NO_2 and N_2O along with trace amounts of HNCO which was noted only at some temperatures.

Since the total input from the urea injector was 165 ppm, total exit gas species should sum to 330 ppm. A number of "N" containing species were detected: NO_2, NO, N_2O and NH_3. Other species like N_2 would also account for "N" atoms. N_2 was a gas species present in a large amount in the exhaust gas stream and FTIR could not detect it. Apart from N_2, FTIR was not capable of detecting the exact amount of H_2O that was formed during the decomposition process. Even if FTIR had the capability, it would not account for the condensation of H_2O which was done prior to the FTIR using the water condenser. Some of the H_2O was also found to condense on the metal flanges hence it could not be quantified by the FTIR. The complete urea-water decomposition process can be written by this overall global reaction (along with other reactions mentioned after):

$$NH_2CONH_2 + H_2O \rightarrow 2NH_3 + CO_2 \tag{6.1}$$

6.1.1 Urea-water decomposition products

The following figures (41 to 45) in the subsequent pages show the major and the minor products of urea decomposition. An attempt has been made to balance the input species with the output species to confirm possible reaction mechanisms. The complete urea-water decomposition reactions have been explained in the later chapters. As stated before, major species from thermal decomposition of an aqueous solution of urea were NH_3, NO, CO_2 and H_2O along with the presence of minor species such as NO_2, HNCO, and N_2O.

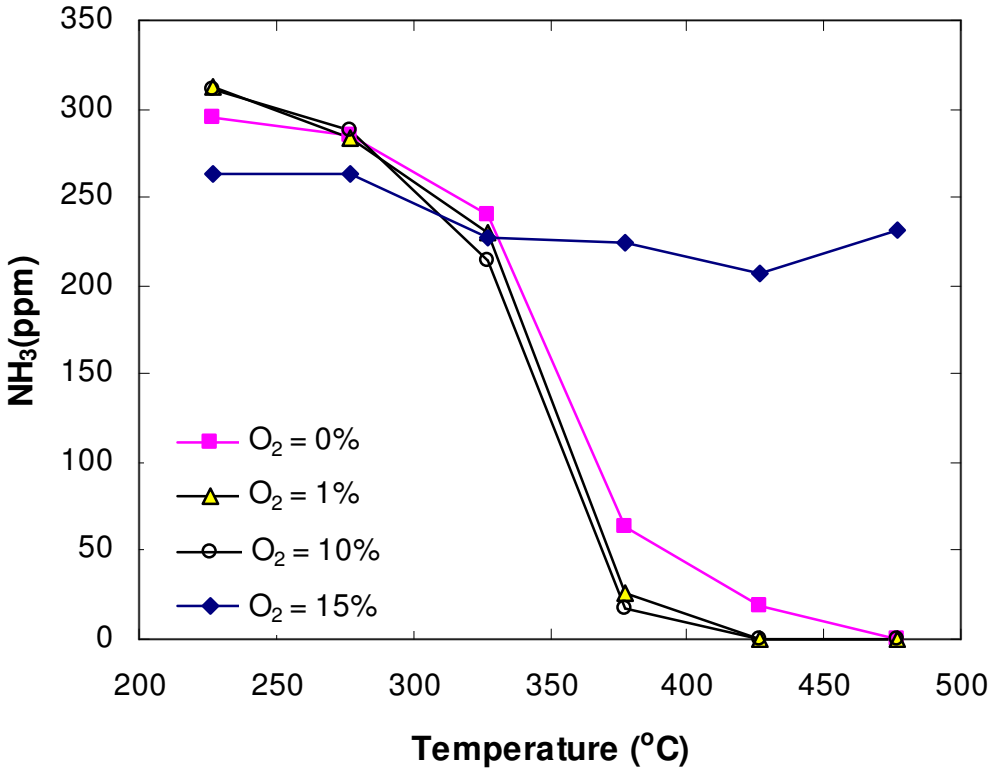

Figure 41. Ammonia (NH_3) concentration as a function of temperature for four oxygen levels over V_2O_5-WO_3/TiO_2. Reaction conditions: [$(NH_2)_2CO$] = 165 ppm, 0-15% O_2, heating area of zones 1 + 2 + 3, and SV = 10500 h^{-1}.

Figure 41 shows the ammonia (NH_3) concentration as a function of temperature for four different oxygen concentrations (0%, 1%, 10% and 15%). Since 165 ppm of urea was the input from the urea injector, 330 ppm of "N" containing species should be detected. NH_3 concentration was almost constant for 0% O_2 concentration at around 250 ppm. With the introduction of O_2 into the gas stream, NH_3 concentration was found to decrease considerably. When O_2 was introduced, NH_3 concentration decreased slowly to 277°C and for temperatures higher than 277°C, NH_3 concentration was found to decrease sharply. For oxygen concentrations of 10% and 15%, NH_3 concentration reached close to 0 ppm at a temperature of 427°C. The trend curves for NH_3 variation with temperature for 10% and 15% O_2 concentration lie very close to each other. For 1% O_2 con-

centration, NH_3 concentration reached 0 ppm at 477°C. The decrease in NH_3 concentration with temperature in the presence of oxygen can be attributed to the oxidation of NH_3 to give species like NO, N_2O and NO_2. This has been confirmed by the results for the other "N" containing species in the following figures. Another possibility could be the reduction of NO with the liberated ammonia favored by the high temperature conditions over the surface of the catalyst.

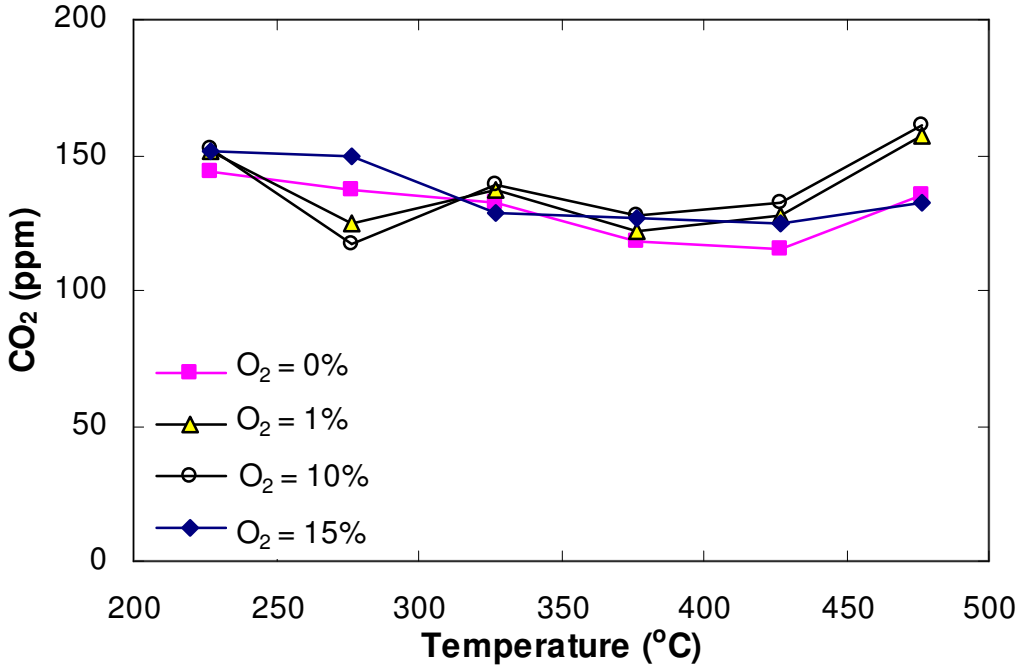

Figure 42. Carbon dioxide (CO_2) concentration as a function of temperature for four oxygen levels over V_2O_5-WO_3/TiO_2. Reaction conditions: $[(NH_2)_2CO]$ = 165 ppm, 0-15% O_2, heating area of zones 1 + 2 + 3, and SV = 10500 h^{-1}.

Figure 42 shows the variation of CO_2 concentration at different temperatures. CO_2 concentration was found to be relatively constant at about 135 ppm for all cases. Strictly speaking, 165 ppm of urea-water solution would result in 165 ppm of CO_2 upon complete decomposition (equation 6.1). Between 227°C and 277°C, CO_2 concentration was found to decrease with temperature for higher O_2 concentrations. At 277°C, CO_2

concentration was found to reach the lowest value of 117 ppm for 15% O_2 case. The curves for 0% and 1% O_2 concentration follow similar trend and same can be seen for 10% and 15% O_2 cases. Between 277°C and 327°C, CO_2 concentration was found to increase linearly with temperature for 10% and 15% O_2 concentration while it decreased for 0% and 1% O_2 concentration cases. Maximum CO_2 concentration at 327°C was 139 ppm for 15% O_2 case. Between 327°C and 427°C, CO_2 concentration was found to be

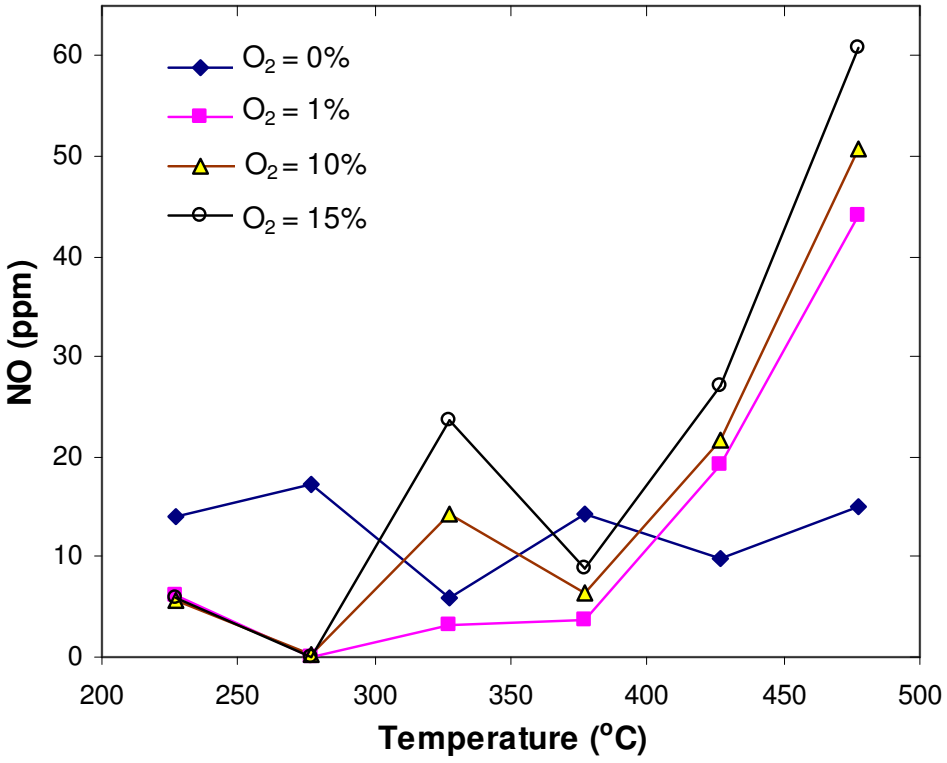

Figure 43. Nitric oxide (NO) concentration as a function of temperature for four oxygen levels over V_2O_5-WO_3/TiO_2. Reaction conditions: [$(NH_2)_2CO$] = 165 ppm, 0-15% O_2, heating area of zones 1 + 2 + 3, and SV = 10500 h^{-1}.

almost constant for all O_2 cases. For temperatures higher than 427°C, CO_2 concentration was found to increase for all O_2 concentrations and reached a maximum value of 160 ppm for 15% O_2 case.

Figure 43 shows the NO concentration as a function of temperature. For 0% O_2 case, NO concentration remained almost steady at 10 ppm. As the oxygen concentration was increased, higher NO production was found to take place. Between 227°C and 277°C, NO concentration decreased linearly for higher O_2 concentrations reaching a lowest value of 0.02 ppm at 15% O_2 concentration. Between 277°C and 377°C, fluctuations were noticed in the NO concentration for 1%, 10% and 15% O_2 cases. Highest NO concentration at 327°C (23 ppm) was observed for the 15% O_2 case. For temperatures higher than 377°C, NO concentration increased for cases in the presence of O_2 and reached a maximum value of 60 ppm at 477°C for 15% O_2 case.

Several important characteristics are revealed by the results from figure 43. As the O_2 concentration was increased, detected amount of NO increased due to the presence of more O_2 molecules to oxidize the "N" atoms. The curve fluctuations noticed between 277°C and 327°C may be the result of the oxidation of the solid urea deposits that were found inside the reactor leading to secondary emissions. One more important observation to be made is the reduction in the concentration of NO produced between 327°C and 377°C for higher O_2 concentrations (10 and 15%). Figure 41 also reports steep decrement in the NH_3 concentration in that same temperature range. This clearly suggests the reduction reaction of NO with NH_3 being active over the catalyst surface in this temperature range. The reduction reactions and results from SCR reduction of NO_x are presented later in this chapter.

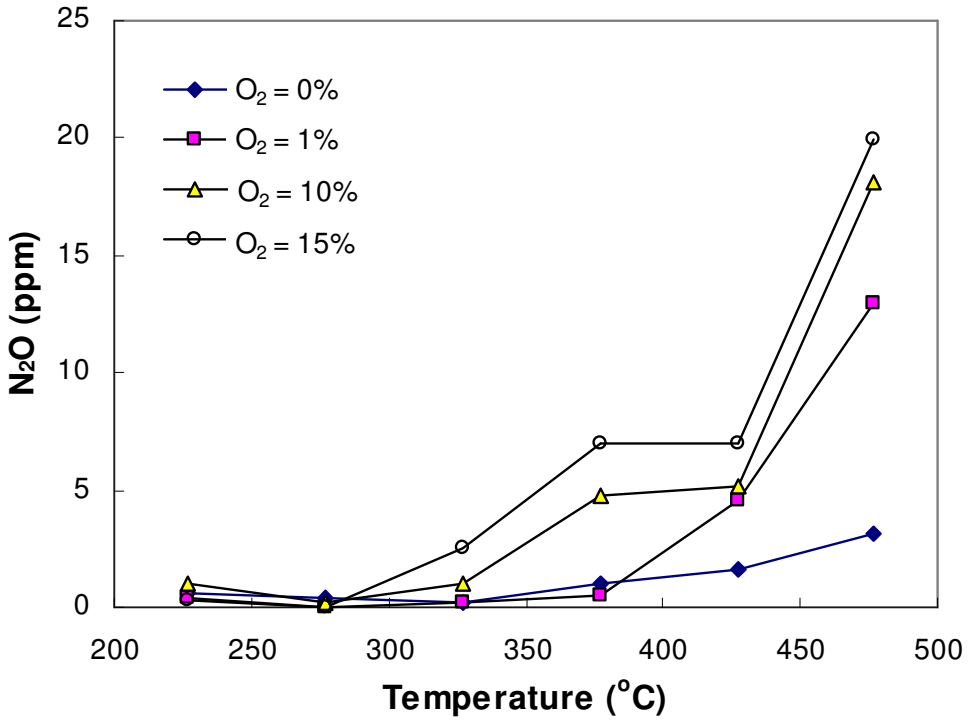

Figure 44. Nitrous oxide (N_2O) concentration as a function of temperature for four oxygen levels over V_2O_5-WO_3/TiO_2. Reaction conditions: $[(NH_2)_2CO]$ = 165 ppm, 0-15% O_2, heating area of zones 1 + 2 + 3, and SV = 10500 h^{-1}.

Figure 44 shows the variation of N_2O concentration with temperature for different O_2 concentrations. N_2O follows a similar trend as NO and was found to increase for higher O_2 concentrations to a maximum value of 20 ppm at 477°C. For 0% oxygen case, N_2O concentration almost remained zero till 327°C and then increased with temperature. For higher oxygen concentrations between 227°C and 277°C, N_2O concentration remained at 0 ppm and increased thereafter for higher temperatures. For example, for 1 % O_2 case about 0.05 ppm of N_2O was detected at 277°C which then increased to 12.98 ppm at 477°C (figure 44). 10% and 15% O_2 cases followed similar trends to each other and increased with temperature.

An important conclusion can be made from the N_2O behavior between 327°C and 377°C. For higher oxygen concentrations (greater than 0%), a drop in NO and NH_3 concentration in that temperature range (327°C to 377°C) was observed while the N_2O curve registered its first steep increment over the temperature range. This can be attributed to the undesirable reaction/oxidation of NH_3 leading to the formation of N_2O. This undesirable reaction has been discussed in more detail in section 2.2.1.

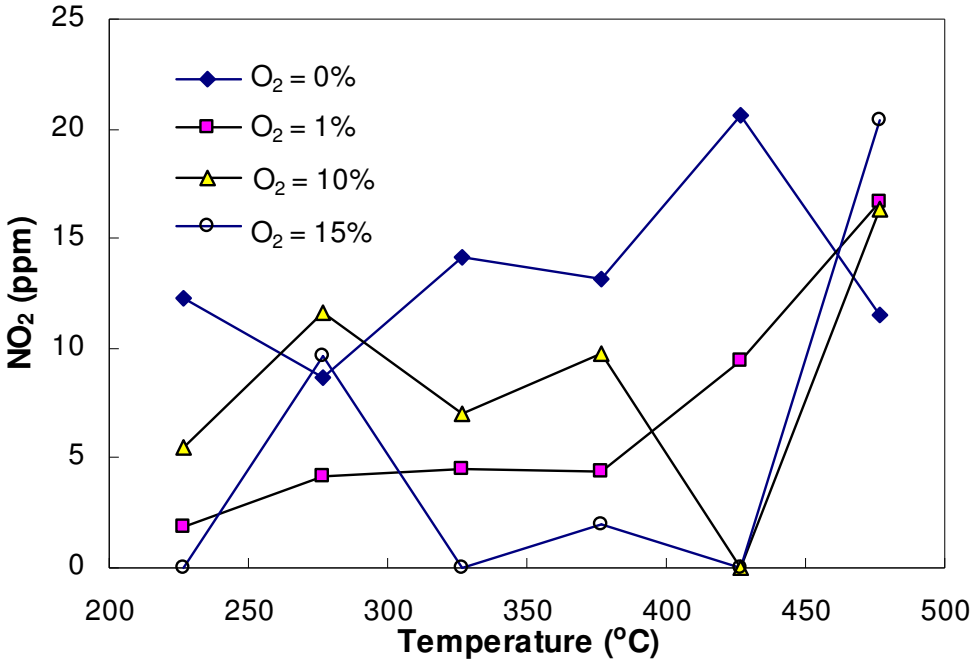

Figure 45. Nitrogen dioxide (NO_2) concentration as a function of temperature for four oxygen levels over V_2O_5-WO_3/TiO_2. Reaction conditions: [$(NH_2)_2CO$] = 165 ppm, 0-15% O_2, heating area of zones 1 + 2 + 3, and SV = 10500 h^{-1}.

Figure 45 shows the variation in NO_2 concentration with temperature. NO_2 was detected at low levels for all the O_2 concentrations. Large fluctuations in concentration were seen over the entire span of temperatures. At 227°C, NO_2 concentration was found to decrease for higher O_2 concentrations except for 10% case. 10% and 15% O_2 cases were found to match closely with each other over the entire temperature range. For 0%

O_2 case, NO_2 concentration remained fairly constant at 12 ppm till 377°C after which it was found to increase until 427°C and then decrease again to 11.5 ppm at 477°C. For 1% O_2 case, NO_2 concentration was found to increase slightly from 1.8 ppm to about 4 ppm between 227°C and 277°C. Between 277°C and 377°C, NO_2 remained fairly constant for 1% O_2 case. Then it increased linearly till 477°C. 10% and 15% O_2 cases followed similar trends with lot of fluctuations occurring between 227°C and 427°C. For 10% O_2 concentration, NO_2 was found to increase from 5.4 ppm at 227°C to 11.6 ppm at 277°C. Between 277°C and 327°C, NO_2 concentration dropped down to 7 ppm and then increased to 9.7 ppm at 377°C. NO_2 decreased sharply to 0 ppm at 427°C and then increased to 16.3 ppm at 427°C. For 15% O_2 case, NO_2 concentration increased from 0 ppm to 9.6 ppm between 227°C and 277°C and then again decreased to 0 ppm at 327°C. For higher temperatures it increased to 2 ppm at 377°C before dropping down to 0 ppm at 427°C and finally reaching a maximum value of 20.3 ppm at 477°C. These fluctuations suggested that NO_2 formation was a result of more than one intermediate reaction and was temperature sensitive.

In order to detect HNCO, wave number of 2282 cm^{-1} was used. No calibration gas was available for HNCO, so only qualitative assessments were possible. HNCO was detected but only at very low levels (absorbance of 0 – 0.3). These results agree very well with the studies conducted by Sullivan et al. [55]. These detection results for HNCO lead to some very important conclusions and inferences as discussed later.

Previous studies have reported the presence of HNCO in treated exhaust downstream of undersized Vanadia-based catalysts [33, and 35]. Studies conducted by Sluder et al. [43] did not show the presence of HNCO downstream of the SCR monolith which was a zeolite formulation that did not contain Vanadia.

From the atom balance of the reported species in this study, it can be inferred that species other than the ones reported in this study were also formed. These could be molecular nitrogen, solid/gaseous urea, CO, higher molecules like cyanuric acid or any other reaction by-products. Species other than the ones mentioned above might also be present in the gas system and were not detected. Using urea as a reducing

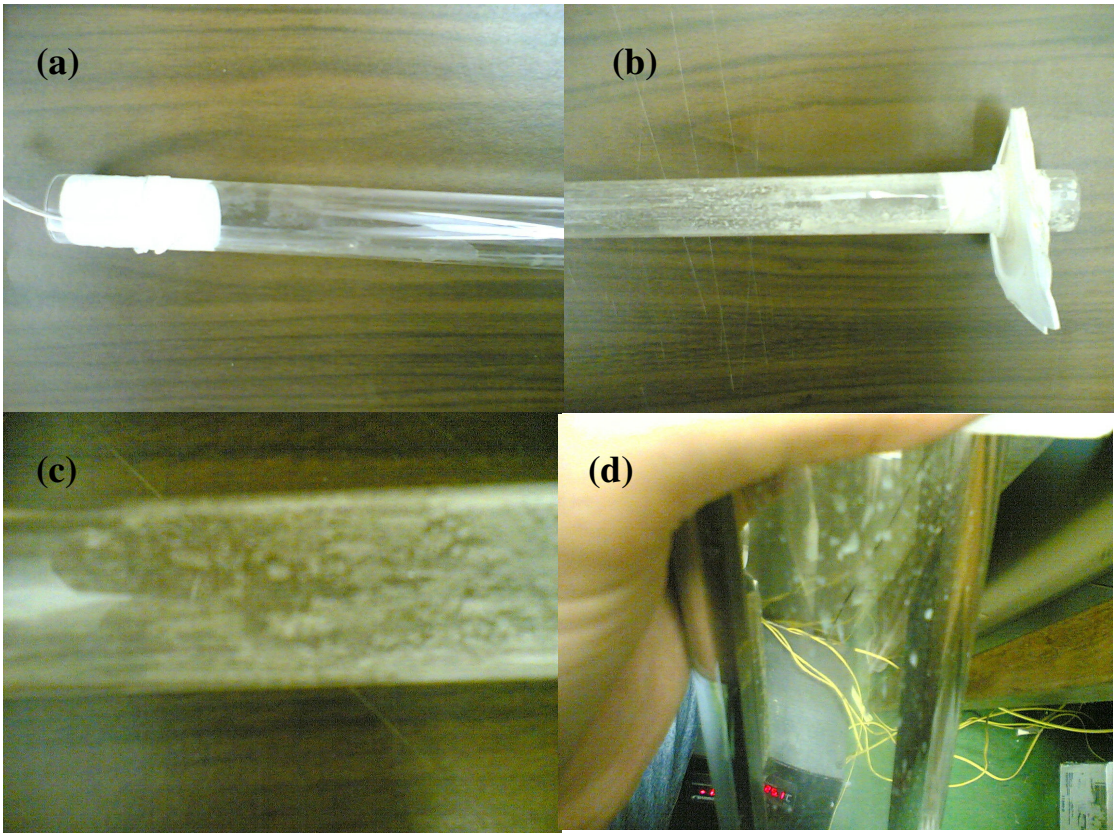

Figure 46. Formation of deposits throughout the quartz tube and the water condenser. (a) deposits formed at the end of quartz tube, (b) deposits formed at the entry of the quartz tube, (c) deposits formed in the middle of the quartz tube near the catalyst, (d) deposits formed inside the water condenser.

agent could result in at least eight thermal decomposition products and compounds such as cyanate ion, melamine, ammeline, ammelide, urea, ammonia, biuret and cyanuric acid [36]. Old calibration files for carbon monoxide (CO) were used but the amount of CO concentration was too small to be detected (0 ppm to 2 ppm). It was not clear whether the detected peaks for wavenumbers corresponding to CO were due to the actual presence of the specie or were due to the background noise. This is the reason why CO has not been reported in this study.

6.1.2 Urea-water decomposition deposits analysis

Deposit formation deactivates catalytic performance by not only consuming part of the ammonia produced during urea decomposition but also by degrading the structural and thermal properties of the catalytic surface [47]. The formation of stable decomposition products also means that higher amounts of urea would be required than the theoretical value for producing a certain amounts of ammonia. Deposit formation could be a function of the spraying effectiveness of the urea solution.

After a series of runs for each oxygen concentration, the quartz tube was inspected for any deposits and it was cleaned before the next set of readings were taken. Small patches of white precipitates which might comprise solid urea were noticed both near the inlet and the outlet of reactor. Figure 46 shows the pictures that were taken of the quartz tube and the water condenser for the deposits that were formed inside them. These precipitates were easily dissolvable in water. The presence of white deposits was noticed at two places in the experimental setup. Firstly white deposits, similar to resolidified urea were found after every run inside the quartz tube. These deposits are responsible for the discrepancy in the data obtained while working at the same temperature for a long time. These deposits could result in secondary NH_3 emissions and thereby an increase in the overall NH_3 detected by the FTIR. Secondly, resolidification of urea was also found to occur just prior to the reactor but after the urea injection port. The white deposits were similar to the ones obtained in the above case. These deposits extended from the point of urea-water injection up to the flange before the quartz tube. A second type of deposits that was detected remained insoluble in water and were formed downstream near the catalyst. Hence cleaning the quartz tube after every run was necessary to minimize secondary emissions.

Seker et al. [58] have also reported similar “white precipitates” but they have not discussed their chemical composition. Greenish-brown deposits were also found on the glass surface of the water condenser. Some deposits were found just ahead of the catalyst and were not soluble in water. Their composition is unknown and needs to be investigated. Fang et al. [47] reported similar solid deposits during the thermolysis of neat urea

without catalyst. The experiments conducted by Fang et al. reported a severe deposit formation along the exhaust pipe prior to the catalyst if the urea spray was not appropriately monitored. The deposit had a pale beige color at an early period of operation which changed to dark brown after a long period of heating, and the morphology changed from a turbostratic structure into a relatively amorphous solid. Their study showed that urea thermolysis exhibits two decomposition stages involving ammonia generation and consumption. Decomposition occurring after the second stage leads to the production of melamine complexes, $(HNC{=}NH)_x(HNCO)_y$, that hinder the overall performance of the catalyst. They asserted that polymeric melamine complexes can be formed both with and without the catalyst and they do not undergo further decomposition (at least up to 320^{o}C).

6.1.3 Possible decomposition mechanism - discussion

The amount of HNCO registered with the FTIR (at a wave number of 2282 cm^{-1}) was negligible (absorbance of 0 – 0.3). This means that the hydrolysis reaction was very active at the temperature range being investigated in these experiments. The aqueous solution was heated to 160^{o}C after the injector capillary and prior to entry into the gaseous stream. This would result in the complete evaporation of water molecules from the aqueous solution leading to solid urea:

$$(NH_2)_2CO\ (\text{aqueous}) \rightarrow (NH_2)_2CO\ (\text{solid}) + x\ H_2O \qquad (6.2)$$

The melting point of urea used is 132.9°C [46]. Schaber et al. [45] studied pyrolysis of urea and found that a complete melt of urea is not achieved until 135°C. Hence solid urea would melt after the urea injector to give molten urea:

$$(NH_2)_2CO\ (\text{solid}) + \text{heat} \rightarrow (NH_2)_2CO\ (\text{melt}) \qquad (6.3)$$

$$(NH_2)_2CO\ (\text{melt}) + \text{heat} \rightarrow (NH_2)_2CO\ (\text{gas}) \qquad (6.4)$$

Also urea decomposition begins at around 152°C noted by vigorous gas evolution from the melt [33, 47, and 48].

$$(NH_2)_2CO\ (melt) + heat \rightarrow NH_3\ (gas) + HNCO\ (gas) \quad (6.5)$$

The next step in the process of urea decomposition is the hydrolysis of isocyanic acid (HNCO) formed to produce additional NH_3. HNCO is very stable in the gas phase, but it hydrolyzes easily with the water arising from the combustion process:

$$HNCO\ (gas) + H_2O\ (gas) \rightarrow NH_3(gas) + CO_2(gas) \quad (6.6)$$

SCR catalysts are very effective for the above reaction. Since no HNCO (negligible) was reported at the FTIR, it means that the above hydrolysis reaction took place readily over the surface of the catalyst. More details of the Urea-water decomposition mechanism can be found in section 2.1.1.

6.2 Nitric oxide removal using urea as a reducing agent

Different reducing agents have been used before and have been investigated for SCR reduction of NO_x such as NH_3, HNCO and hydrocarbons (HCs). Urea has also been identified as an effective reducing agent which can be used as a solid or in an aqueous form to generate NH_3. Urea SCR has been gaining popularity because of its high effectiveness and non-toxicity. The following description deals with the results from the study of removal of nitric oxide from the simulated exhaust gas.

The selective catalytic reduction (SCR) of nitric oxide (NO) with urea over V_2O_5-WO_3/TiO_2 monolithic honeycomb catalysts has been widely investigated. The results presented in this paper are unique in the sense that experimental analysis using a simulated exhaust gas stream in a controlled laboratory reactor environment has not been investigated in detail before. Also many additional gas species (like N_2O) have been quantified in the results though there might be a number of gas products which still need to be investigated.

Table 12. Experimental parameters for NO_x reduction experiments.

Parameter	**Value/Source**
Urea	Extra Pure (EM Industries)
Distilled water	OmniSolv with purge gas in bottle
Temperature Range	127-477^{o}C
Total Flow Rate	1100 sccm
Urea in water solution (mass percentage)	0.76%
Temperature after injector	160 ^{o}C
Inlet Species (concentration in the reactor)	
Urea ($(NH_2)_2CO$)	165 ppm, 220 ppm
Oxygen (O_2)	0%, 0.5%,1%, 3%
Nitrogen (N_2)	Balance

Table 12 presents the experimental cases and injection conditions for the NO reduction experiments that were conducted using urea-water solution. Urea injection rate was kept constant and O_2 was varied for four different cases (0%, 0.5%, 1% and 3%). Temperature of the reactor was varied from 127^{o}C to 477^{o}C in steps of 50^{o}C. The catalyst was placed inside zone 2 of the reactor and the urea-decomposition products were measured and analyzed using FTIR. The major species noted in the output were NH_3, CO_2, NO, and H_2O. Minor species that were noted were NO_2 and N_2O along with trace amounts of HNCO which was noted only at some temperatures.

Table 13 summarizes the experimental cases which were performed on the V_2O_5-WO_3/TiO_2 catalyst in the current study. During the analysis, deposit formation was noticed and the deposits formed during the SCR study were similar to the ones formed during the urea-water decomposition study. Size of the catalyst (a sample of 2 cm in length) used resulted in space velocity of 10500 h^{-1}. The number of heating zones activated included zones 1, 2 and 3. Heating of all the zones of the reactor was essential to prevent moisture from condensing inside the reactor resulting in spoilage of the catalyst placed in zone 2. Two urea injection rates of 165 ppm and 220 ppm of urea were investigated which resulted in β ratios of 1:1 ([NH_3] = 330 ppm, [NO] = 330 ppm) and 1.33:1 ([NH_3] = 440 ppm, [NO] = 330 ppm). Four different oxygen concentrations of 0, 0.5, 1 and 3.0% were tested for all cases over V_2O_5-WO_3/TiO_2 catalysts.

Table 13. Experimental cases performed on the V_2O_5-WO_3/TiO_2 catalyst.

NO	Urea	β- Ratio	O_2	Reactor Temperature Zone1+ Zone2 + Zone3 (^oC)
330	165	1	0%	127 177 227 277 327 377 427 477
330	165	1	0.5%	127 177 227 277 327 377 427 477
330	165	1	1%	127 177 227 277 327 377 427 477
330	165	1	3%	127 177 227 277 327 377 427 477
330	220	1.3	0%	127 177 227 277 327 377 427 477
330	220	1.3	1%	127 177 227 277 327 377 427 477

6.2.1 Product species for β ratio of 1 for various O_2 concentrations

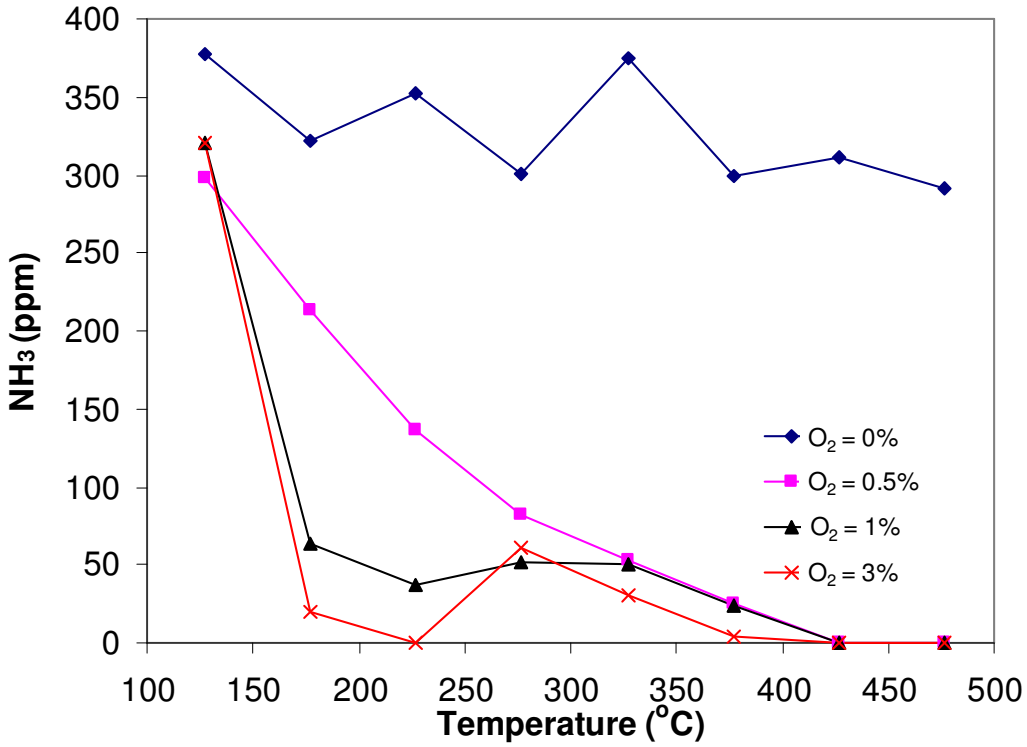

Figure 47. NH_3 concentration as a function of the reaction temperature at various oxygen concentrations over V_2O_5-WO_3/TiO_2 catalyst. Reaction conditions: [NO] = 330 ppm, [urea] = 165 ppm, 0 - 3.0% O_2, heating area of zone 1 + 2 + 3, and SV = 10500 h^{-1}.

In the SCR applications utilizing NH_3 or urea for NO_x reduction, the amount of NH_3 that comes out in the product gases is undesirable and is referred to as 'ammonia slip'. Figure 47 shows NH_3 concentration as the temperature of the reactor was increased from 127°C to 477°C in steps of 50°C for four different levels of O_2 concentration. For 0% O_2, NH_3 concentration fluctuated a bit at 327°C but on an average remained constant at around 335 ppm. For higher O_2% cases NH_3 concentration decreased continuously with increase in temperature for 0.5% and 1% O_2 case. For 0.5% O_2 case, NH_3 concentration reached 0 ppm at a temperature of 427°C. For 1% O_2 case, NH_3 concentration decreased from 320 ppm to 30 ppm at 227°C and remained almost steady till 327°C after which a decline in NH_3 was observed till it dropped down to 0 ppm at 427°C. For the case of 3% O_2 concentration, NH_3 concentration decreased rapidly from 127°C (320

ppm) to 227°C (0 ppm) and then a rise in the NH_3 conversion (slip) was observed at 277°C. NH_3 slip again decreased from 60.6 ppm at 277°C to 0 ppm at 427°C.

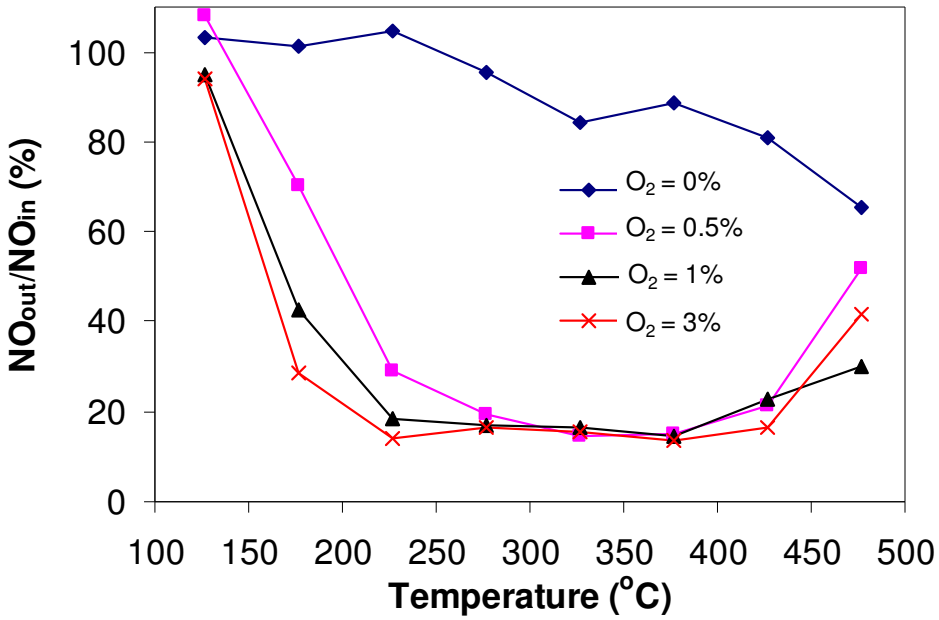

Figure 48. NO reduction as a function of the reaction temperature at various oxygen concentrations over V_2O_5-WO_3/TiO_2 catalyst. Reaction conditions: [NO] = 330 ppm, [urea] = 165 ppm, 0 - 3.0% O_2, heating area of zone 1 + 2 + 3, and SV = 10500 h^{-1}.

Figure 48 shows NO reduction with temperature for four different oxygen concentrations. It presents the NO reduction as a function of the reaction temperature at various oxygen concentrations at a space velocity of 15000 h^{-1}. Catalytic reactions take place for the conditions of [NO] = 330 ppm and [urea] = 165 ppm and heating area of zone 1+2+3.

In figure 48, NO reduction of 86.4% was found to take place at 377°C for 3% O_2 concentration. For 0% O_2 case, NO remained constant at 330 ppm till 277°C after which it decreased to 278 at 327°C and then to 216 ppm at 477°C. With the introduction of a slight amount of O_2 in the gas stream, NO reduction process was greatly accelerated.

For 0.5% O_2 case, NO concentration reduced from 350 ppm at 127°C to 47 ppm at 327°C. NO_x reduction of 85.6% was obtained at a temperature of 327°C. After attaining the minimum concentration at that temperature, NO concentration increased to a value of 171 ppm at 477°C. The NO reduction graphs for 1% and 3% O_2 concentration lie close to each other over the entire temperature range. For 3% O_2 concentration, NO concentration decreased from 309 ppm to 46 ppm from 127°C to 227°C and remained constant at that value till 427°C. From 427°C to 477°C, NO concentration again increased to a value of 134 ppm at 477°C. Thus, the temperature window of 200°C (from 227°C to 427°C) was obtained for NO reduction of 84% or more achieved for 3% O_2 case. NO

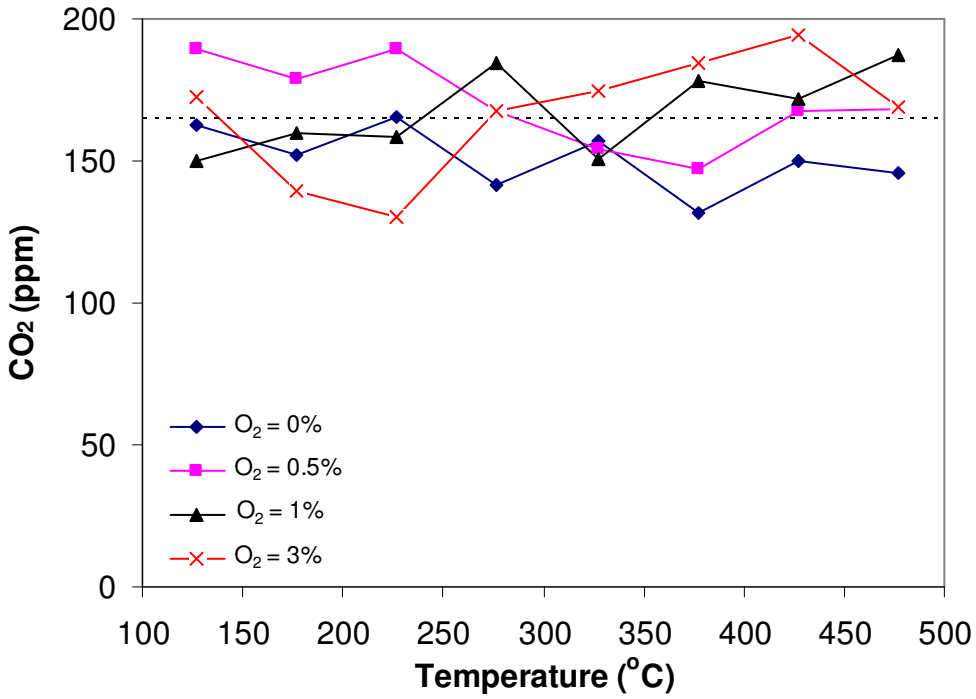

Figure 49. CO_2 concentration as a function of the reaction temperature at various oxygen concentrations over V_2O_5-WO_3/TiO_2 catalyst. Reaction conditions: [NO] = 330 ppm, [urea] = 165 ppm, 0 - 3.0% O_2, heating area of zone 1+2+3, and SV = 10500 h^{-1}.

reduction reached a maximum value for 0.5% O_2 concentration at 327°C and for 1% maximum NO_x reduction was found to take place at 377°C.

Figure 49 shows the CO_2 concentration as a function of the reaction temperature at various oxygen concentrations over V_2O_5-WO_3/TiO_2 catalyst. CO_2 concentration was found to remain almost constant at all the O_2 concentrations. For 0% O_2 case CO_2 concentration remained between 163 ppm and 132 ppm reaching the lowest value at a temperature of 377°C. For 0.5% O_2 case, CO_2 concentration remained at a constant value of 185 ppm from 127°C to 227°C after which it decreased to 167 ppm at 277°C and further to 147 ppm at 377°C. Increase in CO_2 was again noticed from 377°C to 477°C. For 1% O_2 case, CO_2 remained almost constant reaching a maximum value of 187 ppm at 477°C. For 3 % O_2 case, CO_2 concentration decreased from 173 ppm at 127°C to 129 ppm at 227°C. From 227°C to 427°C, CO_2 concentration increased to a maximum value of 194 ppm and then decreased to 169 ppm at 427°C.

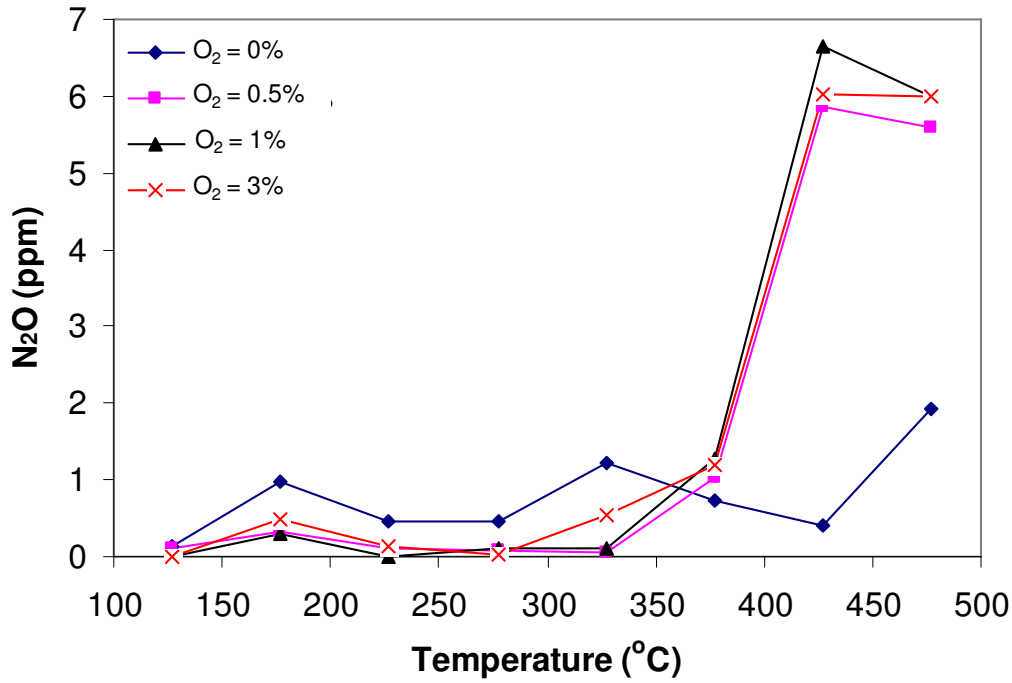

Figure 50. N_2O concentration as a function of the reaction temperature at various oxygen concentrations over V_2O_5-WO_3/TiO_2 catalyst. Reaction conditions: [NO] = 330 ppm, [urea] = 165 ppm, 0 - 3.0% O_2, heating area of zone 1+2+3, and SV = 10500 h^{-1}.

Figure 50 shows the variation in N_2O concentration with temperature for different cases of O_2 concentration under investigation. N_2O was detected at very low concentrations and for 0% O_2 case it remained almost constant over the entire temperature range. For O_2 greater than 0%, N_2O remained at a very low value until 327°C after which it increased rapidly with temperature to a maximum value at 427°C and decreased slightly thereafter till 477°C.

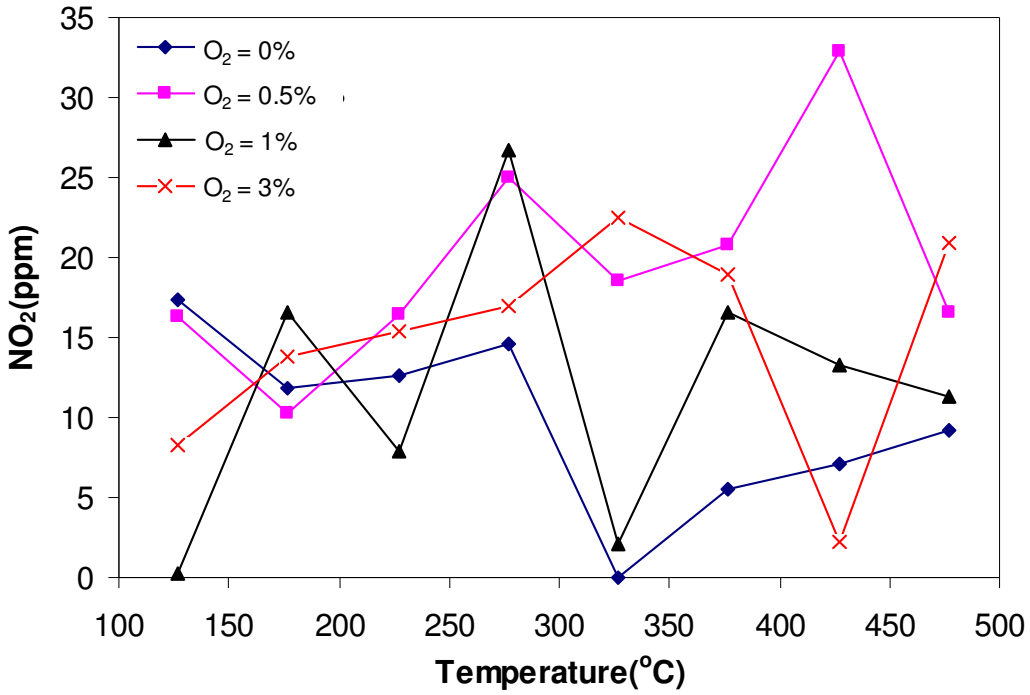

Figure 51. NO_2 concentration as a function of the reaction temperature at various oxygen concentrations over V_2O_5-WO_3/TiO_2 catalyst. Reaction conditions: [NO] = 330 ppm, [urea] = 165 ppm, 0 - 3.0% O_2, heating area of zone 1+2+3, and SV = 10500 h^{-1}.

Figure 51 shows the concentration of NO_2 as a function of the reaction temperature at various oxygen concentrations over V_2O_5-WO_3/TiO_2 catalyst. Amongst all the gaseous species shown, NO_2 was the only gaseous specie to show the largest variation in concentration over the entire temperature range. NO_2 was detected at low levels for all O_2 concentrations. Large fluctuations in concentration were seen over the entire span of

temperature variation. These fluctuations suggested that NO_2 formation was a result of more than one intermediate reaction and was temperature sensitive.

6.2.2 Product gas species for a β ratio of 1.33 for various oxygen concentrations

Experimental results were also obtained for urea injection of 220 ppm leading to 440 ppm of NH_3 generation in an ideal case. Gaseous products were obtained for two O_2 cases of 0% and 1% with temperature variation from 127°C to 477°C in steps of 50°C. Figure 52 shows NH_3 concentration with temperature for two different oxygen concentrations. It presents the NH_3 concentration as a function of the reaction temperature at various oxygen concentrations at a space velocity of 10500 h^{-1}.

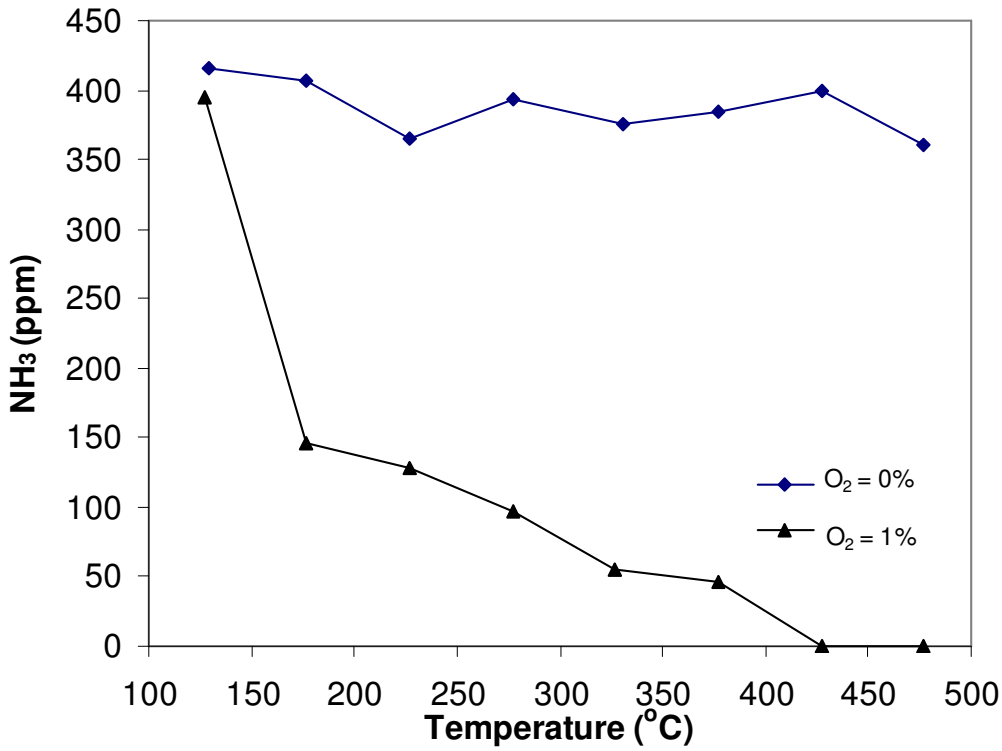

Figure 52. NH_3 concentration as a function of the reaction temperature at various oxygen concentrations over V_2O_5-WO_3/TiO_2 catalyst. Reaction conditions: [NO] = 330 ppm, [urea] = 220 ppm, 0% and 1.0% O_2, heating area of zone 1+2+3, and SV = 10500 h^{-1}.

Catalytic reactions take place for the conditions of [NO] = 330 ppm and [urea] = 220 ppm and heating area of zone 1+2+3. As seen in earlier case (β=1), NH_3 concentration remained constant for 0% O_2 case but was found to decreased rapidly with temperature with the introduction of O_2 in the exhaust gas flow. For 0% O_2 case, NH_3 remained constant at around 400 ppm, decreasing to 364 ppm at 227°C and 360 ppm at 477°C. For 1 % O_2 case, NH_3 slip was found to decrease considerably from a value of 395 ppm at the starting temperature of 127°C to 0 ppm at 427°C. Thus operating at higher temperatures leads to lower ammonia slip which is good as less toxic ammonia is produced.

Figure 53 shows NO reduction (%) with temperature for 0% and 1% O_2 cases.

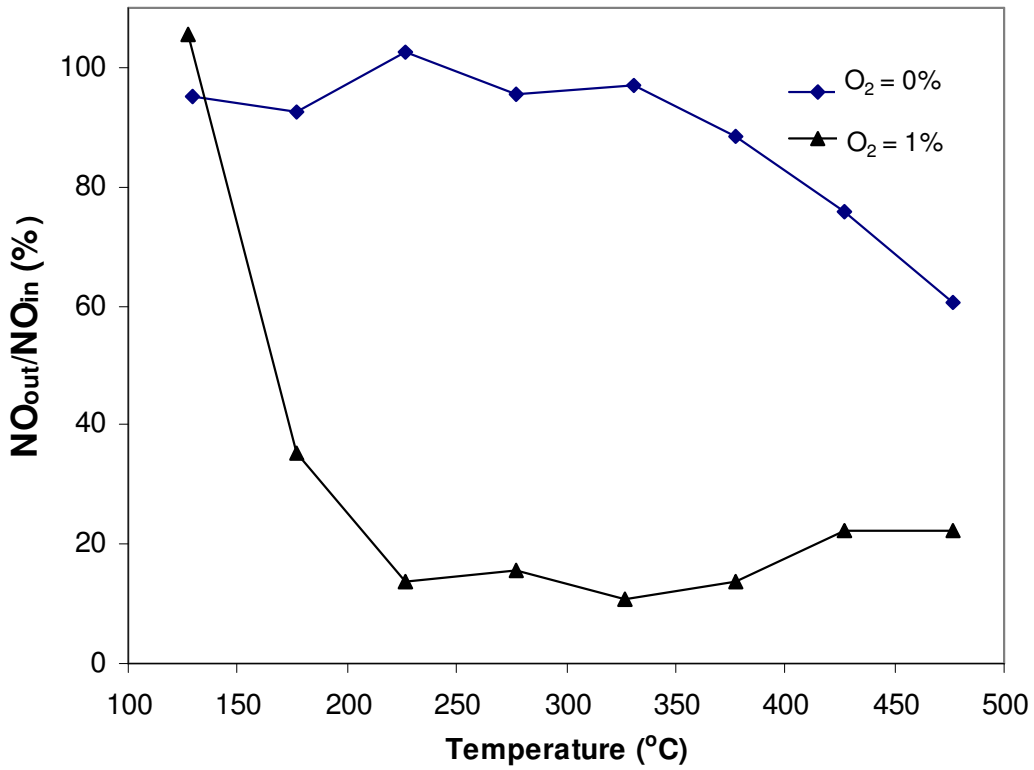

Figure 53. NO reduction as a function of the reaction temperature at various oxygen concentrations over V_2O_5-WO_3/TiO_2 catalyst. Reaction conditions: [NO] = 330 ppm, [urea] = 220 ppm, 0% and 1% O_2, heating area of zone 1 + 2 + 3, and SV = 10500 h^{-1}.

For 0% O_2 case, the catalyst was not very active for NO reduction below 327°C, after which NO reduction was found to take place at a higher rate from 3% at 327°C to 40% NO reduction obtained at 477°C. When O_2 concentration was increased to 1%, NO reduction of up to 90% was obtained at a temperature of 327°C which then decreased at higher temperatures to about 88% at 477°C. NO_x reduction obtained for the higher β ratio was higher as can be compared from the two β ratio cases shown in this section.

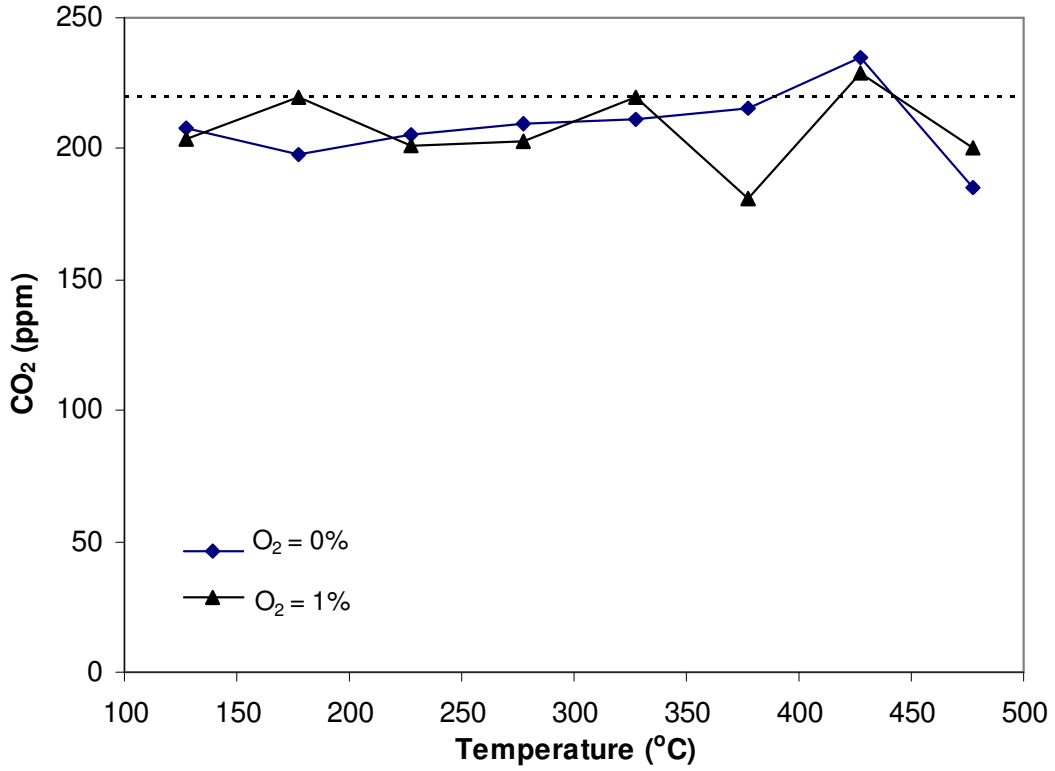

Figure 54. CO_2 concentration as a function of the reaction temperature at various oxygen concentrations over V_2O_5-WO_3/TiO_2 catalyst. Reaction conditions: [NO] = 330 ppm, [urea] = 220 ppm, 0% and 1% O_2, heating area of zone 1+2+3, and SV = 10500 h^{-1}.

Figure 54 shows CO_2 concentration as a function of temperature for different O_2 concentrations (0% and 1%). Similar to the trend followed for β=1, CO_2 was found to be almost constant over the entire range of temperatures for both O_2 concentrations. For 0%

O_2 case, CO_2 remained constant at an average value of 200 ppm. For 1% O_2 case, CO_2 remained almost constant till 277°C after which it increased to 220 pm at 327°C and then decreased again to 181 ppm at 377°C. An increase in CO_2 was observed from 377°C to 427°C followed by a decrease in its concentration at 477°C.

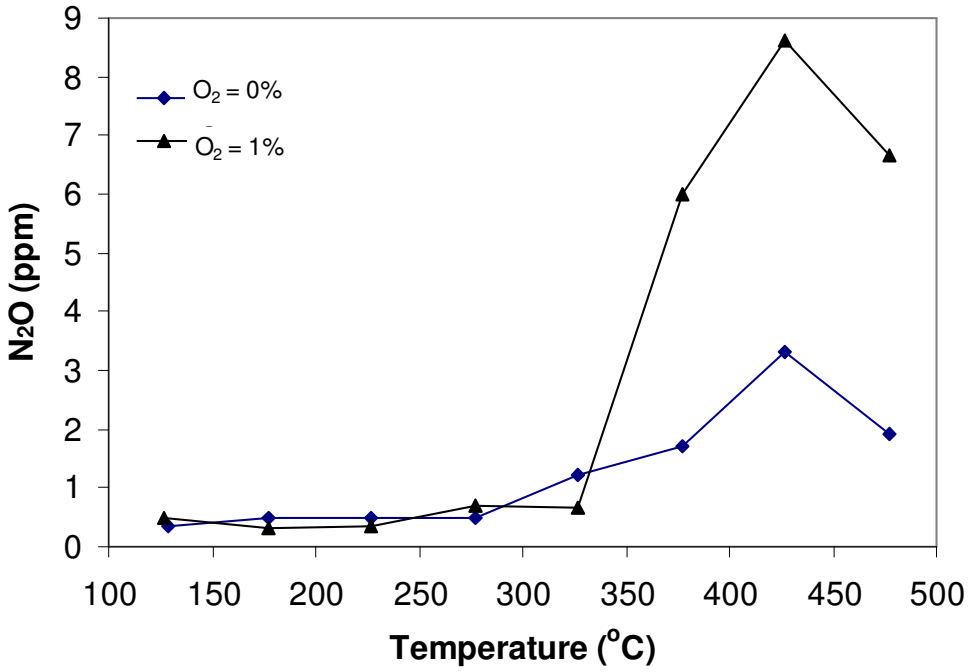

Figure 55. N_2O concentration as a function of the reaction temperature at various oxygen concentrations over V_2O_5-WO_3/TiO_2 catalyst. Reaction conditions: [NO] = 330 ppm, [urea] = 220 ppm, 0% and 1% O_2, heating area of zone 1+2+3, and SV = 10500 h^{-1}.

Figure 55 shows N_2O concentration as a function of the reaction temperature at various oxygen concentrations over V_2O_5-WO_3/TiO_2 catalyst for β ratio of 1.33. N_2O was a species that was detected at very low concentrations over the entire temperature range. For both O_2 concentrations, N_2O was found to remain almost constant to 277°C after which it was found to increase rapidly. For 0% O_2 case, N_2O remained almost constant at around 0.44 ppm till 277°C after which it increased to 3.31 ppm at 427°C and was found to decrease again to 1.92 ppm at 477°C. For 1% O_2 case, N_2O increased from

0.5 ppm to 0.71 ppm from 127°C to 277°C. N_2O was found to remain constant between 277°C and 327°C after which it increased at a sharp rate to 8.6 ppm at 427°C. N_2O reached a final concentration of 6.66 ppm at 477°C.

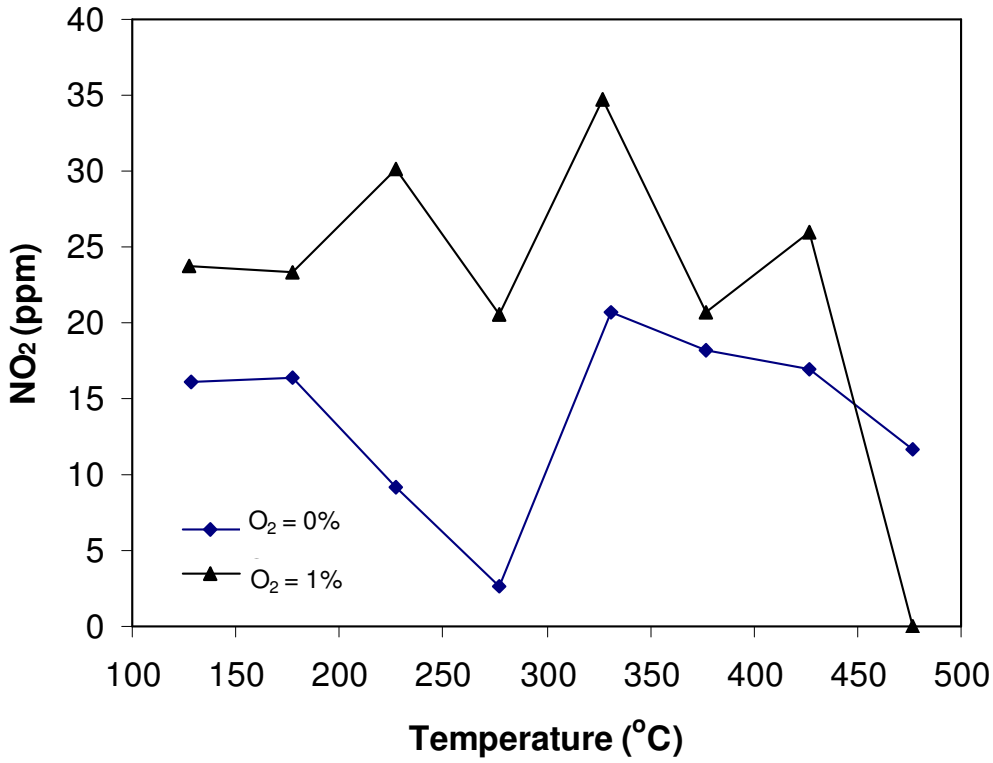

Figure 56. NO_2 concentration as a function of the reaction temperature at various oxygen concentrations over V_2O_5-WO_3/TiO_2 catalyst. Reaction conditions: [NO] = 330 ppm, [urea] = 220 ppm, 0% and 1% O_2, heating area of zone 1+2+3, and SV = 10500 h^{-1}.

Figure 56 shows the concentration of NO_2 as a function of the reaction temperature at various oxygen concentrations over V_2O_5-WO_3/TiO_2 catalyst for a β ratio of 1.33. As found in the earlier case (β ratio of 1), amongst all the gaseous species shown, NO_2 was the only gaseous specie to show large variations in concentration over the entire

temperature range. NO_2 was detected at low levels for higher O_2 concentrations. Large fluctuations in concentration were seen over the entire temperature range.

6.2.3 Product gas species for different β ratios (β=1, 1.33)

Figures in this subsection present combinations of the previous results for variations of NH_3-to-NO ratio. The results of NH_3 conversion in figures of 47 and 52 are combined together into figure 57. For the reduction of NO, the results in figures 48 and 53 are combined together into figure 58. These results are for NH_3-to-NO ratios of 1.33 (solid lines with open symbols), and 1.0 (dashed lines with open symbols). The symbols indicate oxygen concentrations of 0% (◊), 1% (◊) for β=1.33, and oxygen concentration of 0% (*), 1% (*) for β=1.

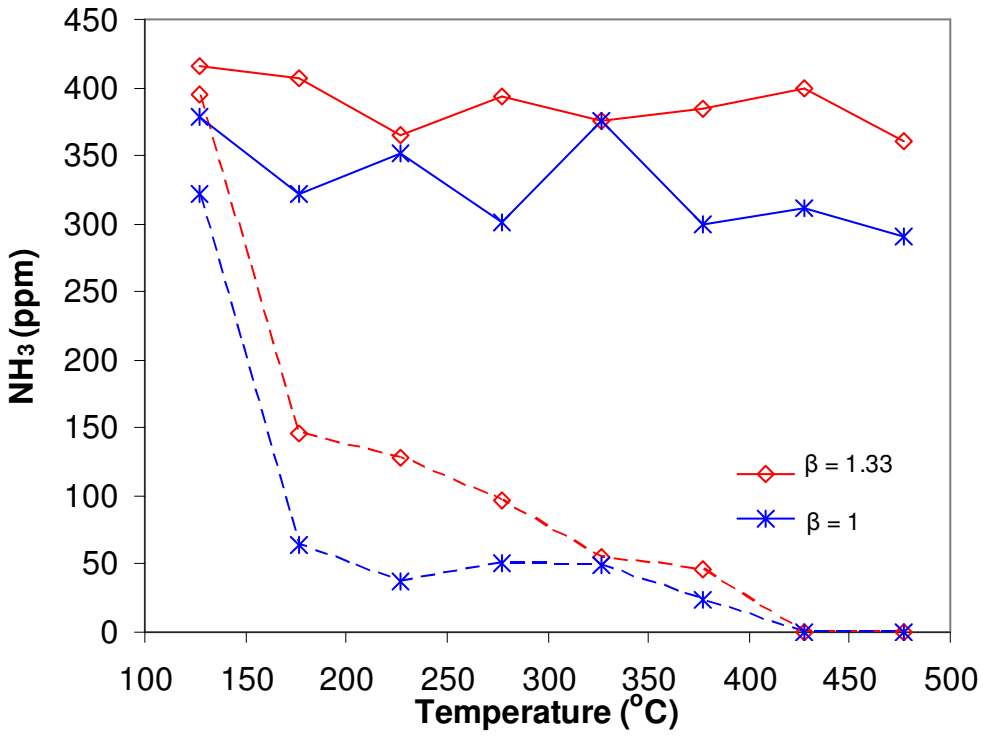

Figure 57. NH_3 conversion as a function of the reaction temperature at various NH_3-to-NO ratios over V_2O_5-WO_3/TiO_2. Reaction conditions: 0% (solid lines), 1% O_2 (dashed lines), SV = 10500 h^{-1}, and NH_3-to-NO ratio = 1.33 (red), and 1 (blue).

Figure 57 shows the effect of the variation of NH_3-to-NO ratio on NH_3 conversion as a function of the reaction temperature. NH_3 slip was found to increase with increase in the β ratio from 1 to 1.33. For 0% O_2 case, NH_3 concentration (slip) was found to be constant for both the β ratios and the slip for β=1 was found to be lower than for β=1.33. The temperature of 100% NH_3 conversion was found to be same for both β ratios in the presence of O_2. NH_3 slip curve for β=1.33 followed almost the same trendas for β=1 but was higher than the β=1 curve.

Figure 58 describes the effect of the variation of NH_3-to-NO ratio on NO reduction as a function of the reaction temperature. The curves for 1% O_2 case follow almost the same trend for different β ratios. For 0% O_2 case, NO reduction was found to remain

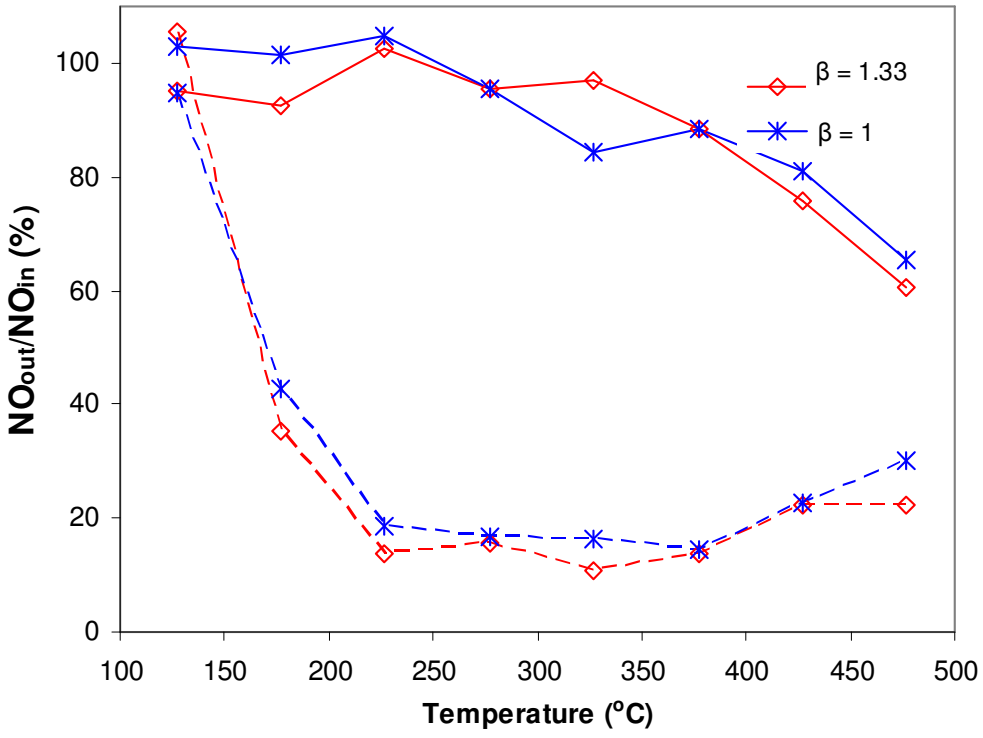

Figure 58. NO reduction as a function of the reaction temperature at various NH_3-to-NO ratios over V_2O_5-WO_3/TiO_2. Reaction conditions: 0% (solid lines), 1% O_2 (dashed lines), SV = 10500 h^{-1}, and NH_3-to-NO ratio = 1.33 (red), and 1 (blue).

constant between 227°C and 327°C for β=1.33. On the other hand, NO reduction for β=1 was found to increase from 0% to 16% between 227°C and 327°C. This means that though an increase in the β ratio leads to a higher amount of NH_3 slip, it doesn't considerably increase the NO reduction.

Figure 59 shows the effect of variation of variation of NH_3-to-NO ratio on the concentration of CO_2. As can be seen from the figure, CO_2 concentration was found to be almost steady over the entire temperature range for both the β ratios and for both the O_2 concentrations of 0% and 1%. CO_2 measured at the FTIR was found to be lower in case of β=1 than for β=1.33. This is consistent with the fact that a greater amount of urea solution would produce a greater amount of CO_2.

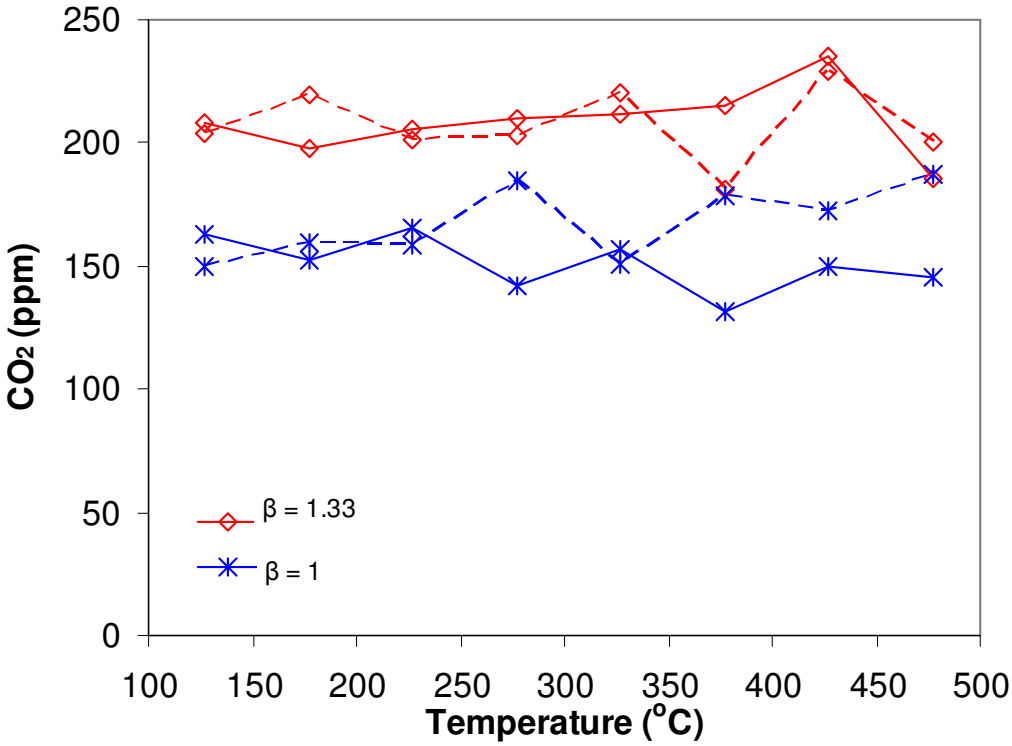

Figure 59. CO_2 concentration as a function of the reaction temperature at various NH_3-to-NO ratios over V_2O_5-WO_3/TiO_2. Reaction conditions: 0% (solid lines), 1% O_2 (dashed lines), SV = 10500 h^{-1}, and NH_3-to-NO ratio = 1.33 (red), and 1 (blue).

Figures 60 and 61 show the effect of variation of NH_3-to-NO ratio on the concentrations of NO_2 and N_2O, respectively.

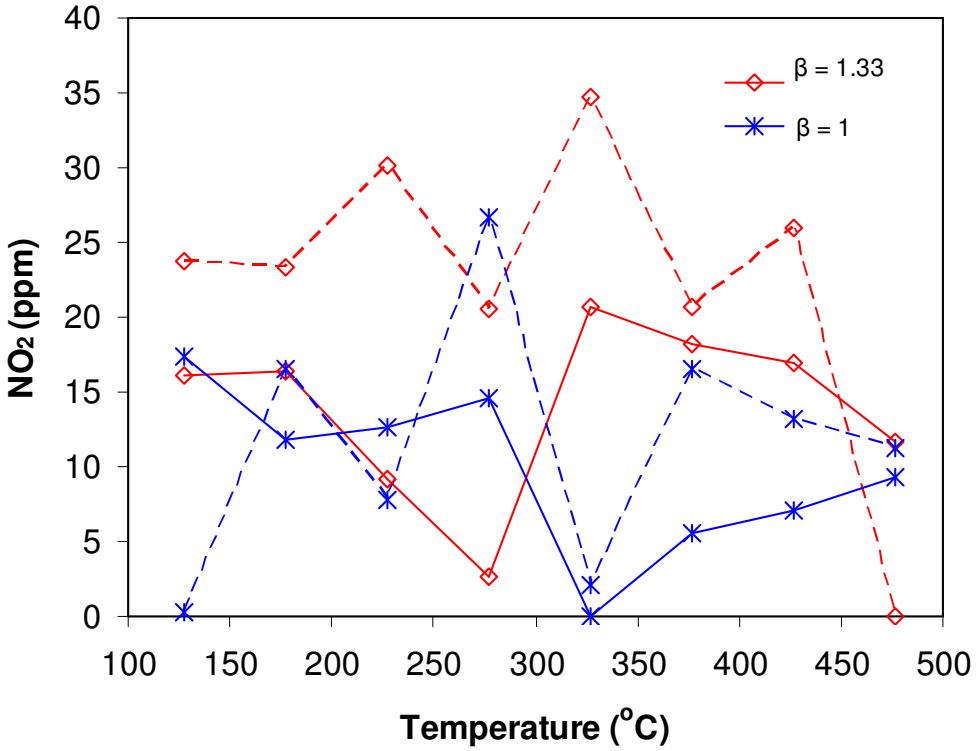

Figure 60. NO_2 concentration as a function of the reaction temperature at various NH_3-to-NO ratios over V_2O_5-WO_3/TiO_2. Reaction conditions: 0, 1% O_2, SV = 10500 h^{-1}, and NH_3-to-NO ratio = 1.33 (solid lines with open symbols), and 1 (dashed lines with open symbols).

For both the β ratios, a large fluctuation in the NO_2 concentration was found to occur over the entire temperature range. The fluctuations suggest that NO_2 was a highly temperature dependent specie and could also be formed from the deposits that were found in the quartz tube.

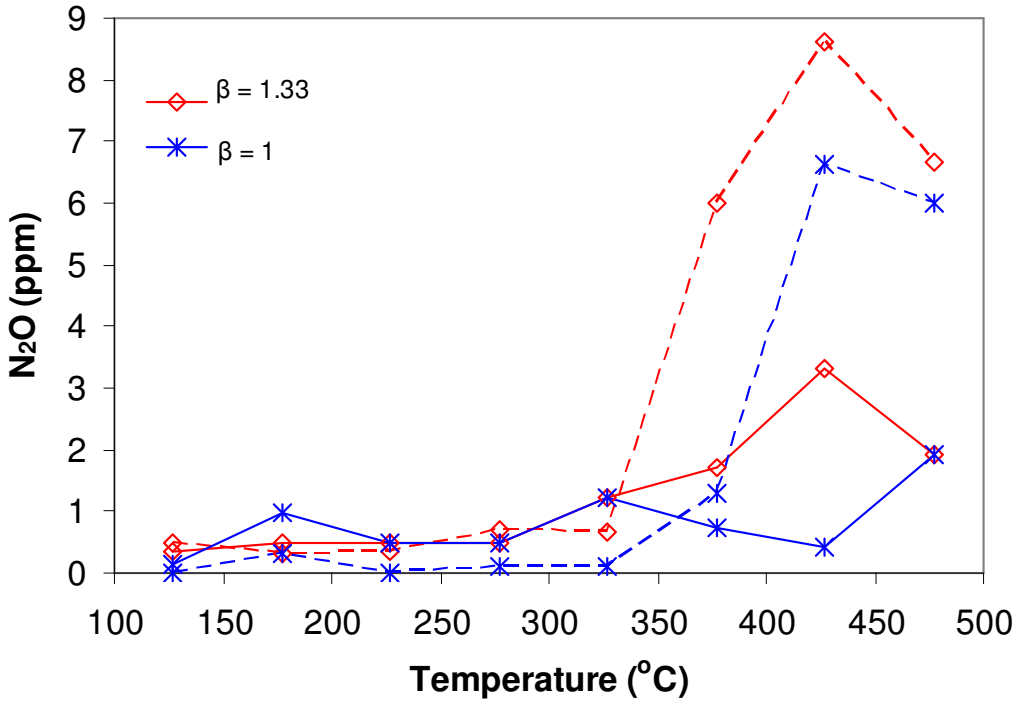

Figure 61. N_2O concentration as a function of the reaction temperature at various NH_3-to-NO ratios over V_2O_5-WO_3/TiO_2. Reaction conditions: 0, 1% O_2, SV = 10500 h^{-1}, and NH_3-to-NO ratio = 1.33 (solid lines with open symbols), and 1 (dashed lines with open symbols).

Table 14. The reaction temperatures of the maximum NO reduction.

O_2 concentration (%)	Temperature of maximum NO reduction (°C)	
	SV = 10500 h^{-1}	
	β ratio = 1	β ratio = 1.33
0	477	477
0.5	327	-
1.0	377	327
3.0	377	-

Table 14 lists the reaction temperatures of the maximum NO reduction at various oxygen concentrations for SV = 10500 h^{-1} and β ratios of 1 and 1.33. For β = 1 case, NO reduction was found to take place at higher temperature with increase in O_2 concentration from 0.5% to 1%. For 0% and 0.5% case, maximum NO reduction temperature was 327^{o}C which increased to 377^{o}C for 1% and 3% O_2 cases. With an increase in β ratio, an opposite trend was observed. Maximum NO reduction temperature was 477^{o}C for 0% O_2 case which decreased to 327^{o}C for 1% O_2 case.

Table 15. The lowest reaction temperatures of 100% NH_3 conversion.

Oxygen concentration (%)	Lowest temperature of 100% NH_3 conversion (°C)	
	SV = 10500 h^{-1}	
	β ratio = 1	β ratio = 1.33
0	-	-
0.5	427	-
1.0	427	-
3.0	427	427

Table 15 lists the lowest temperatures of 100% NH_3 conversion at various oxygen concentrations with space velocity of 10500 h^{-1} and β ratios of 1 and 1.33. Reaction temperature for 100% NH_3 conversion is found to be the same (427^{o}C) for all cases of O_2 concentrations greater than 0%.

6.3 Comparison of results between NH_3 and urea in NO_x removal

The selective catalytic reduction (SCR) of nitric oxide (NO) with ammonia over V_2O_5-WO_3/TiO_2 monolithic honeycomb catalysts has been studied in a previous investigation [63]. The comparisons of the results between NH_3 and urea-water solution as a reducing agent is presented and discussed case by case for the different reaction conditions.

Table 16 lists the experimental cases for V_2O_5-WO_3/TiO_2 monolithic honeycomb catalysts as investigated by Oh [63]. A number of possible catalyst arrangements were also investigated by Oh [33], but only those relevant to the present study have been listed in the table and discussed subsequently. For comparison, β ratio of 1 was tested with the previous study. One thing to be noted here is that in the present study all the zones (zone 1+ 2 + 3) were heated and this case has been compared to work done by Oh [63] for heating zones 2 + 3 only. Hence the exact experimental conditions may not be the same but this comparison gives a good idea of the difference in NO_x reduction with NH_3 or urea. The space velocity used for the comparison was same in both the cases (SV = 10500 h^{-1}). The oxygen concentration in the present study was varied at 0%, 0.5%, 1% and 3% while for the case to be compared, it was varied at 0%, 0.1%, 0.5% and 3%. The catalyst used for both the studies to be compared was obtained from the same company and hence this comparison is a useful study for comparing the effectiveness of NH_3 and urea as reducing agents. The experimental apparatus used for both the studies to be compared was the same including the flow reactor, FTIR, quartz tube and the mass flow controller. As stated earlier, heating all three reactor zones in the present study was imperative in order to ensure no water condensation took place inside the reactor thus preventing deactivation of the catalyst sample from moisture condensation. In the previous study, temperature variation of the reactor was effected from ambient (25^{o}C) to 450^{o}C in steps of 50^{o}C or 100^{o}C. In the present study, temperature was varied from 127^{o}C to 477^{o}C. Catalyst upper limit for the operating temperature was 450^{o}C.

Table 16. Experimental cases performed on V_2O_5-WO_3/TiO_2 catalysts [63].

Catalysts condition	Space velocity (h^{-1})	Heating area	NH_3-to-NO ratio	Oxygen concentration (%)
Standard arrangement	10500	Preheating (zone 2 + 3)	0.8 ([NO] = 330 ppm $[NH_3]$ = 264 ppm)	0 0.1 0.5 3.0
			1.0 ([NO] = 330 ppm $[NH_3]$ = 330 ppm)	0 0.1 0.5 3.0
			2.0 ([NO] = 330 ppm $[NH_3]$ = 660 ppm)	0 0.1 0.5 3.0

Results from the previous work for V_2O_5/TiO_2 monolithic honeycomb catalysts in the presence of oxygen are reviewed as follows [63]:

(1) An increase in oxygen concentration from 0% to 3.0% reduced the reaction temperature for the maximum NO reduction and slightly improved the maximum NO reduction. In the presence of O_2, the N_2O production declined with an increase in oxygen concentration simultaneously. NO_2 concentrations at 0 and 0.5% O_2 were not detected in the prior experiments. NO_2 production at 3.0% O_2 was zero for reaction temperatures below 400°C. The maximum concentration of NO_2 was about 7 ppm at the reaction temperature of 250°C at 0.1% O_2.

(2) For reaction temperatures below 200°C, no great difference was observed with an increase in NH_3-to-NO ratio at the same O_2 concentration (for the cases with non-zero oxygen). However, for reaction temperatures above 200°C, noticeable increase

of NO reduction was observed with an increase in NH_3-to-NO ratio in the presence of oxygen. Thus NO reductions increased with an increase in NH_3-to-NO ratio.

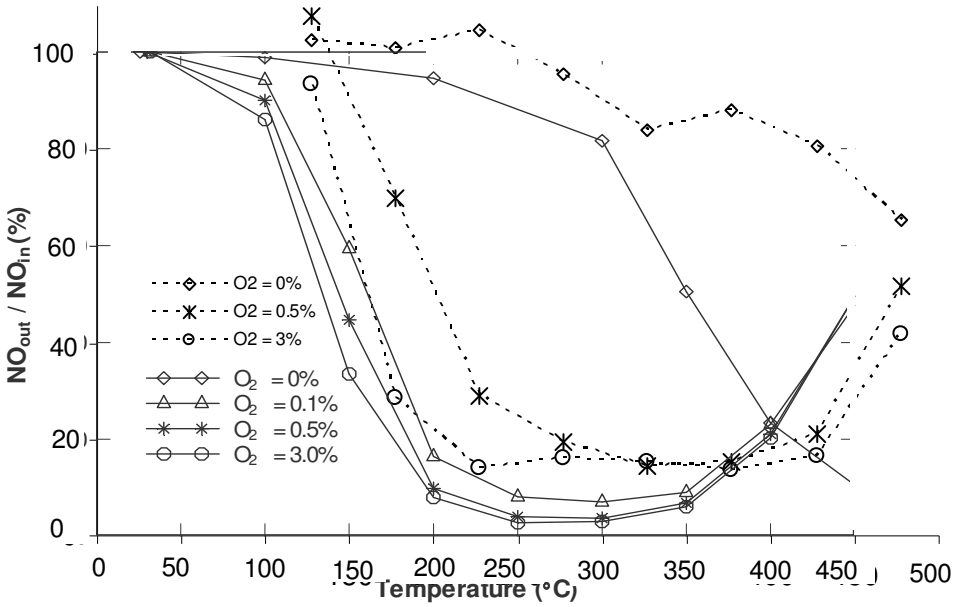

Figure 62. NO reduction as a function of the temperature over V_2O_5-WO_3/TiO_2 catalyst for different NO reducing agents. Reaction conditions: [NO] = [NH_3] = 330 ppm, 0%, 1% and 3.0% O_2, SV = 10500 h^{-1}, heating zones 2+3 for NH_3 (solid lines) [63], and heating zones 1+2+3 for urea (broken lines).

6.3.1 Effect of oxygen concentration

Figures 62 and 63 show the effect of using different reducing agents (NH_3 or urea) on NO reduction and NH_3 conversion, respectively, for the conditions of [NO] = 330 ppm, [NH_3] = 330 ppm, 0.1 - 3.0% O_2, SV = 10500 h^{-1} over V_2O_5-WO_3/TiO_2 for NH_3(solid lines), and urea (broken lines). All data for the NO reduction using NH_3 were collected from the previous study [63].

In figure 62, for the NH_3 as a reducing agent case, temperature was varied from 25°C to 450°C. On the other hand for the current study, temperature was varied from 127°C to 477°C as stated before. Looking at the NH_3 case, NO reduction was found to be greater for all the O_2 cases as compared to the case when urea was used as a reducing agent. For NH_3 case, higher NO reduction was found with an increase in O_2 concentration for the entire temperature range, and the result of 3.0% O_2 was the best performance for the preheating case. NO reductions over 83% were achieved for reaction temperatures between 200 and 350°C in the presence of O_2. NO reduction increased with an increase in O_2 concentration at reaction temperatures for the entire temperature range. The maximum NO reduction was found to be 97% at 250°C at 3.0% O_2. On the other hand for the urea case, maximum NO reduction of 86.4% was found to take place for 3% O_2 concentration at a temperature of 377°C. A temperature window of 200°C (from 227°C to 427°C) was obtained for NO reduction of 84% or more achieved for 3% O_2 case. One reason for greater NO reduction in case of NH_3 being used as a reducing agent could be that when urea was used as a reducing agent, the solution was heated and ideally it would generate enough amount of NH_3 for NO reduction. However, practically 100% conversion of urea into twice the amount of NH_3 is not possible leading to lower values of NO_x reduction in case of urea.

In figure 63, NH_3 conversion as a function of the reaction temperature over V_2O_5-WO_3/TiO_2 catalyst is shown at various O_2 concentrations for NH_3 as a reducing agent [63]. It was observed that high conversions of ammonia could be achieved in the presence of small amounts of oxygen, while very poor NH_3 conversions were obtained in the absence of oxygen in the entire temperature window. The presence of small amounts of oxygen concentration facilitated the oxidation of ammonia. Though higher NH_3 conversion was obtained with an increase in oxygen concentration from 0.1 to 3.0%, the differences were small.

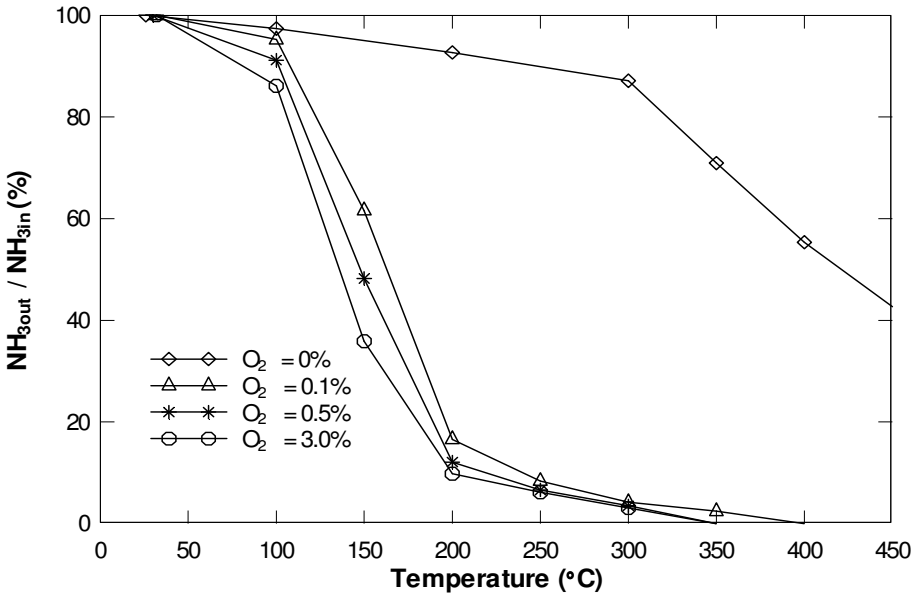

Figure 63. NH_3 conversion as a function of the reaction temperature at various O_2 concentrations over V_2O_5-WO_3/TiO_2 for NH_3 as a reducing agent. Reaction conditions: [NO] = 330 ppm, [NH_3] = 330 ppm, 0 - 3.0% O_2, heating area of zones 2 + 3 (preheating case), and SV = 10500 h^{-1} [63].

Comparing the above results with the present study using urea-water solution as a reducing agent, in case of urea absence of O_2 led to a very high NH_3 slipover the entire temperature range of the catalyst. Introduction of O_2 led to a considerable decrease in NH_3 slip with temperature and it reduced to zero at a temperature of 427^{o}C. Minimum ammonia slip for found to occur for 3% O_2 case. For higher O_2% cases NH_3 concentration decreased continuously with increase in temperature for 0.5% and 1% O_2 case. For 0.5% O_2 case, NH_3 concentration reached 0 ppm at a temperature of 427^{o}C. For 1% O_2 case, NH_3 concentration decreased from 320 ppm to 30 ppm at 227^{o}C and remained almost steady till 327^{o}C after which a decline in NH_3 was observed till it dropped down to 0 ppm at 427^{o}C.

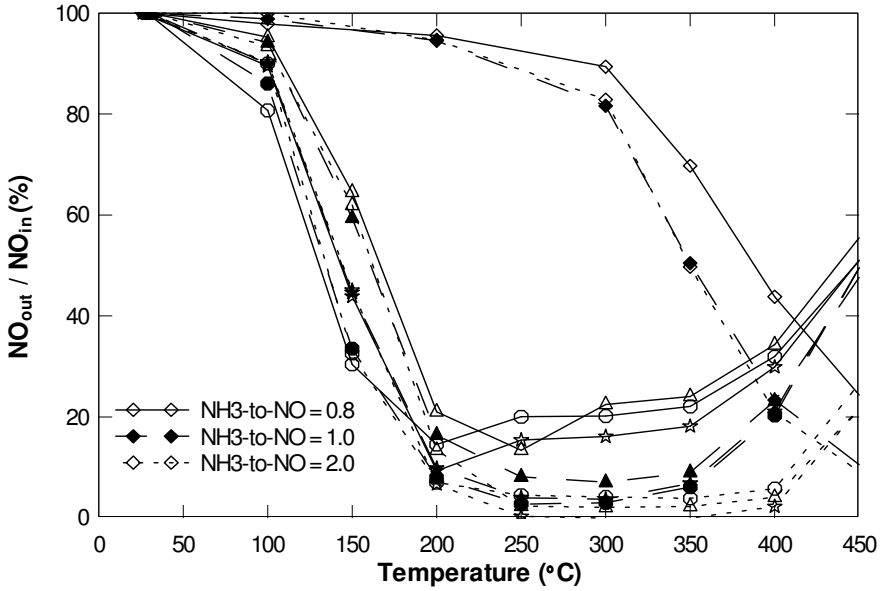

Figure 64. NO reduction as a function of the reaction temperature at various NH_3-to-NO ratios over V_2O_5-WO_3/TiO_2. Reaction conditions: 0 - 3.0% O_2, preheating case, SV = 10500 h^{-1}, and NH_3-to-NO ratio = 0.8 (solid lines with open symbols), 1.0 (broken lines with closed symbols), and 2.0 (dashed lines with open symbols) [63].

6.3.2 Effect of NH_3-to-NO ratio

Figures 64 and 65 describe the effect of the variation of NH_3-to-NO ratio on NO reduction and NH_3 conversion, respectively, as a function of the reaction temperature at space velocity of 10500 h^{-1} over V_2O_5-WO_3/TiO_2 catalyst for the case when NH_3 was used as a reducing agent. All data of were provided from the previous investigation [63]. The NH_3-to-NO ratio of 1 (broken lines with closed symbols) would be used as a measure to compare the NH_3 with urea case.

Figure 64 describes the effect of the variation of NH_3-to-NO ratio on NO reduction as a function of the reaction temperature. For reaction temperatures below 200°C, no great difference was observed with an increase in NH_3-to-NO ratio at the same O_2 concentration (for the cases with non-zero oxygen). However, for reaction temperatures above 200°C, noticeable increase of NO reduction was observed with an increase in NH_3-to-NO ratio in the presence of oxygen. Hence NO reductions increased with an in-

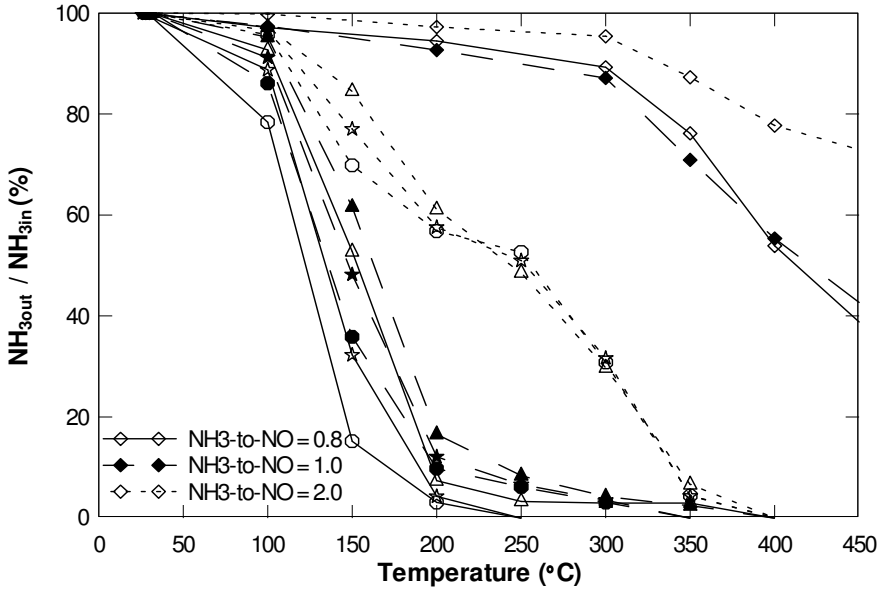

Figure 65. NH_3 conversion as a function of the reaction temperature at various NH_3-to-NO ratios over V_2O_5-WO_3/TiO_2. Reaction conditions: 0 - 3.0% O_2, preheating case, SV = 10500 h^{-1}, and NH_3-to-NO ratio = 0.8 (solid lines with open symbols), 1.0 (broken lines with closed symbols), and 2.0 (dashed lines with open symbols) [63].

crease in NH_3-to-NO ratio. In case of present study similar trends were observed. When O_2 concentration was increased to 1%, NO reduction of up to 90% was obtained at a temperature of 327°C which then decreased at higher temperatures to about 88% at 477°C. NO_x reduction obtained for higher β ratio was higher as can be compared from the two β ratio cases shown in the previous section.

For the case when NH_3 was used as a reducing agent, NH_3 conversion decreased with an increase in NH_3-to-NO ratio in the presence of oxygen. Figure 65 shows that at temperatures below 200°C for NH_3-to-NO ratios of 0.8 and 1.0, NH_3 conversion dropped rapidly. The temperature of 100% NH_3 conversion increased with an increase in NH_3-to-NO ratio.

For the present case and for β=1, NH_3 concentration remained constant for 0% O_2 case but was found to decreased rapidly with temperature with the introduction of O_2 in the exhaust gas flow. The temperature of 100% NH_3 (427°C) conversion was found to be same for both β ratios in the presence of O_2.

6.4. Transient characteristics of NO and NH_3 concentrations over a Vanadia-based (V_2O_5-WO_3/TiO_2) catalyst

To obtain the final concentration values at the reaction temperature, not only the NO concentration should be stabilized, but also the concentration of ammonia species should reach the steady state. According to a result of this study, the NH_3 species takes a longer time to reach steady state than the NO species at the same reaction temperature.

For the selective non-catalytic reduction (SNCR) of NO with NH_3, 20 - 30 minutes were required to obtain the final value at a single reaction temperature [17]. That is to say, the concentrations of both NO and NH_3 reached steady state within about 30 minutes.

On the other hand, more time was required to perform the selective catalytic reduction (SCR) of NO with NH_3. The average times to obtain the final values for each reaction temperature are listed in table 10. The average time decreases with an increase in the reaction temperature. During a single experiment, to stabilize the concentration of both NO and NH_3, the average times ranged from 26 to 134 minutes for the V_2O_5/Ti-PILC catalyst, depending on the reaction temperature. The presence of a catalyst explains this phenomenon. Initially when the gas species started to flow, the catalyst sample apparently absorbed mostly NH_3. Thus, the concentration of NH_3 in the output gases very gradually increased up to 330 ppm (initial NH_3 concentration) at the ambient temperature. It is the reason that the time for the stabilization of NH_3 at ambient takes the longest. It was observed that a sudden burst of the NH_3 concentration was detected by the FTIR spectrometer when the reaction temperature increased from the previous lower temperature. The sudden burst was significant at lower reaction temperatures. This also lengthens the time for stabilization of NH_3 at the reaction temperature.

Unlike the NH_3 species, a sudden decrease of NO concentration was observed when the reaction temperature increased from the previous lower temperature. A sudden burst of the NH_3 species occurred followed by a sudden decrease of NO concentration. The sudden decrease of NO species was significant at lower reaction temperatures.

In this section, the transient characteristics of the concentrations of NO and NH_3 over V_2O_5-WO_3/TiO_2 is described from their initial values until they become stabilized.

6.4.1 Transient characteristics of NH_3 concentration

Temperatures increase and stabilize within 10 minutes for the following figures in this section, and this result is from figure 38. Though the temperature of the reactor reached the set temperature in about 10 minutes (for every 100°C temperature increase), species likes NH_3 and NO took a longer time to stabilize. For example, after the final value (approximately 330 ppm) at 100°C was obtained, the temperature was increased to the next higher temperature (i.e., 200°C). The "zero" line (dotted line) for these figures is when the temperature increases from the ambient to the set temperature. Approximately 5 minutes are required to reach the temperature of 100°C.

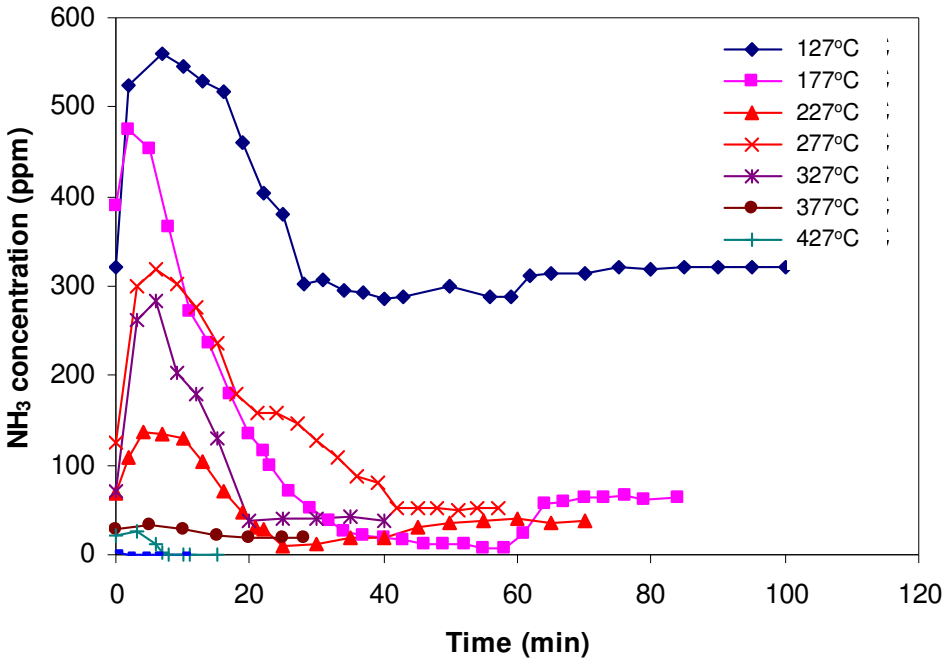

Figure 66. NH_3 concentration as a function of time at different reaction temperatures over V_2O_5-WO_3/TiO_2. Reaction conditions: [NO] = 330 ppm, [urea] = 165 ppm, 1% O_2, heating area of zones 1 + 2 + 3, and SV = 10500 h^{-1}.

Every time the reaction temperature increases from a lower temperature to the next higher temperature, 5 minutes or less are required. Figure 66 shows the transition of NH_3 concentrations over time over V_2O_5-WO_3/ TiO_2 for the reaction conditions of 1% O_2, heating area of zones 1 + 2 + 3, and SV = 10500 h^{-1}.

The initial urea concentration is 165 ppm at ambient which would ideally produce 330 ppm for NH_3. A sudden burst of NH_3 is observed during the first 10 minutes. Then, the NH_3 concentration reaches the maximum value (up to 550 ppm), and this increase declines at higher temperatures. The sudden burst is significant for temperatures below 327°C. The concentration starts to stabilize after 30 minutes but minor fluctuations still prevail at every temperature which might take more than 60 more minutes to stabilize. Then, after the maximum level, the ammonia concentrations decline slightly lower than the final value. Then, the ammonia concentrations increase very slowly to reach the steady state values.

6.4.2 Transient characteristics of NO concentration

Figure 67 shows the transition of NO concentrations over time over V_2O_5-WO_3/ TiO_2 for the reaction conditions of heating area of zones 1 + 2 + 3 , 1% O_2, and SV = 10500 h^{-1}. The initial NO concentration is 330 ppm at ambient (25°C). During the first 10 minutes, the temperature increases from the previous lower temperature and stabilizes as shown in figure 38. Unlike the ammonia species, the concentration of NO decreases until about 20 minutes after that point when the reaction temperature started to increase (at 0 minute). The NO concentration decreases more than half of its initial concentration at 177°C. For reaction temperatures below 277°C, the NO concentration after the minimum level increases until it stabilizes, and the large increasing is obtained. Therefore, a great decrease and increase sequentially is observed between 0 and about 70 minutes.

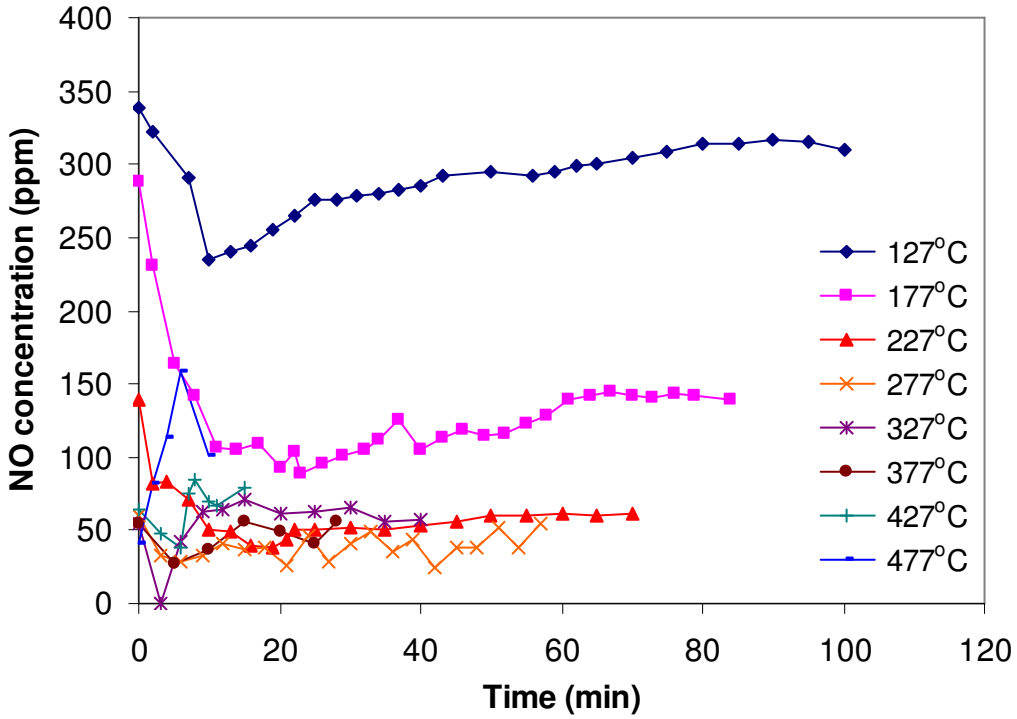

Figure 67. NO concentration as a function of time at different reaction temperatures over V_2O_5-WO_3/TiO_2. Reaction conditions: [NO] = 330 ppm, [urea] = 330 ppm, 1% O_2, heating area of zones 1 + 2 + 3 (preheating case), and SV = 10500 h^{-1}.

However in case of reaction temperatures above 377°C, the NO concentration trends are different. Though the sudden decrease of NO concentration is observed, the concentration does not increase. After it reaches the minimum concentration, it gradually stabilizes.

The time required to overcome this transient phase causes a time delay to determine the final concentration of NO species. Care should be taken to ensure that both NH_3 and NO have been stabilized before readings can be taken. The concentration of NO species takes less time to reach steady state than the concentration of NH_3 species at the same reaction temperature. The lower temperatures require more time to stabilize NO and NH_3 species. These phenomena are observed for every single experiment.

7. SUMMARY AND CONCLUSIONS

The thermal decomposition of urea-water solution in the presence of a catalyst and the selective catalytic reduction (SCR) of nitric oxide (NO) with urea as the reducing agent from simulated exhaust streams in a laboratory laminar-flow reactor were investigated. The experiments used a number of O_2 gas compositions to simulate different combustion gases. The catalyst was a Vanadia-based (V_2O_5-WO_3/TiO_2) monolithic honeycomb catalyst.

The effect of temperature on the urea-water decomposition was investigated. The results can be summarized as below:

A number of species were detected by the FTIR for urea-water thermal decomposition experiments (NH_3, NO, CO_2, NO_2 and N_2O). HNCO was too low to be detected. NH_3 concentration was almost constant for 0% O_2 concentration at around 250 ppm. With the introduction of O_2 into the gas stream, NH_3 concentration was found to decrease considerably. CO_2 concentration was found to be relatively constant at about 135 ppm for all cases. For 0% O_2 case, NO concentration remained almost steady at 10 ppm. As the oxygen concentration was increased, higher NO production was found to take place. N_2O follows a similar trend as NO and was found to increase for higher O_2 concentrations to a maximum value of 3 ppm at 477^{o}C. NO_2 was detected at low levels (~0-20 ppm) for all the O_2 concentrations and large amount of fluctuations in concentration were seen over the entire span of temperature variation.

The effects of two parameters were investigated for SCR using the V_2O_5-WO_3/TiO_2 catalysts. The results can be summarized as below:

(1) The effect of the inlet oxygen concentration variations from 0 to 3% was observed. For 0% O_2 case, NH_3 slip was high and remained constant over the entire temperature range. An increase in oxygen concentration increased the removal of both NO and NH_3 species. High NO reductions and low NH_3 slip were obtained in the presence of a small amount of oxygen, however, increasing oxygen concentration from 1 to 3.0% had no significant influence on the removal of NO. With the increase in O_2, NH_3

slip decreased continuously with temperature unlike NO which reached a minimum (~377^{o}C) and then increased at higher temperatures. An increase in oxygen concentration increased the production of N_2O in the presence of oxygen, but had the effect on NO_2 could not be related to a specific trend due to large fluctuations. CO_2 was found to be almost constant throughout the entire O_2 concentration range.

(2) The effect of β ratio (or inlet urea concentration) was investigated from 1 (urea = 165 ppm) to 1.33 (urea = 220 ppm). An increase in urea-to-NO ratio increased the NH_3 slip but the relative increase in NO reduction was not much. Lowest temperature for 100% NH_3 conversion remained the same for both the β ratios. CO_2 production was found to increase with increase in the β ratio for both the O_2% values. NO_2 again had a lot of fluctuation for both the values of β ratio whereas N_2O was found to increase very slightly with increase in the β ratio.

Transient behavior was documented for both NH_3 and NO concentrations. For typical conditions, almost two hours was needed to attain steady state values.

8. RECOMMENDATIONS

Recommendations for future work are listed as below:

(1) The effect of space velocity needs to be investigated for a V_2O_5-WO_3/TiO_2 catalyst.

(2) The effect of different heating area needs to be investigated for a V_2O_5-WO_3/TiO_2 catalyst. One drawback of using urea-water solution is that all the heating zones need to be activated in order to prevent moisture condensation hence different heating areas could not be investigated.

(3) The effect of various arrangements of a catalyst needs to be investigated for a V_2O_5-WO_3/TiO_2 catalyst. The catalyst can be tried for different positions and twist angles to obtain the best possible arrangement.

(4) The effect of the presence of water (H_2O) and sulfur dioxide (SO_2) needs to be investigated for a V_2O_5-WO_3/TiO_2 catalyst.

(5) The effect of NO_2 concentration in the simulated exhaust gas stream on the NO reduction needs to be investigated (fast SCR).

(6) An input and output species atom balance needs to be investigated for validation of the experimental results. One of the drawbacks of using FTIR for gas analysis is the incapability to quantify diatomic gases like N_2 and O_2 in the output gas stream.

REFERENCES

1. R.Y. Saleh, I.E. Wachs, S.S. Chan, C.C. Chersic, J. Catalysis 98 (1986) 102-114.

2. Department of Environment and Conservation, Principal Air Pollutants, http://www.epa.nsw.gov.au/envirom/princairpol.htm (Accessed May 1, 2005).

3. D. H. F. Liu, B. G. Liptak, Air Pollution, Lewis Publishers, New York, 2000.

4. C. C. Freudenrich, How Ozone Pollution Works - What Is Ozone, http:// science.howstuffworks.com/ozone-pollution1.htm, (Accessed November 2004).

5. M. J. Prather, J. A. Logan, Combustion's Impact on the Global Atmosphere, in: 25th Symposium (International) on Combustion, The Combustion Institute: Pittsburgh, (1996).

6. Environmed Research Inc., Car Exhaust - Health Effects, http://www.nutramed-comenvironment/carsepa.htm (Accessed May 6, 2005).

7. S. R. Turns, An Introduction to Combustion, McGraw-Hill, New York, 1996.

8. B.J. Smith, J.P. McGreevy, Urban Stone Decay and Acid Deposition: An Introduction to the Problem and Its Causes, http://www.qub.ac.uk/geog/documents-/research/weathering/usd.html (Accessed May 6, 2005).

9. K.-H. Baek, Selective Non-Catalytic Reduction of NO_x by Ammonia: Experiments and Model Calculations, Ph.D. Dissertation, Texas A&M University, College Station, 2003.

10. World Bank, Environment Department, Sulfur Oxides: Pollution Prevention and Control, Pollution Prevention and Abatement Handbook, World Bank Group, Washington, DC, 1998.

11. M. Radojevic, Environmental Pollution 102, Sl (1998) 685-689.

12. J. R. Mondt, Cleaner Cars: The History and Technology of Emission Control Since the 1960s, Warrendale, PA, Society of Automotive Engineers, 2000.

13. F. N. Alasfour, Applied Thermal Engineering 12 (1998) 245-256.

14. A. M. G. Gentemann, J. A. Caton, Decomposition and Oxidation of Urea-Water Solution as Used in Selective Non-Catalytic Removal(SNCR) Processes, Proceedings of the 2nd Joint Meeting of the United States Sections: The Combustion Institute, Oakland, California (2001).

15. Bosch, H., and F. Janssen, Catalysis Today 2 (1998) 369-532.

16. J. R. Mondt, Cleaner Cars: The History and Technology of Emission Control since the 1960s, Warrendale, PA, Society of Automotive Engineers, 2000.

17. Pollution Control Division, Harris County Ozone, http://www.harriscountyhealth.com/pcd/ozone/home.htm, (Accessed May 4, 2005).

18. Lets Talk About Health and Air Quality, http://www.hc-sc.gc.ca/hecs-sesc/air_quality/talk.htm, (Accessed April 28, 2005).

19. G. Baumbach, Air Quality Control, Springer, Berlin, Germany, 1996.

20. Turbine Technology NO_x Formation, http://www.netl.doe.gov/coalpower/environment/nox/howNOx.html (Accessed October 25, 2004).

21. TMTS Associates, Inc. and J. J. Santoleri, NO_x Control for Stationary Sources, http://www.mindspring.com/~tfmcgowan/presentation/nox.ppt, (Accessed April 28, 2005).

22. D. Acton, H. Taplin, Steam Efficiency Workshop II, The Gas Company Energy Resource Center, Downey, California, 2002.

23. C. P. Fenimore, 13th Symposium (International) on Combustion, The Combustion Institute: Pittsburgh, Pennsylvania, 1970, 373-380.

24. J. A. Caton, "Regulatory Considerations – Lecture No. 6", Cogeneration Systems, Texas A&M University, College Station, August 2003, 15-25.

25. J. Thomas, Complex Behavior in Heavy-Duty Urea SCR, Fourth CLEERS Workshop, Oak Ridge National Laboratory, Ann Arbor, Michigan, 2002.

26. Environmental Protection Agency, Diesel Emission Standards for Heavy-Duty On- and Off-Road Engines, http://www.cleanairfleets.org/standards.html, (Accessed April 30, 2005).

27. M. Koebel, M. Elsener, G. Madia, Industrial and Engineering Chemistry Research 40 (2001) 52-59.

28. C. R. Ferguson, A. T. Kirkpatrick, Internal Combustion Engines: Applied Thermodynamics, Second Edition, John Wiley & Sons, New York, 2001.

29. W. Kind, Beitrag zur NO_x-Verminderung im Abgas von Dieselmotoren durch selektive katalytische Reduktion mit Harnstoff, Fortschritts-Berichte VDI, Düsseldorf, Germany (1998).

30. A. B. Jensen, H. Topsøe, Scandinavian Shipping Gazette 3 (2000), 37-38.

31. H. Bosch, F. Janssen, Catalysis Today 2 (1988) 369-379.

32. P. Forzatti, Catalysis Today 62 (2000) 51-65.

33. M. Koebel, M. Elsener, M. Kleemann, Catalysis Today 59 (2000) 335-345.

34. Selective Catalytic Reduction, The most promising technology to comply with the imminent Euro IV and Euro V emissions standards for HD engines, final report, European Automobile Manufacturer's Association (ACEA), June 2003.

35. M. Koebel, M. Elsener, G. Madia, Recent Advances in the Development of Urea-SCR for Automotive Applications, SAE Paper Number 2001-01-3625, Society of Automotive Engineers, Warrendale, 2001.

36. J. C. Ball, A Toxicological Evaluation of Potential Thermal Degradation Products of Urea, SAE Paper Number 2001-01-3621, Society of Automotive Engineers, Warrendale, 2001.

37. M. Radojevic, Environmental Pollution 102, S1 (1998) 658-689.

38. S. W. Ham, I. Nam, The Royal Society of Chemistry, 2002, Catalysis 16, senior reporter, C. Kemball; reporters A. D. Caunt, London: Chemical Society, c1977.

39. S. T. Choo, Young Gil Lee, In-Sik Nam, Sung-Won Ham, Jeong-Bin Lee, Applied Catalysis A 200 (2000) 177-188.

40. R.Q. Long, R.T. Yang, Applied Catalysis B 24 (2000) 13-21.

41. H. J. Chae, I. Nam, H. S. Yang, S. L. Song, I. D. Hur, Journal of Chemical Engineering of Japan 34, No 2 (2001) 148-153.

42. B. Maurer, E. Jacob and W. Weisweiler, MTZ 60 (1999) 308-313.

43. C. S. Sluder, J. M. E. Storey, S. A. Lewis, L. A. Lewis, Low Temperature Urea Decomposition and SCR Performance, SAE Paper Number 2005-01-1858, Society of Automotive Engineers, Warrendale, PA (2005).

44. L. Stradella, M. Argentero, Thermochimica Acta 219 (1993) 315-323.

45. P. M. Schaber, J. Colson, S. Higgins, E. Dietz, D. Thielen, B. Anspach, J. Brauer, American Laboratory 31 (1999) 13-21.

46. EM Industries, MSDS Urea, OmniPur ®, http://www.emdchemicals.com/analytics-/doc/msds/msds-display.asp?materialid=9510, (Accessed June 2005).

47. H. L. Fang, H. F. M. Dacosta, Applied Catalysis B: Environmental 46 (2003) 17-34.

48. M. Kleeman, M. Elsener, M. Koebel, A. Wokaun, Ind. Eng. Chem. Res. 39 (2000) 4120-4126.

49. P. G. Blakeman, G. R. Chandler, G. A. John, A. J. J. Wilkins, Investigations into NO_x Aftertreatment with Urea SCR for Light-Duty Diesel Vehicles, SAE Paper Number 2001-01-3624, Society of Automotive Engineers, Warrendale, 2001.

50. M. Koebel, E. O. Strutz, Journal of Industrial and Engineering Chemistry Research 42, Number 10. (2003) 2093-2100.

51. H. Luders, R. Backes, G. Huthwohl, D. A. Ketcher, R. W. Horrocks, R. G. Hurley, R. H. Hammerle, An Urea Lean NO_x Catalyst System for Light Duty Diesel Vehicles, SAE Paper Number 952493. Society of Automotive Engineers, 1995.

52. G. Madia, M. Koebel, M. Elsener, A. Wokaun, Journal of Industrial and Engineering Chemistry Research 41, Number 16 (2002) 4008-4015.

53. E. Jacob, G. Emmerling et al., NO_x-Verminderung für Natzfahrseugmotoren mit Harnstoff-SCR-Kompaktsystemen (GD-KAT). p 366, 19th Int. Vienna Motor Symposium, May 7-8, 1998.

54. E. Jacob, A. Döring, GD-Kat: Abgasnachbehandlungssystem zur simultanen Kohlenstoffpartikel-Oxidation und NO_x-Reduktion für EURO 4/5-Nfz-Dieselmotoren. 21st Int. Vienna Motor Symposium, May 4-5, 2000.

55. J. A. Sullivan, J. A. Doherty, Applied Catalysis B: Environmental 55 (2005) 185-194.

56. C. A. Jones, D. Stec, S. C. Larsen, Journal of Molecular Catalysis A: Chemical 212 (2004) 329-336.

57. M. Koebel, M. Elsener, Journal of Chromatography A 689 (1995) 164-169.

58. E. Seker, N. Yasyerli, E. Gulari, C. Lambert, R. H. Hammerle, Applied Catalysis B: Environmental 37 (2002) 27-35.

59. A. Miyamoto, K. Kobayashi, M. Inomata, Y. Murakami, Journal of Physical chemistry 86(1982) 2945-2950.

60. G. Busca, L. Lietti, G. Ramis, F. Berti, Applied Catalysis B: Environmental 18 (1998) 1-36.

61. Y. H. Park, An Investigation of Urea Decomposition and Selective Non-Catalytic Removal of Nitric Oxides with Urea, Thesis, Master of Science, Texas A&M University, College Station, 2003.

62. A. M.G. Gentemann, Flow Reactor Experiments on the Selective Non-Catalytic Removal of Nitrogen Oxides, Thesis, Master of Science, Texas A&M University, College Station, 2001.

63. H. Oh, Selective Catalytic Reduction (SCR) of Nitric Oxide (NO) with Ammonia over Vanadia-Based and Pillared Interlayer Clay-Based Catalysts, Thesis, Master of Science, Texas A&M University, College Station, 2004.

64. Swagelok Company, FW, F and TF Series Filters - Complete Catalog, http://www.swagelok.com (Accessed April 2005).

65. S. Gupta, Selective Catalytic Reduction (SCR) of Nitric Oxide with Ammonia Using Cu-ZSM-5 and Va-Based Honeycomb Monolith Catalysts: Effect of H_2 Pretreatment, NH_3-to-NO Ratio, O_2, and Space Velocity, Thesis, Master of Science, Texas A&M University, College Station, 2003.

66. J. A. Caton, D. L. Siebers, Combustion Science and Technology 65 (1989) 277-293.

APPENDIX A

MASS FLOW CONTROLLERS CALIBRATION PROCEDURE

A.1 Objectives and description

A Mass Flow Controller (MFC) is a precision flow device used to regulate the flow of gas with high precision. Calibration of MFC is essential for their experimental application and has to be done before the main experiment can be started. This chapter describes the theory behind and the procedure to produce calibration curves for the MFC. The aim of the calculations is to provide information about the desired gas flow rates and the actual set points of the flow controllers in order to get the desired flow rate values.

A.2 Theory

In order to ensure the total mass flow of 1100 sccm, the flow rate of the different gases have to be controlled properly and accurately. This calculation is done with the help of an Excel spreadsheet.

A H_2O displacement method is used to measure the amount of gas that flows through the system in a measured amount of time. By measuring the weight of water in the flask before and after the gas has been added to the flask, the weight of the water displaced can be determined. Density of water is determined from the tables by the inverse of specific volume. Density and the time required to run the calibration are then used to calculate a mass flow rate in standard cubic centimeters per minute (SCCM).

$$\dot{\forall} = \frac{\partial V}{\partial t} = \frac{M_1 - M_2}{\rho_{H_2O} t} \tag{A.1}$$

where $\dot{\forall}$ is the volume flow rate of the gas, M_1 and M_2 are weights of water at the beginning and the end, t is the time allowed for the flow of gas and ρ_{H2O} is the density of water.

The volume displacement should be adjusted for the difference in pressure between the N_2 in the flask and atmospheric pressure. This is done using a simple manometer method.

Table A-1. Example calculation for the flow composition using an excel calibration spreadsheet

Date	MFC #	Set Flow Rate (%)	Actual Flow Rate (%)	Calculated Uncertainty (%)	Remarks
					NO
2/9/2004	1-3	100	106.7849	0.41685	
2/9/2004	1-3	80	92.87956	0.385224	
2/9/2004	1-3	60	63.08547	0.279666	
2/9/2004	1-3	40	42.51347	0.139334	
2/9/2004	1-3	20	21.71846	0.090238	
2/9/2004	1-3	2	2.204959	0.044813	

Table A-1 gives an example of the calculation of actual flow rate for MFC #1-3 used for NO, with the help of an Excel spreadsheet. Also from the ideal gas law of the pure gas ($P\forall = mRT$), the volume flow rate ($\dot{\forall}$) can be corrected to the initial volume flow rate ($\dot{\forall}_0$) at T_0 and P_0.

$$\dot{\forall} = \dot{\forall}_o \left(\frac{P_0}{P}\right)\left(\frac{T}{T_0}\right) \tag{A.2}$$

$$\dot{\forall}_0 = \left(\frac{P}{P_0}\right)\left(\frac{T_0}{T}\right)\left(\frac{M_1 - M_2}{\rho_{H2O} \cdot t}\right) \tag{A.3}$$

where T_0 is the ambient temperatures, P_0 is P_{atm}, T is also the temperature inside the flask which is equal to the ambient temperatures because the calibration process is performed under fixed conditions

The pressure inside the flask after the displacement is less than the outside pressure which is atmospheric (P_{atm}).

$$P_{flask} = P_{atm} - \rho_{H_2 0} gh \tag{A.4}$$

The flow rate should then recognize the pressure adjustment. The pressure adjustment can make a difference of around one percent.

$$\frac{\partial V_{adjusted}}{\partial t} = \left(\frac{P_{atm} - \rho_{H_2} ogh}{P_{atm}} \right) \left(\frac{M_1 - M_2}{\rho_{H_2} ot} \right) \tag{A.5}$$

A.3 Equipment required

In order to calibrate the MFCs, the equipment required is the following: a 2 liter flask, a basin to contain the water acting as a reservoir, and N2 source which is a pressurized cylinder, a stopwatch to measure the time for which the gas is allowed to collect at the bottom of the flask, a thermometer in order to measure the ambient and the water temperature, correctly installed MFC with tubing and connectors, and a ruler in order to measure the height of the water column in the bucket.

The Mass Flow Controller is a self contained control system and flow controller capable of controlling the volumetric flow rate of certain gases for low flow rates. Precision Flow Devices manufacture the MFC.

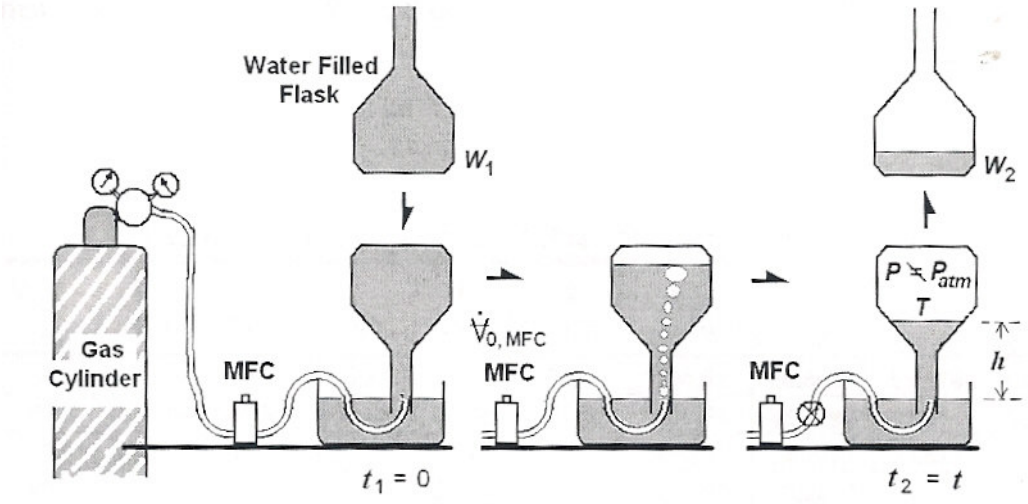

Figure A-1. MFC calibration setup using water displacement method [9].

A.4 Procedure

The calibration procedure takes around one hour for each of the MFC. Figure A-1 gives a schematic of the steps involved during the calibration of the MFC. The entire process of calibration can be subdivided into two parts: the first one involved pre-calibration of the MFC and the latter part involved actual calibration steps. For pre-calibration, water was added to the tub (reservoir) and it was allowed to warm and attain the room temperature. MFC which was required to be calibrated was turned on and allowed to warm up for about half an hour. This is necessary in order to ensure the stability and consistency in the readings obtained from the MFC. The MFC was checked for zero set point to confirm no gas was flowing through it. MFC was then set to the required set point in order to ensure the desired flow rate through it. Now the actual calibration steps of MFC were required to be performed. The temperature of the water was tabulated and the related density was obtained through water-steam tables (Moran and Shepiro's thermodynamics, 3rd edition's tables contain specific volume which is the inverse of density). The flask was filled totally with water ensuring that there were no water bubbles trapped inside it. The flask was then weighed using a balance and the weight was noted down in a tabular format. Top of the flask was then covered and it was inverted carefully without spilling any water and ensuring no air escaped into it. It was then clamped in an inverted position in such a way that the flask neck was totally immersed inside the water, again making sure no air entered the flask. All the valves except the one after the MFC were turned to an open position which allowed N_2 to flow from the cylinder through the pipe connection to the MFC. Then the valves after the MFC was turned on and N_2 was permitted to flow out into the atmosphere till the MFC reading stabilized. By careful inspection, N_2 was allowed to fill the water column in the inverted flask by simultaneously switching on the stop watch. After allowing N2 to flow for sometime, the flow and the stop watch were stopped simultaneously and the reading for the stop watch was noted down. With the help of the ruler, height of the remaining water column from the free surface inside the tub was also noted down. The flow reading from

the MFC was noted down as well and it may not be the same as the set flow rate. The flask was then unclamped and by securely covering its top, it was removed from the tri-pod stand and weighed on the balance. The difference between the weight of the flask before and after the experiment gave the mass of water that remained in the flask. The afore-mentioned procedure was repeated for different flow rates so as to come up with a calibration data for the MFC. Figure A-2 gives the calibration plot MFC #1-3 used for NO. Figure A-3 gives the calibration plot for MFC #1-4 used for N2. Figure A-4 and Figure A-5 give the calibration plot for MFC #2-4 and MFC #2-4 used for O_2 and N2 respectively.

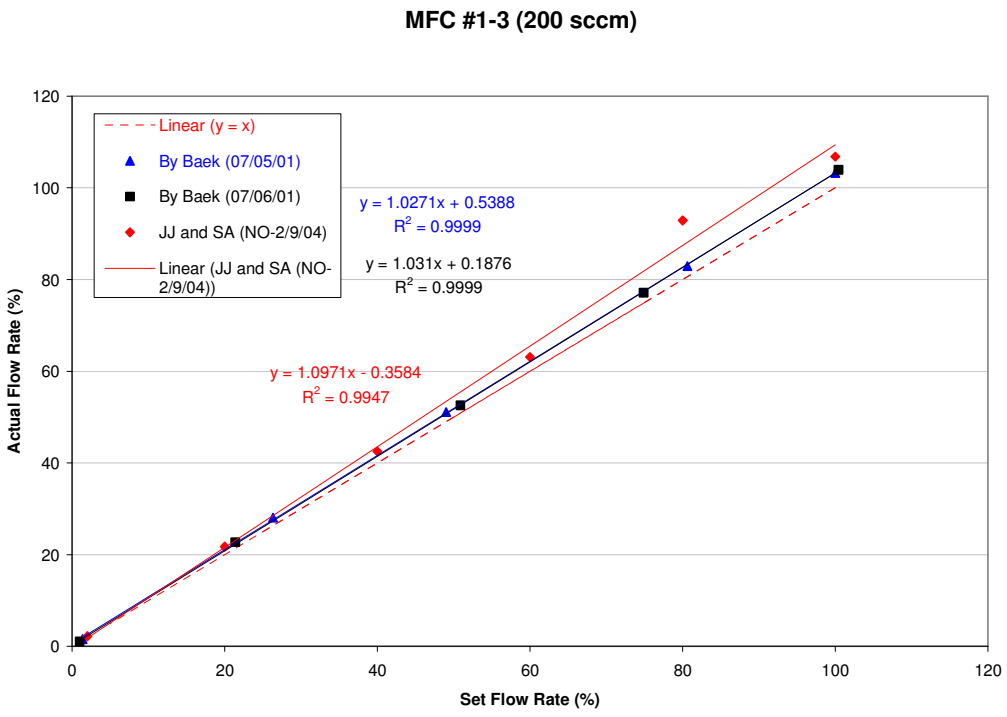

Figure A-2. MFC calibration plots for mass flow controller 1-3 (200 sccm) for NO.

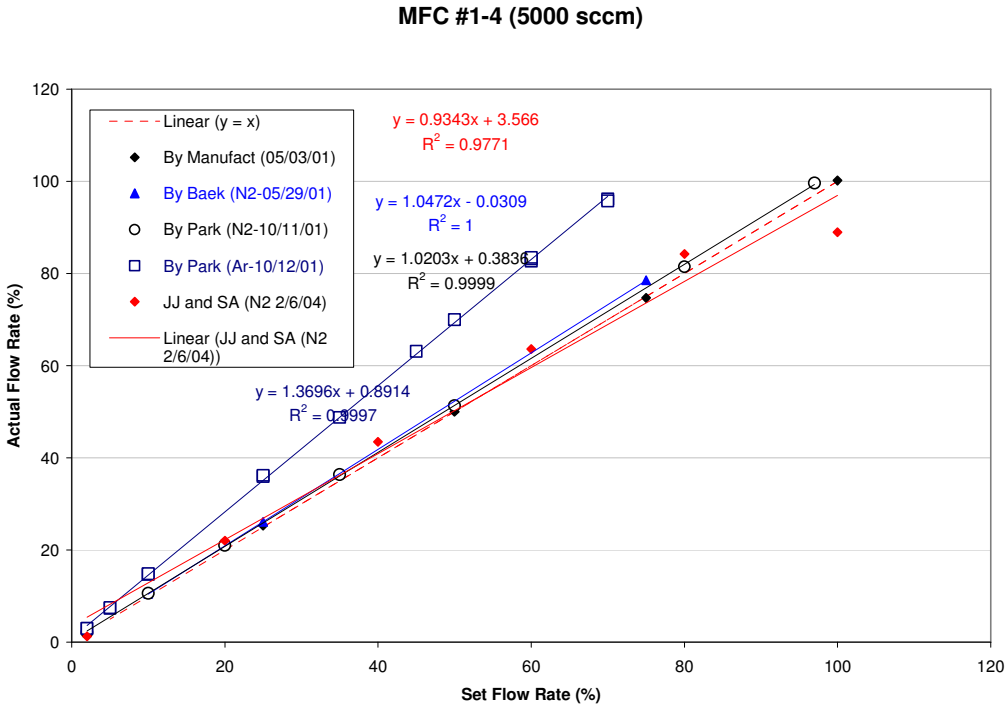

Figure A-3. MFC calibration plots for mass flow controller 1-4 (5000 sccm) for N_2.

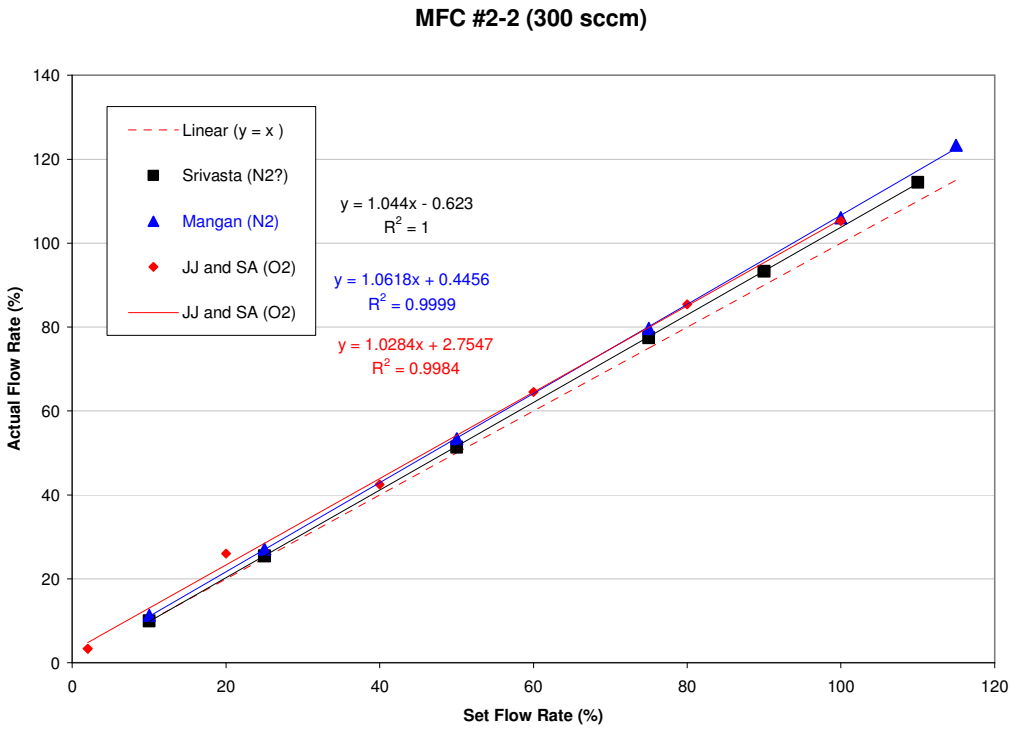

Figure A-4. MFC calibration plots for mass flow controller 2-2 (300 sccm) for O_2.

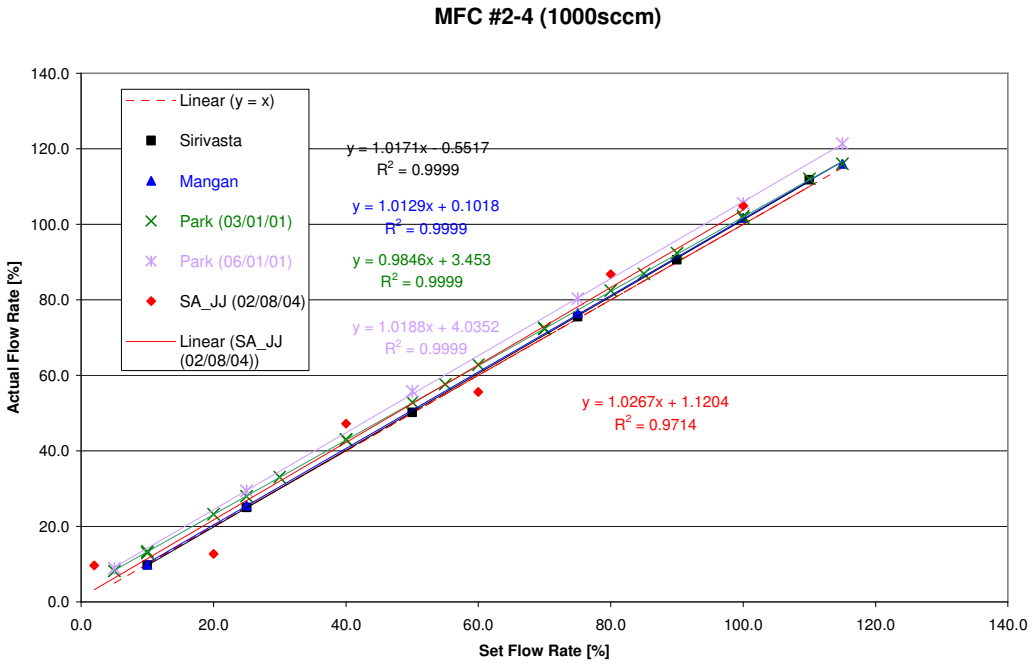

Figure A-5. MFC calibration plots for mass flow controller 2-4 (1000 sccm) for N_2.

.

Table A-2. Coefficients of the curve-fit functions for the four MFCs.

MFC number	Used gas	y = mx + c	
		m	c
#1-3	NO/N_2	1.0971	-0.3584
#1-4	N_2	0.9343	3.566
#2-2	O_2	1.0284	2.7547
#2-4	N_2	1.0267	1.1204

With all data from above procedures between the MFC set flow rates and its calibrated flow rates ($\dot{\forall}_0$ in %), the linear fits and their functions in the form of y = mx + c for MFC #1-3, 1-4, 2-2, 2-4 are illustrated in figures . The linear fits were found to be of root-mean square accuracy of about 0.999. Coefficients of the linear fit functions have been given in Table A-2 for different gas species.

APPENDIX B

UREA INJECTOR CALIBRATION

B.1 Urea injection calibration data

The following table gives the calibration data for the urea injector. While taking the calibration readings, it was ensured that the injector calibration was done as close to the final configuration as possible. This was achieved by connecting the injector to the whole setup and heating all the three zones of the reactor. Filters were also attached to the setup and pure N_2 was allowed to flow through the setup at the rate of 1100 sccm. Adding filters at the outlet of the reactor caused a back pressure as a result of which, the urea injector required a higher injection pressure. For each pressure case, three readings were taken and averaged in order to plot the average flow rate with the injection pressure. Table B-1 gives the details regarding the calibration data.

Table B-1. Calibration data for the urea injector pressured by N_2.

Sno.	Time (sec)	Initial level (cm)	Final Level (cm)	Pressure (psig)	Furnace Temperature Zone 1	Zone 2	Zone 3	Flow Rate (ml/min)	Average flow (ml/min)
1	45.0786	2.4	2.5	2.4	150	150	150	0.06	
2	45.92583	2.5	2.6	2.4	150	150	150	0.06	
3	46.39667	7.6	7.7	2.4	150	150	150	0.06	0.06
4	52.12633	8.1	8.2	0.7	150	150	150	0.05	
5	53.766	8.2	8.3	0.7	150	150	150	0.05	
6	52.942	8.3	8.4	0.7	150	150	150	0.05	0.05
7	52.4092	7.9	8	1	150	150	150	0.05	
8	54.72017	8	8.1	1	150	150	150	0.05	
9	96.41083	8.1	8.3	1	150	150	150	0.06	0.05
10	49.55333	7.6	7.7	1.3	150	150	150	0.06	
11	48.62	9.2	9.3	1.3	150	150	150	0.06	
12	47.51433	9.3	9.4	1.3	150	150	150	0.06	0.06
13	39.54933	7.9	8	3.8	150	150	150	0.07	
14	39.5	8	8.1	3.8	150	150	150	0.07	
15	74.7495	8.1	8.3	3.8	150	150	150	0.08	0.07

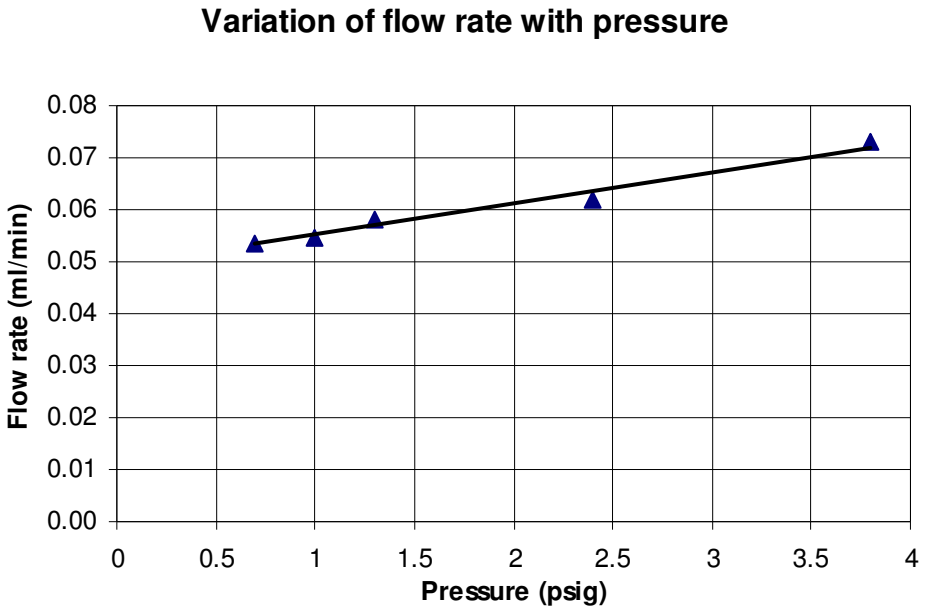

Figure B-1. Linear relationship between the injection pressure and the flow rate.

Figure B-1 was plotted from the data obtained in Table B-1. After plotting all the data points for the average flow rate readings, a linear curve was used to fit the graph and the data points fit very well with a linear profile. This curve was taken as the basis for running all the experiments. The voltage that was set for the heating tape installed after the injector was 72 V. The temperature of the reactor was kept constant at 150^{o}C for all the three zones. Capillary size used for the calibration was 28 gauge with outer diameter of 0.014 inch and inner diameter of 0.007 inches.

Table B-2. Excel spreadsheet for determining amount of urea to be added to the water for desired urea ppm.

	Milliter	Time (Min)	Feed Rate (ml/min)	Water (ml)	Desired Urea (ppm)
Input Data	200	4000	0.05	250	330

Density (kg/m3)	Mole Mass H_20 (kg/kmole)	Total Flow (sccm/min)	STP	M (urea)
998	18.016	1100	22.41354	60.056

	Mole Flow (kmole/s)	Total Mole Flow (kmole/s)	Mole Fraction H_20	H_20 (%)	ppm
Calculated	4.61627E-08	8.17958E-07	0.053421558	5.342155816	53421.55816

N'(urea) (kmole/s)	m'(urea) (kmole/s)		amount of Urea (gm)	
2.69926E-10	1.62107E-08		0.004863205	

After deciding a feeding rate and set point of heating tape controller, the amount of urea powder that should be mixed with distilled water was calculated. Table B-2 shows the excel spreadsheet which was used to calculate the amount of urea that was required to be dissolved in a given quantity of water in order to prepare the right solution. The right solution would inject the correct amount of urea in ppm into the reactor which would lead to the desired NH_3: NO ratio.

APPENDIX C

ESTIMATION OF WATER INJECTION RATE

C.1 Assumptions

It was necessary to estimate the water injection rate from the urea injector so as to ensure that the water level inside the FTIR does not exceed a maximum limit above which it was too difficult to obtain sensible data from the FTIR. The maximum limit was set to be between 2-5% H_2O based on the earlier FTIR data obtained in the presence of moisture. The flow was assumed to be continuous and no phase change was assumed to take place during urea-water solution injection.

C.2 Methodology

Volume flow rate of gases = 1100 sccm

$$= 22\left(\frac{\text{cm}^3}{\text{min}}\right)$$

Minimum volume flow rate for H_2O

$$= \frac{2}{100}\times 1100\left(\frac{\text{cm}^3}{\text{min}}\right)$$

At STP (0^oC, 1 bar), Volume occupied by 1 kmole of gas = 22.41354 m^3/kmole

$$= 22\times 10^{-6}\left(\frac{\text{m}^3}{\text{min}}\right)\times\left(\left(\frac{1}{22.41354}\right)\left(\frac{\text{kmole}}{\text{m}^3}\right)\right)$$

.

Mole flow rate of water required (N_{H_2O})

$$= 9.815\times 10^{-7}\left(\frac{\text{kmole}}{\text{min}}\right) \quad = 9.815\times 10^{-4}\left(\frac{\text{mole}}{\text{min}}\right)$$

Hence Mass flow rate of water

$$= 9.815\times10^{-4}\times18.016\left(\frac{\text{kg}}{\text{min}}\right)$$

Density of water at room temperature (25^{o}C, 1 atm) = 998 kg/m^3

Hence

$$= 1.768\times10^{-2}\left(\frac{\text{kg}}{\text{min}}\right)$$

Water Injection Rate (minimum)

$$= \frac{1.768\times10^{-2}}{998}\times10^{6}\left(\frac{\text{ml}}{\text{min}}\right)$$

$$= 17.72\left(\frac{ml}{\text{min}}\right)$$

Similarly for 5% H_2O

$$V_{max} = \frac{5}{100}\times1100\times\frac{10^{-6}}{22.4}\times\frac{18.016}{998}\times10^{6}\times10^{3}\left(\frac{\text{ml}}{\text{min}}\right)$$

$$= 44.324\left(\frac{ml}{\text{min}}\right)$$

General formula between desired H_2O percentage in FTIR(X%) and the injection rate is given by:

$$V = \frac{X}{100}\times1100\times\frac{10^{-6}}{22.4}\times\frac{18.016}{998}\times10^{6}\times10^{3}\left(\frac{\text{ml}}{\text{min}}\right)$$

$$\boxed{V\left(\frac{\text{ml}}{\text{min}}\right) = 8.856X(\%)}$$

APPENDIX D

CALCULATIONS FOR ACCOMMODATING AMMONIA AND CO_2 GENERATED FROM UREA-WATER SOLUTION

D.1 Products of thermal decomposition

$$NH_2CONH_2 + H_2O \longrightarrow 2NH_3 + CO_2 \qquad (D.1)$$

The above reaction suggests that one mole of urea reacts with one mole of water at high temperature to give 2 moles of ammonia and one mole of CO_2. The above reaction suggests that if the urea-water solution is heated at high temperature then the products of thermal decomposition should entirely be ammonia and CO_2 at steady state and there should not be any production of water. But while doing our experimentation we also find that water condenses at the flanges and the water condenser. Where does this water come in to picture if the urea solution is giving away only ammonia and CO_2? Also the concentrations of these components by the FTIR confirm that the thermal decomposition is taking place almost completely. The reason is as follows:

D.2 Where does the excess moisture come from?

From the mole flow rates of water and urea coming form the urea-water solution, it is noticed that the rates are not the same. For an injection rate of 0.05 ml/min, water flow rate is 4.62089E-08 moles/min while that of urea being 7.6582E-09 moles/min. This clearly accounts for the excess moisture being present in the gases after thermal decomposition of the solution and this excess water vapor condenses wherever the temperature is low enough for the condensation to take place.

D.3 Why does this excess moisture cause a problem?

The FTIR is very sensitive to the moisture concentration of the gases flowing through it. Any amount of excess moisture (> 5%) would cause the FTIR readings to deviate from the zero line and cause experimental error. The excess moisture condenses in the water condenser as well as the left flange and this moisture concentration builds up from time to time. The building of this water concentration results in the gases being more and more moisture laden as the experiment continues to run. This eventually ruins the FTIR reading after a while. Hence one of the main challenges in this experiment is to maintain the minimum flow rate possible.

D.4 Calculations for ammonia and CO_2

From equation (D.1) it is evident that 1 mole of water and urea at high temperature (around 227^{o}C) give 2 moles of NH_3 and 1 mole of CO_2. Hence the mole flow rate of ammonia and CO_2 would be 1.53165E-08 moles/min and 7.658E-09 moles/min respectively. Converting it to volume flow rate we get the flow rate of ammonia as 0.363 sccm and that of CO_2 as 0.1815 sccm. These are the values which are taken into account while making the flow settings file for the mass flow meters. The balance nitrogen is taken to be the difference of 1100 sccm and the sum of the entire gas flow rate taking place inside the reactor. Hence incorporating the above calculation is important for greater accuracy of experimentation.

After taking into account the flow rate of ammonia and CO_2, following are the mass flow setting values:

Table D-1. Mass flow meter settings taking into consideration NH_3 and CO_2 arising from the injector.

Mass Flow meter settings

Dilution N_2	**Balance N_2**	**NH_3**	**NO**		**β Ratio**	**O_2**	
#1-4	**#2-4**	**ppm**	**ppm**	**#2-1**		**%**	**#2-2**
97	94.8178566	330	330	10.135042	1	0	0
97	93.7399957	330	330	10.135042	1	0.5	0.908304
97	92.6621347	330	330	10.135042	1	1	4.495234
97	88.3506909	330	330	10.135042	1	3	18.84296
97	90.9025347	495	330	10.135042	1.5	0	0
97	89.8246737	495	330	10.135042	1.5	0.5	0.908304
97	88.7468128	495	330	10.135042	1.5	1	4.495234
97	84.435369	495	330	10.135042	1.5	3	18.84296

APPENDIX E
TEMPERATURE DISTRIBUTION IN THE FURNACE

E.1 Objectives

The furnace consists of three separate zones each of which can be heated separately in order to get different heating lengths. In actual practice, temperature inside the furnace is not regular and varies from one location to the other though the temperature controller might show the same temperature in all the three zones. The objective of this study was to measure the temperature distribution of the furnace when all the zones (Zone 1 + Zone 2 + Zone 3) were heated together at the same temperature. Temperature along the whole length of the quartz tube was measured using a thermocouple (OMEGA® Type K) at flow conditions similar to the actual experiments.

E.2 Methodology

The furnace was powered up and was set at a selected temperature for sometime in order to let it reach a steady state. Figure E-1 shows the setup for measuring the reactor temperature along with the 3 zones inside the reactor.

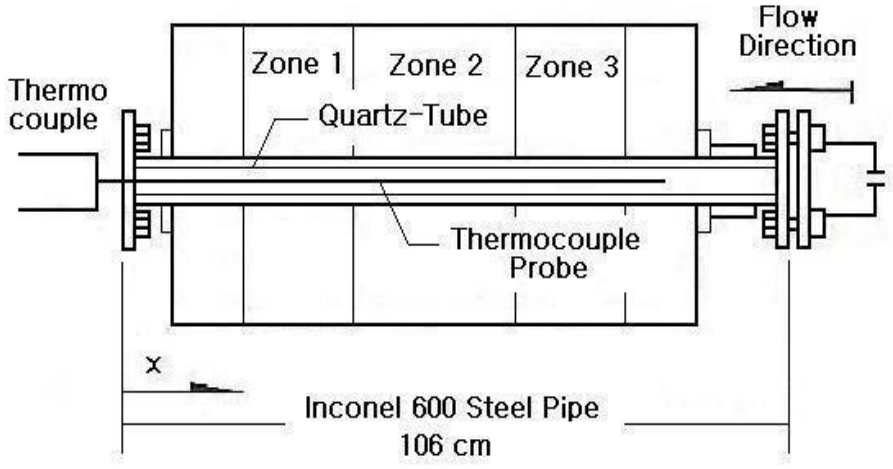

Figure E-1. Reactor temperature measurement using K-type thermocouple [3].

The temperature distribution of the simulated gas was measured by setting the reactor temperature at 227 and 477°C, and the flow rate of 1100 sccm of pure nitrogen was used. The catalyst was not kept inside the reactor during the study because the thermocouple thickness would not allow it to pass through it. The reactor temperatures were taken in axial direction at steps of 6 cm and 4 cm depending upon where the accuracy was more important. The K-type thermocouple was inserted inside of the furnace from the outlet to the inlet side, hence the direction of measurement of the temperature was against the gas flow. The K-type thermocouple theory is explained in greater detail by Baek [53]. Due to the weight of the thermocouple, it was difficult to hold it in the centre of the quartz tube and hence it was allowed to touch the quartz tube bottom for all the readings. The temperature distribution was studies for heating all the three zones together and it gave a better idea of how long and in what ranges the temperature inside the furnace exceeded the set temperature. For both the temperature distribution measurements, the reading of the temperature panel for the reactor was allowed to stabilize and the room conditions were kept the same.

Table E-1. Measured temperature data for all zone activation of reactor by two selected reactor set temperatures.

3 Zone Heating		
x (cm)	Set Temperature (ºC)	
	227ºC	477ºC
0	27.6	26.3
6	58.1	185.3
12	167.8	387.4
18	191.6	437.7
24	212.4	475
30	225.1	474.6
36	225	475.1
40	225.6	474.8
44	224.5	474.8
48	224.6	473.9
52	225.1	473.8
56	225.1	474.3
60	224.6	474.5
64	224.5	475
68	224.2	473.2
70	224.8	472.9
76	224.3	473.2
82	223.9	471.6
88	180.3	377
94	87.4	143
99	52.6	77.2
104	41.5	54.2
108	29.8	34.5

Table E-1 shows the measured temperature data for the cases shown in Figure E-2. The measured temperature data is given in ^{o}C and is tabulated for different axial lengths where temperature measurements were taken. All the temperature measurements were made up to one decimal digit accuracy.

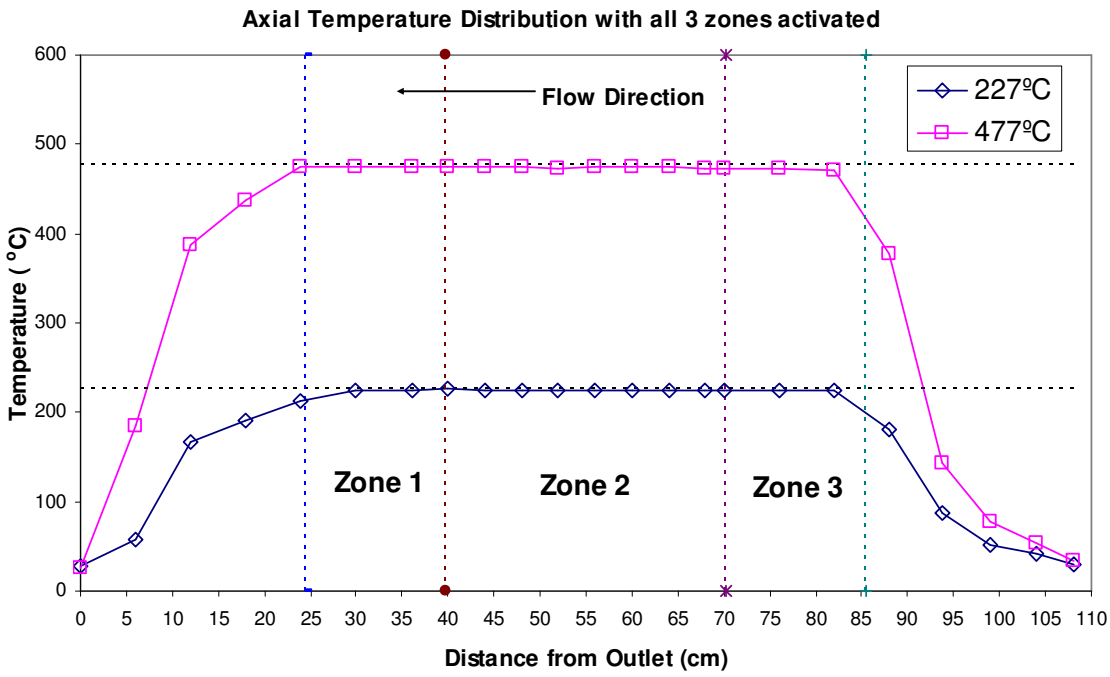

Figure E-2. Axial temperature distribution with zone 1, 2 and 3 activated at 227°C and 477°C.

E.3 Temperature distribution for activation of zone 1, zone 2 and zone 3

Figure E-2 shows the temperature distribution resulting from all the three zones being activated. This was done for both a low temperature of 227°C (500K) and 477°C (750K). The reactor temperature was taken at an interval of 6 cm or 4 cm. The dotted lines in the figure represent the two set temperatures of the reactor. The measured temperatures were found to be lower (~7°C) than the actual set temperatures over the entire length in the axial direction. Looking at the curves, N_2 flows from right to left, with the outlet from the reactor located at the zero mark. The temperature difference between the set temperature and the measured temperature can be attributed to heat losses to the gas, imperfect sealing of the reactor and the effects of convection. Going from left to right in the figure, the curve has a convexity in the region of zone 1, in zone 2 the temperature distribution is almost constant and in zone 3 the curve is concave at the bottom. This

could be due to the convection current due to the flow of gas from right to left. The region of uniform temperature distribution lies at a distance of 25 cm to 85 cm from the outlet of the reactor.

APPENDIX F

THE DETAILS OF THE CATALYST SAMPLE

F.1 V_2O_5-WO_3/TiO_2 honeycomb monolithic catalyst

V_2O_5-WO_3/TiO_2 honeycomb monolithic catalyst sample was provided by KWH Catalysts, Inc. [4] in USA. Table F-1 gives more specifications of the sample. The study was conducted on the sample by cutting it in 2 cm length for a quartz tube of internal diameter of 2 cm.

Table F-1. Specifications of V_2O_5-WO_3/TiO_2 honeycomb monolithic catalyst.

Material	Tetragonal-shaped square-channel titania-vanadia-tungsten based honeycomb monolithic catalyst
Appearance	Dark-green/gray color
Operating temperature (advised)	< 430 ˚C
Height × Width × Length	6 inches × 6 inches × 11 inches
Stability	Stable under normal storage conditions
Specific surface area	1,015 m^2/m^3
pH (potential of hydrogen)	5
Cell size	(1/3) cm × (1/3) cm
Specific gravity	1.8
Potential Health Effects	Skin irritant, eye irritant
Other properties	Toxic and odorless

APPENDIX G

FTIR CALIBRATION SPECTRUM

G.1 Chemical species and spectral bands

The following section shows the absorbance detected for the various species using the FTIR and the wave numbers for detecting different species. The basis for the FTIR calibration of different gas species is Beer's law that governs the linear proportionality relationship between the spectral heights in absorbance and the specie concentrations when exposed to infrared radiations. Figure G-1 is an example of the absorbance spectra for various input gas species along with the wave number range for which peaks are observed.

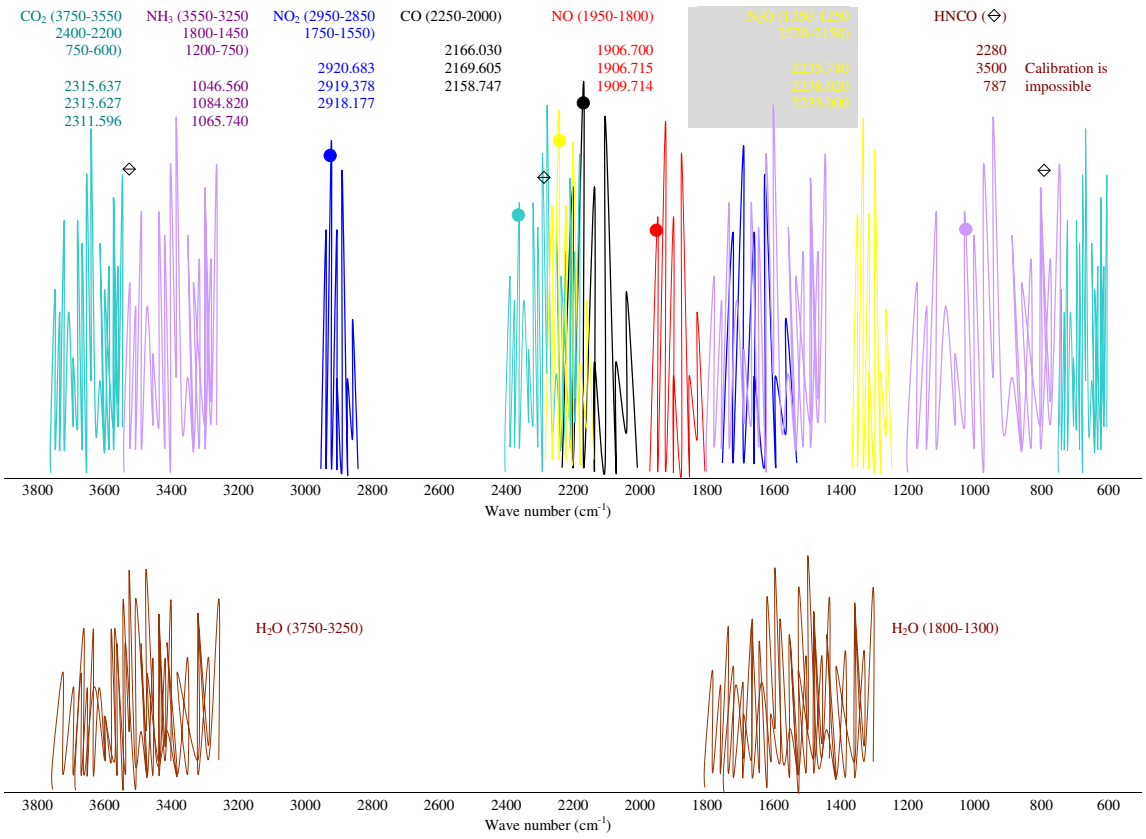

Figure G-1. Absorbance spectra for various species.

Table G-1. Wave numbers used to quantify various species and the estimated lower detection limits.

Species	**Wave Number (cm^{-1})**	**Lower Limit (ppm)**
NO	1906.621 1903.605	5
CO_2	2315.637 2313.627 2311.596	5
N_2O	2235.741 2238.023 2233.005	2
NH_3	1046.499 1065.701 1084.764	5
HCNO	2282.178	-
NO_2	2920.683 2919.378	2

The absorbance intensities (i.e., the maximum peak heights for a spectral band) may not be the same for different species having the same concentration. As can be seen from the figure, typically every species possesses more than one spectral band, while different species may appear in a mixed spectral range. Spectral bands of some species may overlap (eg. H_2O and N_2O) making it difficult to identify each specie separately. This is one reason why H_2O concentration is kept as low as possible (2-5%) in the gas mixture in order to prevent noise and difficulty in detection of other important gas species.

Table G-1 gives a list of all the wave numbers used in order to quantify various gas species and their estimated lower detection limits. For most of the species, more than one wave number was utilized for quantifying the gases. Using more than one wave

numbers helped in obtaining result with higher accuracy. For NO and NO_2 wave numbers 1909.594 and 2918.177 cm^{-1} respectively were discarded since they were obscured by the moisture present in the gases that were analyzed by the FTIR. A minor drawback of the FTIR analysis is the interference of the absorbance bands of NO and NO_2 with the ones of water, thus limiting the lower limit of detection in the measurements of NO_x [5].

G.2 Calibration data and curve fitting

The changes in the spectral peak heights in absorbance with respect to the concentration changes are related by curve fit functions. For the detection of various reactants and possible products from the reactions, each chemical species is sampled with its known concentrations by obtaining an absorbance spectrum at conditions which are exactly similar to the actual experiment.

The results of the calibration for the species, NH_3, NO are presented in the following pages. The plots for each species illustrate the selected absorbance peaks the curve fits, which is used to functionally relate the concentrations of the species to the absorbance peak heights. For the curve fits, the base line spectrum (the background spectrum) contains intrinsic spectral noise along with H_2O, instead of forcing the concentrations to zero. Hence the curve fits can be associated with a second degree polynomial function of the form:

$$X_k = ah^2 + bh + c$$

where X_k represents the species concentration in mole fraction (ppm), ‘h’ represents the absorbance peak height, and the three coefficients ‘a, b, c’, represent the curve fitting constants. Because of the presence of noise in the background spectrum, ‘c’ is not equal to zero.

G.3 Calibration procedure

The following subsection explains the FTIR calibration procedure which was performed prior to running the experiments. Experiment was first started by switching on all the mass flow meters and it was ensured that the connections are properly secured.

The required amount of gas species were allowed to flow through the system. On the FTIR computer, the following path was followed: BioRad →Collect → Rapid Scan → Setup. The settings were switched from interferogram to single beam. Single beam corresponds to the nature of the background scan. After checking the Single beam, checked under processed. Processed corresponds to the sample scan trend. The sample scan button was clicked to check for the water vapor content and noise. On the sample scan, last fluctuation in the spectrum referred to the noise which can be due to vibrations in the instrument. This can be confirmed by tapping the FTIR apparatus slightly and noticing the noise going up in the FTIR spectrum. The middle frequency range showing fluctuations corresponded to CO_2. The whole system was allowed to run for some time in order for it to stabilize and allow the water vapor content to decrease. It was taken great care not to click on the background scan button in the middle of the experiment. Background scan was clicked only once at the starting of the experiments and was not clicked anytime later. For all the ppm of one species taken, the background scan acted as a reference. If by mistake the background scan was clicked in the middle of the experiments then it was immediately aborted. For every ppm of gas, 20-25 sets of reading were taken. Checked the filename ave-check for how its done. This file was present under the jasmeetsherif folder in the E:/ drive. As the readings were taken for the same ppm, it was noticed that the transient state was present earlier leading to variation in the readings. Later on the readings stabilized.

NH_3 took longer time to stabilize than NO. Readings that were close to the average were selected. Going back to the file containing sample scans and all but one scans of that ppm pertaining to the reading close to the average were deleted. For NO, steps taken by were as follows: 0, 50, 100,150,200,250,300,350,400,500…..1000. These set of 20-25 sample scans were then repeated for different ppms. After taking the scans, the next step was to find out the concentration of specie pertaining to the readings we got. Followed the following path after selecting all the readings. Operation → Quantitative Analysis → Simple or Alt O → Q → S or C:\ Winnt\Profiles\Administrator\Personal. Separate files were made for below 350 ppm and above 350 ppm so that in case in the

middle of experimentation when the specie concentration exceeded 350 ppm, the second file could be referred to, otherwise first one would suffice always. Amongst these readings only one was selected based on the one close to the average after transient state had been overcomed. This reading corresponded to the one used in the final case. Thus sample scans for every ppm in the file form had been created. Then clicked on the Baseline Correct button. This was done after getting every ppm reading for both NO and NH_3. On clicking two screens appeared: one for initial and the other for baseline. Initial ones corresponded to the readings taken before baseline correction. Baseline ones corresponded to after correction. The baseline ones were created by clicking at the mid point of the scan obtained at various frequencies before the correction.

G.4 Calibration curves (NO and NH_3)

The results from the calibration of NH_3 and NO have been presented in the next few pages. For NO and NH_3 separate files were created for species concentration of below 350 ppm and another for above 350 ppm. The plots for each species illustrate the selected absorbance peaks the corresponding curve fits, which functionally relates the concentrations of the species to the absorbance peak heights. The functional relationship between the species concentration and the absorbance peaks was taken to be quadratic resulting in a curve fit having $R^2 = 1$.

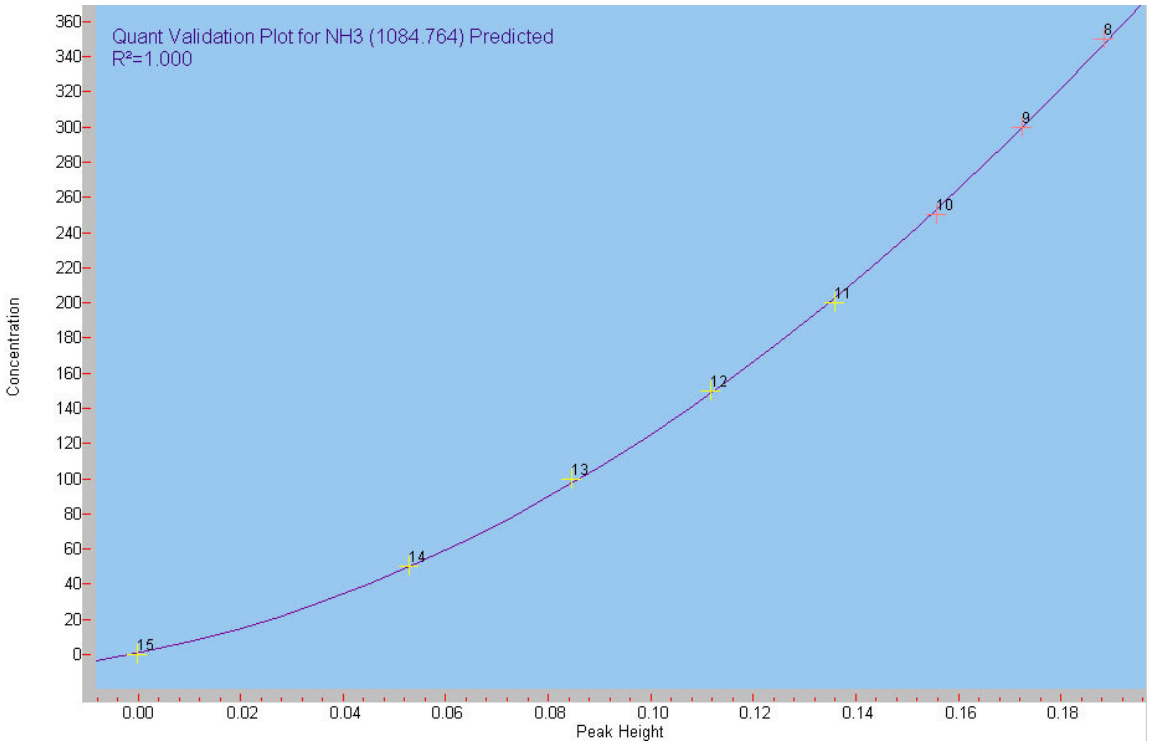

Figure G-2. Calibration curve-fits of peak heights v/s concentrations of NH_3 (0-350 ppm).

Figure G-2 shows the calibration curve which was generated for NH_3 concentrations of less than 350 ppm. NH_3 has well separated absorption bands and a relatively high absorption coefficient. Ammonia has absorption bands in three regions in the infrared (3550 ~ 3250, 1800 ~ 1450, and 1200 ~ 750 cm-1). In the ranges around 3550 ~ 3250 and 1800 ~ 1450 cm-1, the absorbance is interfered with H_2O [2]. For the accurate determination of NH_3, selected absorbance was in the 1200 ~ 750 cm^{-1} region in the spite of interference from carbon dioxide. Among lots of peaks, 3 peaks were selected for the quantification with the wavenumbers (1046.499, 1065.701, and 1084.764cm^{-1}).

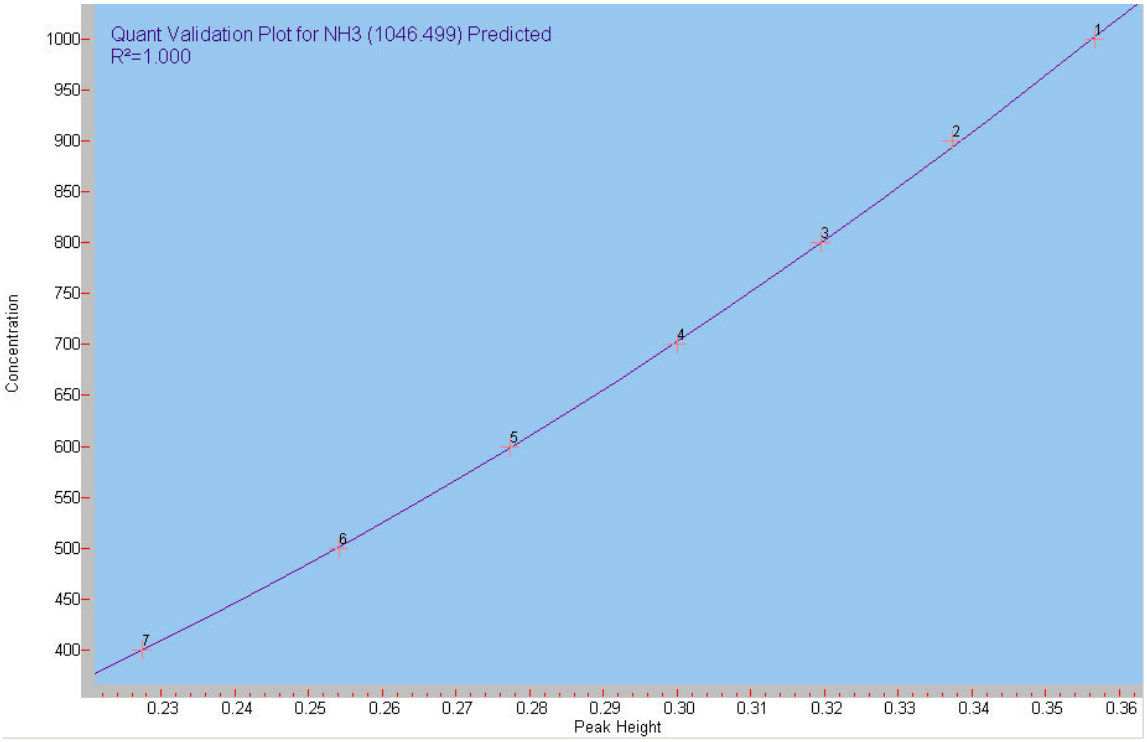

Figure G-3. Calibration curve-fits of peak heights v/s concentrations of NH_3 (350-1000 ppm).

Figure G-3 shows the calibration curve which was generated for NH_3 concentrations lying between 350 ppm and 1000 ppm. For the accurate determination of NH_3, selected absorbance was in the 1200 ~ 750 cm^{-1} region in the spite of interference from carbon dioxide.

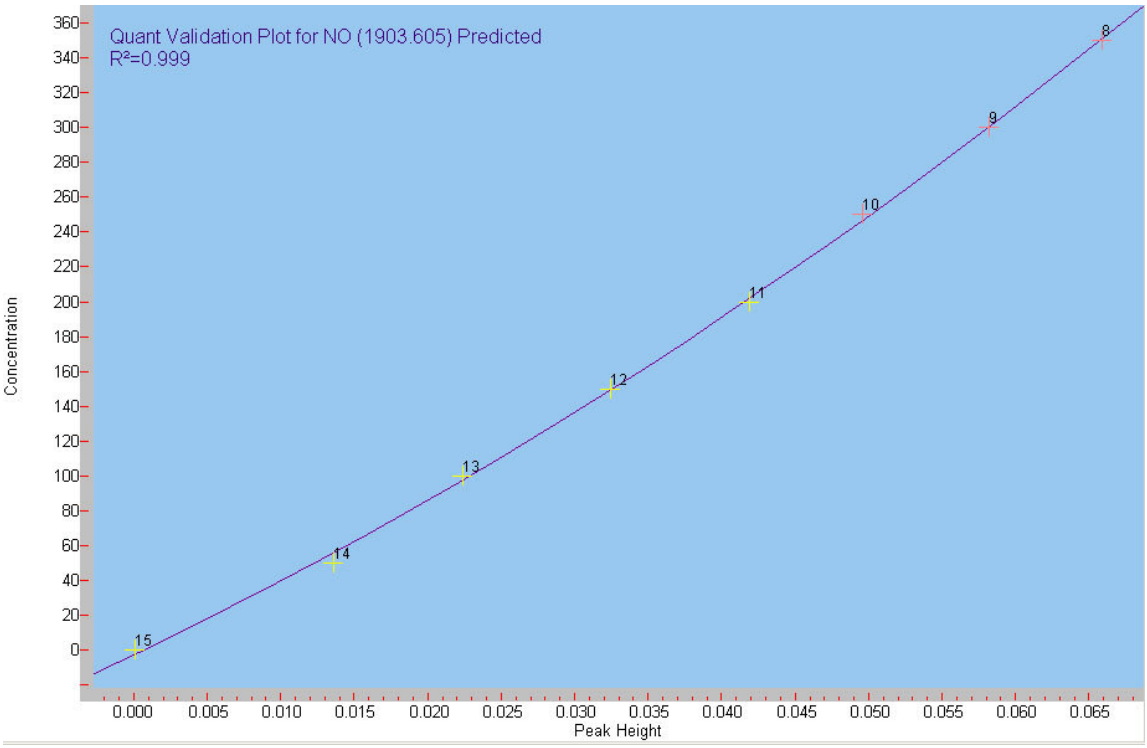

Figure G-4. Calibration curve-fits of peak heights v/s concentrations of NO (0-350 ppm).

Figure G-4 shows the calibration curve which was generated for NO concentrations of less than 350 ppm. NO absorbs infrared radiation only in the range 1950 ~ 1800 cm –1. Among lots of peaks, 2 peaks were selected for the quantification with the wavenumbers (1906.621, and 1903.605 cm^{-1}). Figure G-4 shows the relation between absorbance and concentration of NO. For NO wave number 1909.594 cm^{-1} was discarded since it was obscured by the moisture present in the gases that were analyzed by the FTIR

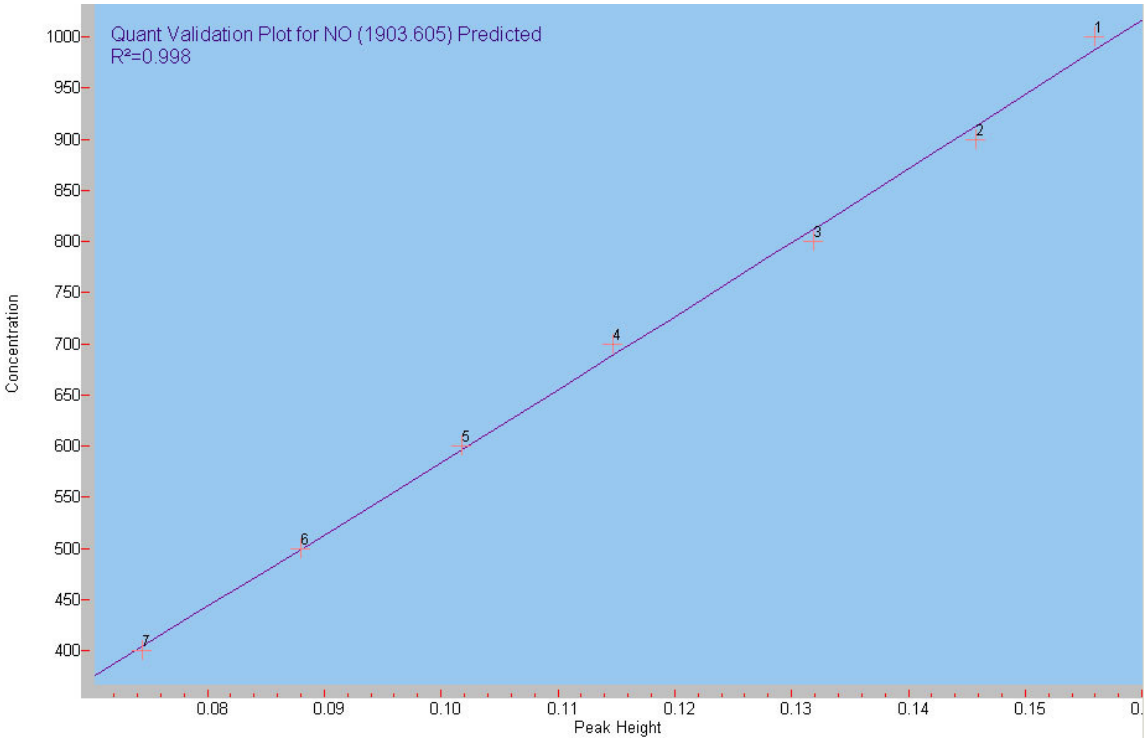

Figure G-5. Calibration curve-fits of peak heights v/s concentrations of NO (350-1000 ppm).

Figure G-5 shows the calibration curve which was generated for NO concentrations lying between 350 ppm and 1000 ppm. Among lots of peaks, 2 peaks were selected for the quantification with the wavenumbers (1906.621, and 1903.605 cm^{-1}). For NO wave number 1909.594 cm^{-1} was discarded since it was obscured by the moisture present in the gases that were analyzed by the FTIR.

VITA

Jasmeet Singh Johar was born in New Delhi, the national capital of India on November 11, 1981. He enrolled in the Bachelor of Engineering program in mechanical engineering at Delhi College of Engineering, University of Delhi, India in the fall of 1999. Soon after graduating in May 2003 with a Bachelor of Science degree, he enrolled at Texas A&M University in the fall of 2003 to pursue a Master of Science degree in mechanical Engineering.

Jasmeet Singh Johar can be reached at e-mail: jasmeet_johar@yahoo.com and will maintain his permanent address at his parents' home:
B-4/11, First Floor, Vasant Vihar, New Delhi, Delhi-110057, India.